LBL-30096

Lawrence Berkeley Laboratory
UNIVERSITY OF CALIFORNIA

Materials & Chemical Sciences Division

Low-Frequency NMR and NQR with a cd SQUID Amplifier

N.-Q. Fan
(Ph.D. Thesis)

November 1990

Prepared for the U.S. Department of Energy under Contract Number DE-AC03-76SF00098.

LBL--30096

DE91 011829

Low-Frequency NMR and NQR with a dc SQUID Amplifier

Nong-Qiang Fan
Ph.D. Thesis

Department of Physics,
University of California
Berkeley, CA 94720

and

Materials Sciences Division
Lawrence Berkeley Laboratory
University of California
Berkeley, CA 94720

November 1990

This work was supported by the Director, Office of Energy Research, Office of Basic Energy Sciences, Materials Sciences Division of the U.S. Department of Energy under contract number DE-AC03-76SF00098.

Low-Frequency NMR and NQR Spectrometer Based on a dc SQUID

by

Nong-qiang Fan

Abstract

A sensitive Fourier-transform spectrometer based on a dc SQUID (Superconducting QUantum Interference Device) has been developed for the direct detection of nuclear magnetic resonance (NMR) in zero applied magnetic field and pure nuclear quadrupole resonance (NQR) at low frequencies. The motivation to detect zero field NMR and NQR is to provide a new high resolution spectroscopy technique at frequencies below 200 kHz to study ultra-weak interactions in chemicals and materials . By comparing the sensitivity of a SQUID amplifier with that of a conventional semiconductor amplifier, it is shown that a SQUID amplifier is essential for the direct detection of low frequency resonant signals. The spectrometer has a frequency response extending from about 10 to 200 kHz, and a recovery time (after the magnetic pulse is removed) of about 50 μs. The spectrometer is used to detect NMR spectra from Pt and Cu metal powders in a magnetic field of 6 mtesla, and NQR spectra from ^{2}D in a tunneling methyl group and ^{14}N in NH_4ClO_4. Finally, the zero field NMR spectrum from a quantum tunneling methyl group is calculated.

ACKNOWLEDGMENT

I would like to thank my research advisors Professor John Clarke, Professor Alex Pines and Professor Erwin Hahn for their support, guidance and encouragement. I would also like express my appreciation to F. C. Wellstood for his enormous help during my research. I thank M. D. Hürlimann for collaboration in the ^{14}N NQR experiment and M. B. Heaney for assistance in SQUID fabrication. I wish to express my appreciation to all my colleagues, past and present, in the Clarke group for their help and their friendship.

Finally I gratefully acknowledge the use of the Microelectronics Facility in the Electronics Research Laboratory of the Electrical Engineering and Computer Science Department, U.C.Berkeley. This work was supported by the Director, Office of Energy Research, Office of Basic Energy Sciences, Materials Sciences Division of the U.S. Department of Energy under contract number DE-AC03-76SF00098.

TABLE OF CONTENTS

CHAPTER 1

INTRODUCTION

In this thesis, I describe a spectrometer involving a dc Superconducting QUantum Interference Device [1] (SQUID) for the direct detection of nuclear magnetic resonance[2] (NMR) and nuclear quadrupole resonance [2] (NQR) at frequencies below 200 kHz. The spectrometer is designed to detect three classes of spectra: (i) NMR spectra, which arise from the interaction of a nuclear spin with an external magnetic field, (ii) NQR spectra, which arise from the interaction of the electric quadrupole moment of a nucleus (with spin $I \geq 1$) with the local electric field gradient, and (iii) zero-field NMR (ZFNMR) spectra[3,4], which arise from the interaction of a nuclear spin with the local magnetic field generated by neighboring spins. While the applications of low-frequency NMR are relatively restricted, for example, low-temperature thermometry using Cu or Pt powder,[5] low-frequency NQR and ZFNMR are of considerable interest in chemistry and condensed matter physics. One example is ^{2}D NQR [4], which can be used to obtain information about organic molecules in which protons are selectively replaced by deuterons; ^{5}Be, ^{11}B and ^{14}N also have low NQR frequencies in nearly symmetric environments (for example, ^{14}N in NH_4^+). In the case of ZNMR, the frequency is low because the local magnetic fields are typically below 1 mtesla; for example, water molecules in hydrated crystals have a frequency of about 42 kHz.

The major difficulty in observing resonance signals at a low-frequency f is their small amplitude. At a given temperature, the power coupled to a tuned circuit with quality factor Q is proportional to Qf^3, so that the power available at low frequencies is many orders of magnitude lower than that from high-frequency resonances at (say) 10's of MHz. Because of this difficulty, methods have been devised to detect low-frequency NQR and ZFNMR indirectly. For example, one can derive the quadrupole or dipole-dipole interactions from a high-field NMR spectrum.[6] This technique usually requires a single

crystal; with a powder sample, much of the quadrupole or dipole-dipole information may be lost because of the broadening of the high-field NMR spectrum by powder averaging.[7] An alternative method is magnetic field cycling[3,4,8], which enables one to obtain high resolution NQR and ZFNMR spectra from powder samples. This technique, however, determines the zero-field free induction decay (FID) signal point by point; since only one point is obtained from each field cycling process, the procedure is time-consuming. The technique also requires the sample to have a long longitudinal relaxation time T_1 to ensure the field cycling process is adiabatic. More recently, a third method of observing ZFNMR has been introduced in which the sample is rotated rapidly in a high magnetic field and appropriate sequences of radio frequency (rf) pulses are applied.[9] To our knowledge, this technique has not yet been applied to NQR.

Compared with indirect detection techniques, direct detection of NQR and ZFNMR has several advantages. It allows one to use powder samples, and to obtain the spectra more quickly, since the entire FID signal is obtained in a single measurement. It enables one to implement two-dimensional spectra[10] techniques more easily. However, to detect the low-frequency signal directly, one needs an extremely low-noise amplifier, and the dc SQUID correctly configured, is by far the most sensitive available in the frequency range of interest. Our spectrometer is based on such a SQUID operated in a flux locked loop with an externally triggered recover circuit , a configuration similar to that developed by Friedman *et al.*[11] to study low-frequency NMR (< 50 kHz) in ^{3}He at millikelvin temperatures. However, our requirements are more demanding: the signal power available at liquid ^{4}He temperatures is many orders of magnitude smaller than that at 20 mK. Furthermore, the transverse relaxation time (T_2) in a solid is short, so that the amplifier must recover very quickly from the rf pulse that initiates the FID. In addition, to excite all the resonances over a large bandwidth with a single magnetic pulse, the pulse length must be short and consequently of large amplitude, compounding the difficulties of a short recovery time. A preliminary report of part of this work has been published previously.[12]

Chapter 2 compares the sensitivity of SQUID and conventional Amplifier. Chapter 3 Compares the difference in spectra resolution between the high field NMR spectra and two other kind of spectra: zero field NMR an pure NQR spectra. Chapter 4 describes the spectrometer based on a DC SQUID and presents some experimental results. Finally, Chapter 5 deals with the zero field NMR spectra from a tunneling methyl group.

1. J. Clarke, NATO ASI Series Vol. 59, *Superconductive Electronics*, edited by M.Nisenoff and H. Weinstock (Springer, Berlin, 1989), p.87.

2. A. Abragram, *Principles of Nuclear Magnetic Resonance* (Oxford, London, 1961); C. P. Slichter, *Principle of Magnetic Resonance* , 2nd edition (Spring-Verlag, Berlin, 1980).

3. D. P. Weitekamp, A. Bielecki, D. Zax, K. Zilm, and A. Pines, Phys. Rev. Lett. **43**, 1791 (1979).

4. D. B. Zax, A. Bielecki, K. W. Zilm, A. Pines and D. P. Weitekamp, J. Chem. Phys. **83**, 4877 (1985).

5. D. P. Hudson, H. Morshak, R. J. Soulen, Jr., and D. B. Utton, J. Low Temp. Phys. **20**,1 (1975).

6. A. Abragram, ref.(2), Chap. VII.

7. G. F. Pake, J. Chem. Phys. **16**, 327 (1948).

8. A. Bielecki, D. B. Zax, K. W. Zilm, and A. Pines, Rev. Sci. Instrum. **57**, 393 (1986).

9. R. Tycko, Phys. Rev. Lett. **60**, 2734 (1988).

10. R. R. Ernst, G. Bodenhausen, and A. Wokaun, *Principle of Nuclear Magnetic Resonance in one and two dimensions* (Oxford, New York, 1987).

11. L. J. Friedman, A. K. M. Wennberg, S. N. Ytterboe, and H. M. Bozler, Rev. Sci. Instrum. **57**,410 (1986).

12. N. Q. Fan, M. B. Heaney, J. Clarke, D. Newitt, L. Wald, E. L. Hahn, A. Bielecke, and A. Pines, IEEE Trans. **MAG-25**, 1193 (1989).

CHAPTER 2

COMPARING SENSITIVITY OF SQUID AND CONVENTIONAL AMPLIFIER

Sensitive SQUID preamplifiers have been developed in a wide frequency range: from magnetometers that operate down to zero frequency to rf amplifiers that operate up to 300 MHz[1]. These sensitive amplifiers have many applications, for example, they can be used as preamplifiers in NMR and NQR spectrometers[2,3]. It is natural, therefore, to ask how much improvement in sensitivity one can achieve by replacing the conventional preamplifier in a NMR system with a SQUID preamplifier. To answer this question, we need to find a figure of merit that can be used to compare these two different classes of amplifiers. One such a figure of merit is the noise temperature of an amplifier , which is defined in Sec. I. In that section, I discuss and compare the noise temperatures of SQUID and conventional amplifiers. In Sec. II, to find out what is the smallest NMR signal one can detect with or without SQUID amplifiers, I calculate the signal to noise ratio in four detection schemas: 1) a tuned circuit with a conventional amplifier, 2) an untuned circuit with a conventional amplifier, 3) a tuned circuit with a SQUID amplifier and 4) an untuned circuit with a SQUID amplifier. By comparing the signal to noise ratios of these circuits, in Sec. III, I conclude this Chapter with the answers to the question as whether a SQUID amplifier should be used, whether a tuned circuit should be used, and more specifically why a SQUID amplifier has to be used to detect directly ZFNMR and low frequency NQR.

I. Noise Temperature of SQUID and Conventional Amplifier

In this section, I first introduce the concept of noise density; then I discuss the noise temperature of conventional amplifiers and SQUID amplifiers; finally, I compare the noise temperatures of conventional and SQUID amplifiers.

A. Noise density

I introduce the concept of *voltage noise density* and *current noise density* with a specific example: the Johnson noise from a resistor. Fig. 1(a) shows a resistor with resistance R at temperature T; the resistor is in an open circuit. Because the electric carriers in the resistor undergo thermal fluctuations, there is a random voltage V_N across the resistor. This noise is the Johnson noise. The time average of V_N is zero, $< V_N > = 0$. If the voltage is measured within a bandwidth B, the time average of the square of V_N is proportional to the observation bandwidth, $< V_N^2 > = S_V B$; the proportional constant S_V is the *voltage noise density*. The voltage noise density due to Johnson noise is given by Nyquist formula,

$$S_V = 4k_B T R. \qquad (2.1)$$

Fig. 1(b) shows the resistor in a closed circuit; the current noise I_N due to the Johnson noise is measured within a bandwidth B. The time average of I_N is zero, $< I_N > = 0$. The time average of I_N^2 is proportional to the observation bandwidth, $< I_N^2 > = S_I B$; the proportional constant S_I is the *current noise density*. The current noise density due to the Johnson noise is given by formula

$$S_V = 4k_B T/R. \qquad (2.2)$$

The concept of noise density can be extended to the case that the noise is not white, where $< V_N^2 >$ and $< I_N^2 >$ are not directly proportional to the observation bandwidth. In general, if the voltage noise density is measured from frequency f_1 to f_2, the time average of V_N^2 is given by

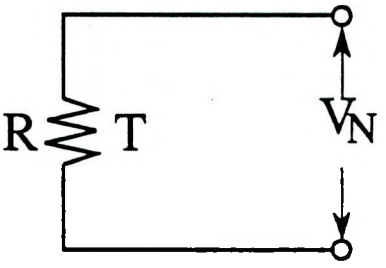

(a)

$$< V_N^2 > = (4\, k_B\, TR)B$$

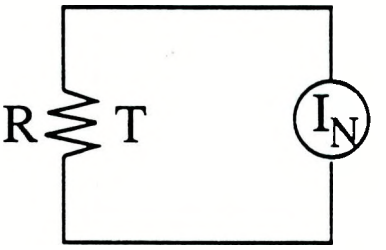

(b)

$$< I_N^2 > = (4\, k_B\, T/R)B$$

XBL 9010-4754

Fig. 2.1 (a) Voltage noise and (b) current noise from resistor R at temperature T.

$$< V_N^2 > = \int_{f_1}^{f_2} S_V(f)\, df, \tag{2.3}$$

where the voltage noise density $S_V(f)$ is a function of frequency. If the observation bandwidth $\Delta B = f_2 - f_1$ is small so that $S_V(f)$ is approximately a constant, the time average of V_N^2 is again directly proportional to the observation bandwidth,

$$< V_N^2 > = S_V(f)\, \Delta B. \tag{2.4}$$

The voltage noise density is defined formally by the Fourier transform of the correlation function $\overline{V_N(0)\, V_N(\tau)}$,

$$S_V(f) = \frac{1}{2\pi} \int_{-\infty}^{+\infty} \overline{V_N(0)\, V_N(\tau)} \exp(j2\pi f\tau)\, d\tau. \tag{2.5}$$

The correlation function $\overline{V_N(0)\, V_N(\tau)}$ is the ensemble average of the product of $V_N(0)$ and $V_N(\tau)$, the voltage noises at time $t = 0$ and at time $t = \tau$, respectively.

Similarly, the current noise density is defined by

$$S_I(f) = \frac{1}{2\pi} \int_{-\infty}^{+\infty} \overline{I_N(0)\, I_N(\tau)}\ \exp(j2\pi f\tau)\, d\tau, \tag{2.6}$$

and the correlation noise density of the voltage and current by

$$S_{VI}(f) = \frac{1}{2\pi} \int_{-\infty}^{+\infty} \overline{V_N(0)\, I_N(\tau)}\ \exp(j2\pi f\tau)\, d\tau. \tag{2.7}$$

Again, if the observation bandwidth ΔB is small,

$$< I_N^2 > = S_I(f)\, \Delta B, \tag{2.8}$$

$$<V_N\, I_N> = S_{VI}(f)\Delta B. \tag{2.9}$$

In the rest of this thesis, I will constantly use ΔB to represent an observation bandwidth within which all the noise densities are constants.

Finally, the random noise processes discussed through out this thesis are both *stationary* and *ergotic*. In a *stationary* process, the ensemble average of a variable A at time t, $\overline{A(t)}$, is equal to the assemble average of the variable at time t+τ, $\overline{A(t+\tau)}$; for example, $\overline{V_N(0)\, V_N(\tau)} = \overline{V_N(t)\, V_N(t+\tau)}$. In an *ergotic.* process the ensemble average of a variable A, $\bar{A}$, is equal to its time average, <A>; for example, $\overline{V_N(t)\, V_N(t)} = \langle V_N^2(t) \rangle$.

B. Noise temperature of conventional amplifier

(a) Definition of noise temperature

Fig. 2.2 shows a circuit in which a resistor with resistance R is connected to the input of an ideal voltage amplifier. The resistor is at temperature T, and the ideal voltage amplifier has an infinite input impedance. The noise properties of an amplifier can be modeled by two independent noise sources as shown in the figure: a voltage noise source (with zero input impedance) which generates a random voltage V_N with $< V_N^2 >$ determined by the voltage noise density of the amplifier S_V, $< V_N^2 > = S_V \Delta B$, and a current noise source which generates a random current I_N with $< I_N^2 >$determined by the current noise density of the amplifier S_I, $< I_N^2 > = I_N \Delta B$. The time average of the square of the total noise voltage $V_{N\Sigma}$ at the input of the amplifier is

$$< V_{N\Sigma}^2 > = 4k_B T R_S \Delta B + S_V \Delta B + S_I R_S^2 \Delta B. \qquad (2.10)$$

The first term is due to the Johnson noise from the resistor, the second term is due to the voltage noise of the amplifier, and the last term is due to the current noise of the amplifier (the current noise injects into the resistor and generates a voltage noise across the resistor). The total voltage noise is higher than the Johnson noise from the resistor R_S at temperature T, but it is equal to the Johnson noise from the resistor at a higher temperature $T + T_N$, that is

$$< V_{N\Sigma}^2 > = 4k_B(T + T_N)R_S \Delta B, \qquad (2.11)$$

where T_N is defined as the noise temperature of the amplifier. Using Eq. 2.10 and Eq. 2.11, we find

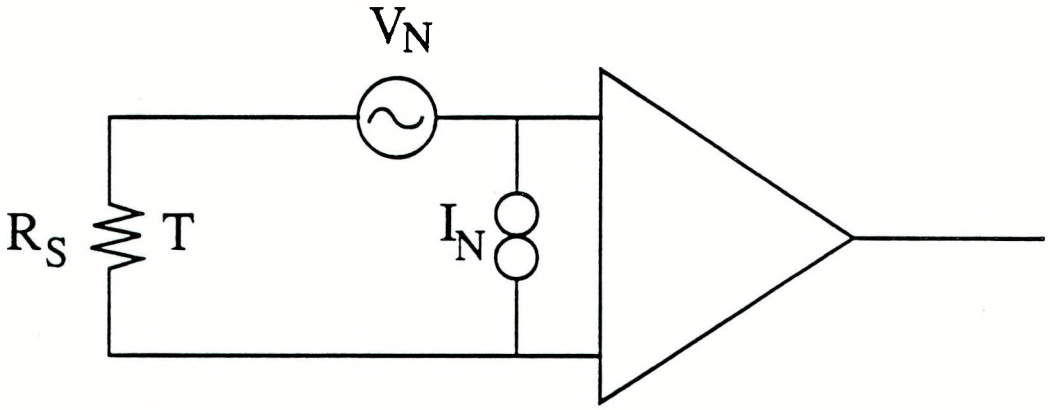

Fig. 2.2 Resistor R_S connected to input of amplifier modeled by voltage noise source V_N and current noise source I_N.

$$4k_B T_N R_S = S_V + S_I R_S^2, \tag{2.12}$$

or

$$T_N = \frac{S_V + S_I R_S^2}{4k_B R_S}. \tag{2.13}$$

The noise temperature T_N, which clearly depends on the source impedance R_S, is optimized if the optimization condition, $\partial T_N / \partial R_S = 0$, is satisfied. The minimal noise temperature is

$$T_N^0 = (S_V S_I)^{1/2} / 2k_B, \tag{2.14}$$

and the optimization condition can be written as

$$R_S = R_N = (S_V / S_I)^{1/2}, \tag{2.15}$$

where R_N is defined as the noise impedance.

In most cases, the source impedance R_S is not equal to the noise impedance R_N and the noise temperature is not optimized. But the noise temperature can be optimized by matching the source impedance with the noise impedance; this can be achieved by using either a transformer or a tuned circuit. Figure. 2.3(a) shows a source resistor connecting to an amplifier via a transformer; Fig. 2.3(b) shows that via a tuned circuit. The transformer has a turns ratio N; the tuned circuit has a quality factor Q. The impedance at the input of the amplifier is $Z = N^2 R_S$ for the case with a transformer, and $Q = N^2 R_S$ for the case with a tuned circuit. The noise temperature of the amplifier in both cases are given by the same equation,

$$T_N = \frac{S_V + S_I Z^2}{4k_B Z}. \tag{2.16}$$

The noise temperature is optimized if the optimization condition $Z = R_N$ is satisfied, and the minimal noise temperature T_N^0 is reached, $T_N^0 = (S_V S_I)^{1/2} / 2k_B$. Therefore, in the case $R_S \neq R_N$, the noise temperature can be minimized by using either a tansformer with a turns ratio $N = \sqrt{R_N / R_S}$, or a tuned circuit with a quality factor $Q = \sqrt{R_N / R_S}$. Because the amplifier is an ideal voltage amplifier, the minimal noise temperature of an untuned amplifier is equal to that of a tuned amplifier.

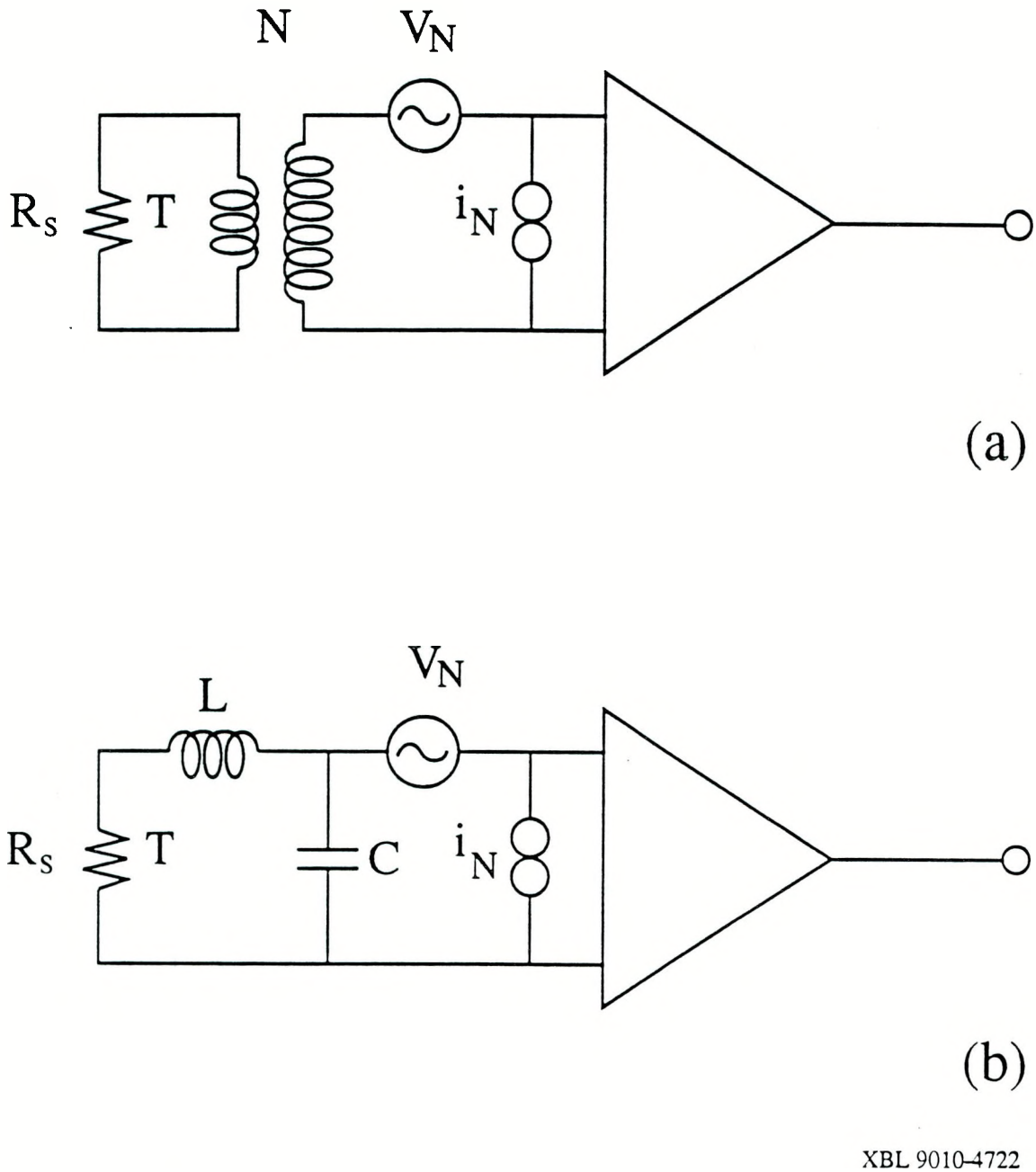

Fig. 2.3 Resistor R_S connected to input of amplifier (a) via transformer, and (b) via tuned circuit.

b) Noise figure and noise number

Other parametersare are also used sometimes to characterize the sensitivity of an amplifier, for example, noise figure and noise number. Noise figure (NF), in units of decibels (dB), is defined by the equation

$$NF = 10\,lg_{10}[\,1+\frac{S_V + S_I R_s^2}{4k_B T_R R_s}\,] \quad (dB), \tag{2.17}$$

where $T_R = 295$ K. The noise figure is related to the noise temperature by

$$NF = 10\,lg_{10}[\,1+ (T_N/T_R)\,] \quad (dB). \tag{2.18}$$

In the limit $T_N << T_R$,

$$T_N \approx 69\,\frac{NF}{(dB)} \quad (K). \tag{2.19}$$

Figure 2.4 shows the noise contours -- noise figures as functions of the input impedance and signal frequency -- of an amplifier, PAR 113. Table 2.1 lists some converting factors between the noise figure and noise temperature. The minimal noise temperature of the amplifier, PAR 113, is about 3 K.

Like noise figure, noise number is also related to the noise temperature; it is defined by [4]

$$n_N = \frac{1}{\exp(\hbar\omega/k_B T_N) - 1}\,, \tag{2.20}$$

which in the $k_B T_N >> \hbar\omega$, reducers to

$$n_N \approx \frac{k_B T_N}{\hbar\omega}\,. \tag{2.21}$$

Here, n_N is the average number of photons (with energy $\hbar\omega$) fluctuating in the circuit [5]. The noise power P_N within a bandwidth ΔB is deterimined by n_N,

$$P_N = n_N \hbar\omega \Delta B. \tag{2.22}$$

Finally, the most sensitive linear phase conserve amplifier is the quantum limited amplifier; its sensitivity is only limited by the Heisenbeg uncertainty principle. The noise number of the quantum limited amplifier is

$$n_N^Q = 1; \tag{2.23}$$

correspondingly, the noise temperature of the quantum limited amplifier is

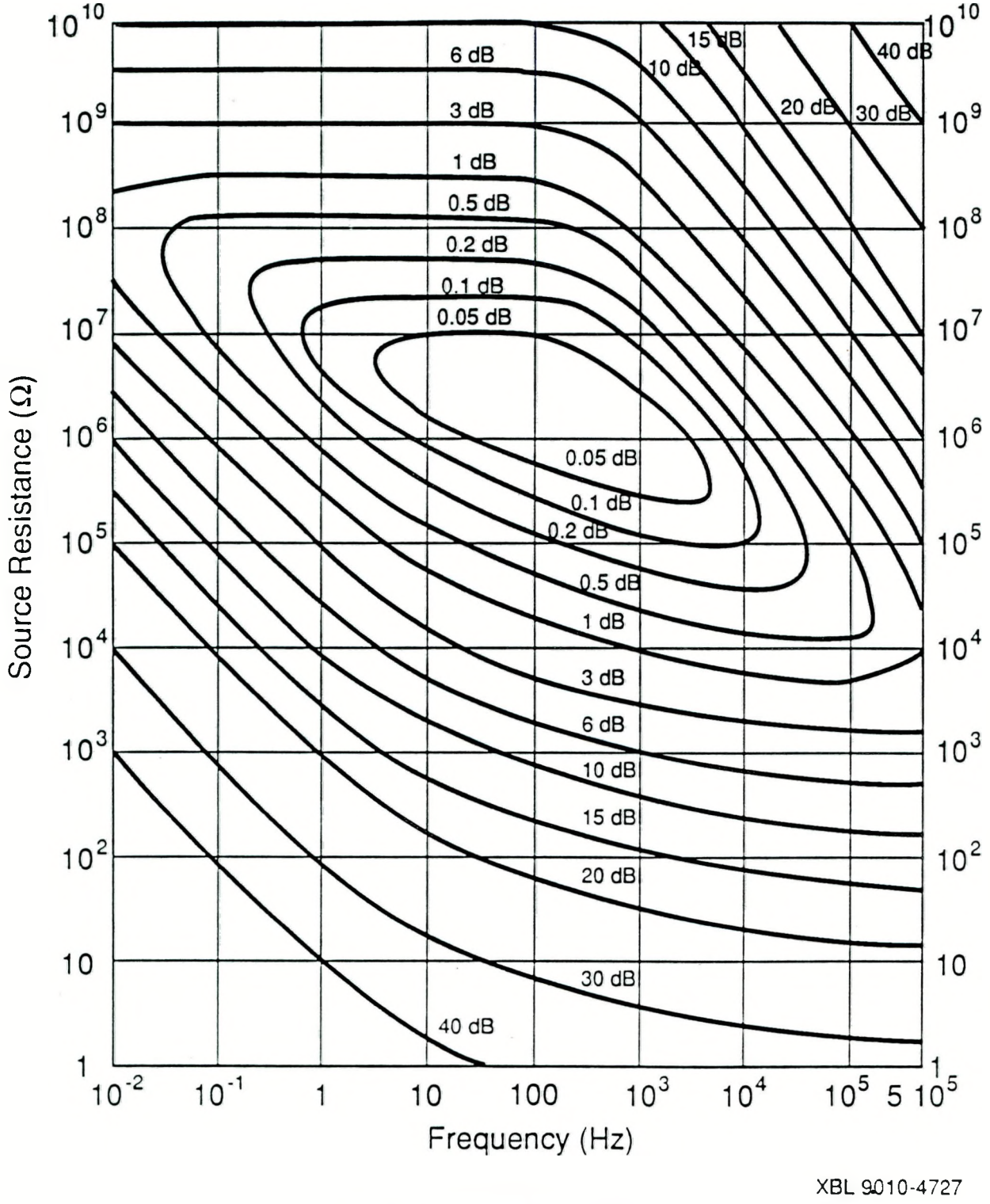

Fig. 2.4 Noise contour of PAR-113.

N. F. (dB)	T_N(K)
0.05	3.4
0.1	6.9
0.2	13.9
0.5	36.0

Table 2.1Converting factors between noise figure and noise temperature.

$$T_N^Q = \frac{\hbar\omega}{k_B \ln 2} \cdot \tag{2.24}$$

Since the quntum limited amplifier has $n_N = 1$, the noise number characterizes how may times less sensitive an amplifier is compared with the quantum limited amplifier.

C. Noise temperature of SQUID amplifier

a) Principle of DC SQUID

A clear and complete discussion of DC SQUIDs can be found in Ref. 1. Before discussing the noise temperatures of SQUID amplifiers, I only summarize some major properties of DC SQUIDs. As shown in Fig. 2.5(a), a DC SQUID consists of a superconducting ring with self inductance L and two Josephson junctions. Each junction has a critical current I_0 and is shunted with a resistor of resistance R. The I - V characteristic of a SQUID depends on the amount of the flux Φ in the superconducting loop; the I – V curves with $\Phi = n\,\Phi_0$ and $\Phi = (n + 1/2)\Phi_0$ are shown in Fig. 2.5(b). When the SQUID is biased properly with a constant current I_b as shown in Fig. 2.5(b), the voltage across the SQUID is a periodic function of Φ. The V– Φ curve is shown in Fig. 2.5(c). Assuming the flux in the loop is biased at a constant flux Φ_b, any changes of flux $\Delta\Phi << \Phi_0$ will induce a change of the voltage across the SQUID ΔV, and the ratio is

$$\frac{\Delta V}{\Delta \Phi} = \left(\frac{\partial V}{\partial \Phi}\right)_{I = I_b} = V_\Phi, \tag{2.25}$$

where V_Φ is the transfer coefficient . Thus, a SQUID is simply a flux to voltage transducer. As an example, at the bottom of Fig. 2.5(c), we show a sinusoidal flux signal with peak to peak value Φ_{pp} as a function of time; at the left side we show the induced voltage signal as a function of time. The peak to peak value V_{pp} is determined by the transfer coefficient V_Φ,

$$V_{pp} = V_\Phi\, \Phi_{pp}. \tag{2.26}$$

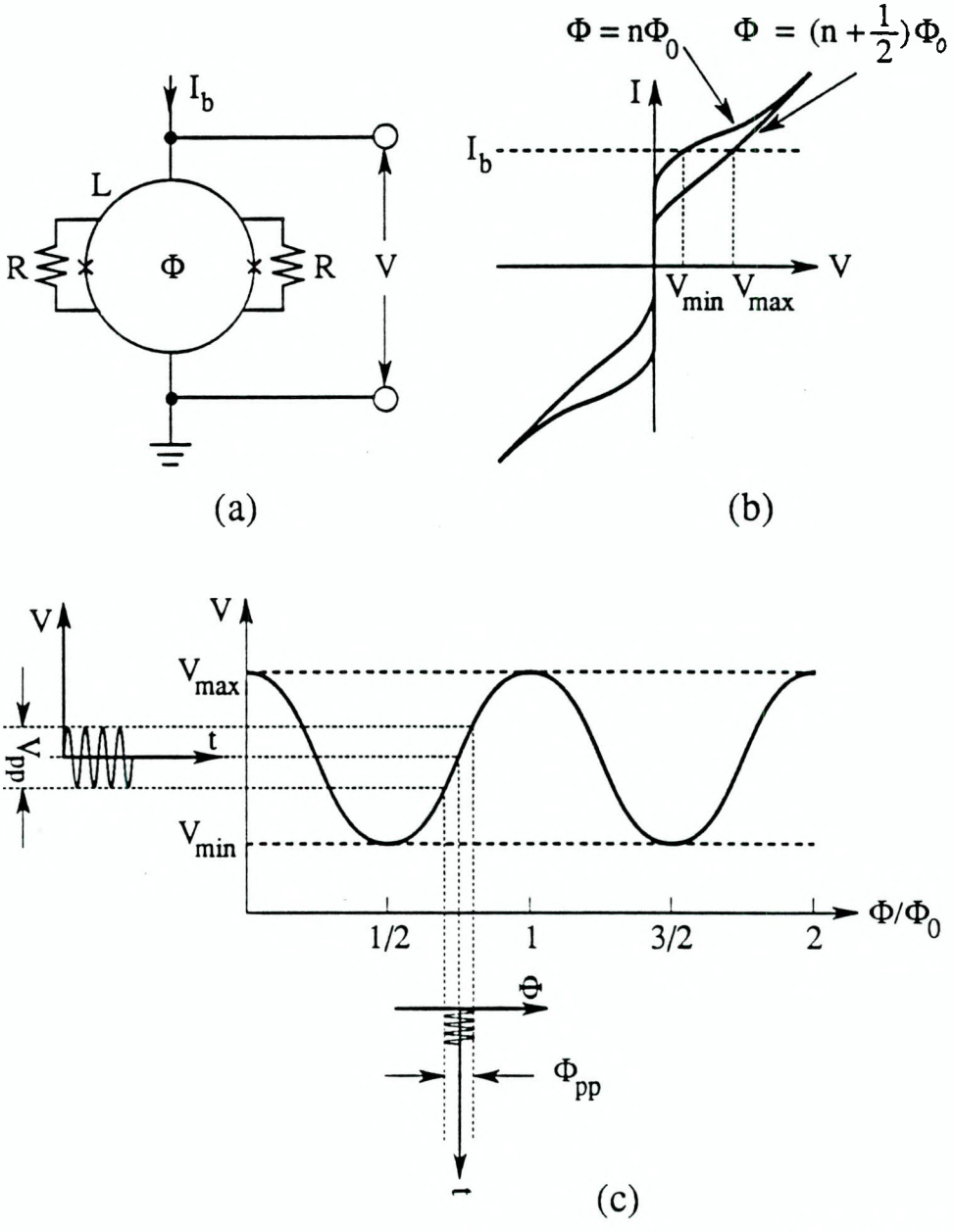

Fig. 2.5 (a) Schematic, (b) I *vs.* V curves, and (c) V*vs.* Φ curve of SQUID, showing input signal converted to voltage signal across SQUID.

b) Noise temperature of SQUID amplifier

The noise properties [6] of a bare SQUID can be characterized by the noise density of the flux in the SQUID loop S_Φ, the noise density of the circulating current in the loop S_J, and the correlation noise density between the flux and the circulating current $S_{\Phi J}$*. The time average of the square of the flux noise $< \Phi_N^2 >$ and of the circulating noise $< J_N^2 >$, and the time average of the product of the flux and the current $<\Phi_N J_N>$ are determined by the equations

$$< \Phi_N^2 > = S_\Phi \Delta B, \tag{2.27}$$

$$< J_N^2 > = S_J \Delta B, \tag{2.28}$$

$$<\Phi_N J_N> = S_{\Phi J} \Delta B . \tag{2.29}$$

For a SQUID of optimized performance, S_Φ, $L^2 S_J$ and $L S_{\Phi J}$ are comparable in amplitude.

In almost all applications, signals are coupled into a SQUID via an input coil. As shown in Fig. 2.6, the self inductance of the input coil is L_i, the self inductance of the SQUID is L, and the mutual inductance between the pick up coil and the SQUID is M. The mutual inductance M is related to L_i and L by $M^2 = \alpha^2 L_i L$, where α^2 is the coupling coefficient ; the impedance connected to the input coil is $R_s + jY$. In general, the dynamic properties (e.g. V_Φ) and the noise properties (e.g. S_Φ, S_J and $S_{\Phi J}$) of a SQUID are influenced by the presence of the input coil and circuit. But one can neglect the influence of the input coil and the circuit in the limit that the coupling coefficient $\alpha^2 << 1$; in this approximation, V_Φ, S_Φ, S_J and $S_{\Phi J}$ are constants.

Because of the input circuit, the total flux noise in the SQUID loop $\Phi_{N\Sigma}$ is the sum of the noise from three sources [7]: the flux noise of a bare SQUID Φ_N, the flux noise induced

---

* As a convention, most authors use parameters S_V, S_J and S_{VJ} to characterize a SQUID. These parameters are related to the parameters used in my thesis by the relations: $S_V = V_\Phi^2 S_\Phi$, $S_J = S_J$ and $S_{VJ} = V_\Phi S_{\Phi J}$. These two sets of parameters are completely equivalent.

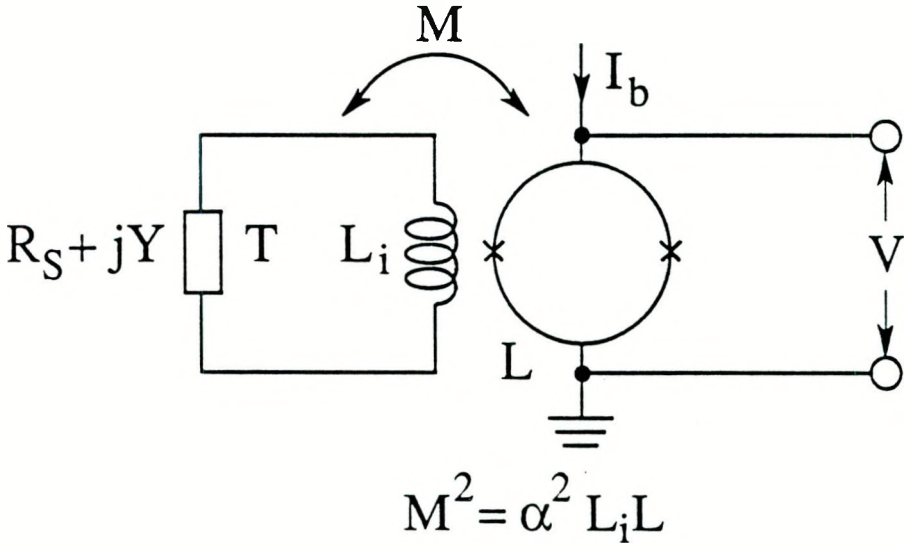

Fig 2.6 Source impedance R_s + Y connected to input coil L_i of SQUID.

by the circulating current noise J_N, and the flux noise induced by the Johnson noise from the disspative elements R_S in the input circuit Φ_{NJ}, that is:

$$\Phi_{N\Sigma} = \Phi_N - \frac{\omega^2 M^2 J_N}{R_S + j(Y+\omega L_i)} + \Phi_{NJ}. \tag{2.30}$$

The time average of the square of the total flux noise is

$$< \Phi_{N\Sigma}^2 > = < \Phi_N^2 > - 2\omega M^2 <\Phi_N J_N> \mathrm{Im}\left(\frac{1}{R_S + j(Y+\omega L_i)}\right) + \left|\frac{\omega^2 M^2 J_N}{R_S + j(Y+\omega L_i)}\right|^2 < J_N^2 > + < \Phi_{NR}^2 >, \tag{2.31}$$

where $< \Phi_N^2 >$, $< J_N^2 >$ and $<\Phi_N J_N>$ are given by Eqs. 2.27, 2.28 and 2.29 respectively, and the noise due to the Johson noise $< \Phi_{NJ}^2 >$ is given by

$$< \Phi_{NJ}^2 > = \frac{4k_B T R_S M^2}{R_S^2 + (Y+\omega L_i)^2} \Delta B. \tag{2.32}$$

Substituting Eqs. 2.27, 2.28, 2.29 and 2.32 into Eq. 2.31, we have

$$< \Phi_{N\Sigma}^2 > = \frac{1}{R_S^2 + (Y+\omega L_i)^2} [\, R_S^2 S_\Phi + (\omega L_i)^2 \tilde{S}_\Phi + 4k_B T R_S M^2] \Delta B, \tag{2.33}$$

where

$$\tilde{S}_\Phi = S_\Phi (1 + Y/\omega L_i)^2 + 2\alpha^2 L S_{\Phi J} (1 + Y/\omega L_i) + \alpha^4 L^2 S_J. \tag{2.34}$$

If we imagine that the total flux noise are induced entirely by the Johnson noise from R_S at a temperature $T+T_N$, then,

$$< \Phi_{N\Sigma}^2 > = \frac{4k_B (T_N+T) R_S M^2}{R_S^2 + (1 + Y/\omega L_i)^2} \Delta B, \tag{2.35}$$

where T_N is the noise temperature of the SQUID amplifier. Comparing Eq. 2.33 and Eq. 2.35, we have the noise temperature given by

$$T_N = \frac{R_S^2 S_\Phi + (\omega L_i)^2 \tilde{S}_\Phi}{4k_B R_S M^2}. \tag{2.36}$$

Since a function $y = ax + b/x$ reaches a minimum $y_{min} = 2(ab)^{1/2}$ when $x = (a/b)^{1/2}$, then the noise temperature reaches a minimum, T_{Nmin}, when

$$R_S = \omega L_i (\tilde{S}_\Phi / S_\Phi)^{1/2}, \tag{2.37}$$

and the minimum noise temperature is given by

$$T_{Nmin} = \frac{\omega(\tilde{S}_\Phi S_\Phi)^{1/2}}{2k_B\alpha^2 L} \quad . \tag{2.38}$$

The minimum noise temperature still depends on the value of Y. In the following I will discuss the minimum noise temperature T_{Nmin} in three situations : T_{Nmin} of an untuned amplifier (Y= 0), T_{Nmin} of a tuned amplifier at the resonant frequency ($Y+ \omega L_i = 0$), and the absolute minimum noise temperature of a tuned amplifier T_N^0, which is obtained by optimizing T_{Nmin} further with respect to Y ($\partial T_{Nmin}/\partial Y = 0$).

(1) Minimum noise temperature of an untuned amplifier (Y= 0) [7]

Substituting Y =0 into Eq. 2.38 and Eq. 2.34, we have the optimization condition of an untuned amplifier,

$$R_S = \omega L_i \left(\frac{S_\Phi + 2\alpha^2 L S_{\Phi J} + \alpha^4 L^2 S_J}{S_\Phi} \right)^{1/2} , \tag{2.39}$$

and minimum noise termperature

$$T_N^{un} = \frac{\omega[S_\Phi(S_\Phi + 2\alpha^2 L S_{\Phi J} + \alpha^4 L^2 S_J)]^{1/2}}{2k_B\alpha^2 L} \quad . \tag{2.40}$$

In terms of the energy sensitivity of a SQUID,

$$\varepsilon = \frac{S_\Phi}{2L} , \tag{2.41}$$

the minimal noise temperature of an untuned amplifier is given by

$$T_N^{un} = \frac{\omega\varepsilon}{k_B\alpha^2}(1 + 2\alpha^2 L S_{\Phi J}/S_\Phi + \alpha^4 L^2 S_J/S_\Phi)^{1/2} \quad . \tag{2.42}$$

In the limit $\alpha^2 << 1$,

$$T_N^{un} \approx \frac{\omega\varepsilon}{k_B\alpha^2} , \tag{2.43}$$

and the optimization condition is

$$R_S \approx \omega L_i . \tag{2.44}$$

(2) Minimum noise temperature of a tuned amplifier on resonance ($Y+ \omega L_i = 0$)[8]

The minimal noise temperature T_{Nmin} is a function of Y, and in general Y is a function of frequency. At the resonant frequency of a tuned amplifier, the imaginary part of the total impedance is zero, that is, $Y+ \omega L_i = 0$. Substituting $1+ Y/L_i = 0$ into Eq. 2.34, we have

$$\tilde{S}_\Phi = \alpha^4 L^2 S_J . \tag{2.45}$$

The minimum noise temperature at the resonant frequency, Eq. 2.38, becomes

$$T_N^{res} = \frac{\omega}{2k_B} (S_J S_\Phi)^{1/2}, \tag{2.46}$$

and the optimization condition becomes

$$R_S = \omega L_i (\alpha^4 L^2 S_J / S_\Phi)^{1/2}. \tag{2.47}$$

(3) Absolute minimum noise temperature of a SQUID amplifier ($\partial T_{Nmin} / \partial Y = 0$)[7]

In the two cases discussed above ($Y= 0$ and $Y+ \omega L_i = 0$), the minimum noise temperature is not optimized with respect to Y. Instead of setting $Y=0$ or setting $Y= - \omega L_i$, the T_{Nmin} can be optimized further by minimizing $\tilde{S}_\Phi$ with respect to Y. Since $\tilde{S}_\Phi$ has the functional form $\tilde{S}_\Phi = ax^2+2bx +c$ ($a = S_\Phi$, $b = \alpha^2 L S_{\Phi J}$, $c = \alpha^4 L^2 S_J$, and $x= 1+Y/\omega L_i$), it has a minimum $\tilde{S}_\Phi^0 = c - b^2/a$, when the optimization condition $x= - b/a$ is satisfied. Therefore, if

$$1+ Y/L_i = -\alpha^2 L S_{\Phi J}/S_\Phi, \tag{2.48}$$

$\tilde{S}_\Phi$ reaches the absolute minimum $\tilde{S}_\Phi^0$:

$$\tilde{S}_\Phi^0 = \alpha^4 L^2 \frac{S_J S_\Phi - S_{\Phi J}^2}{S_\Phi}. \tag{2.49}$$

The optimization condition (Eq. 2.37) becomes

$$R_S = \omega L_i \frac{\alpha^2 L (S_J S_\Phi - S_{\Phi J}^2)^{1/2}}{S_\Phi}, \tag{2.50}$$

and the minimum noise temperature (Eq. 2.38) becomes

$$T_N^0 = \frac{\omega}{2k_B}(S_J S_\Phi - S_{\Phi J}^2)^{1/2}, \tag{2.51}$$

where T_N^0 is the absolute minimum noise temperature of an amplifier based on a DC SQUID. Substituting $Y = -1/\omega C$ into Eq. 48, we have,

$$\omega = \frac{\omega_0}{(1+ \alpha^2 L S_{\Phi J}/S_\Phi)^{1/2}}, \tag{2.52}$$

where ω_0 is the resonant frequency of the circuit. Equation 2.52 indicates that the lowest noise temperature occurs off resonance.

D. Comparing noise temperatures of SQUID and conventional amplifiers

The noise densities of a DC SQUID --S_Φ, S_J and $S_{\Phi J}$ -- can be expressed in terms of dimensionless constants γ_Φ, γ_J and $\gamma_{\Phi J}$,

$$S_\Phi = 2k_B T \gamma_\Phi L^2/R, \tag{2.53}$$

$$L^2 S_J = 2k_B T \gamma_J L^2/R, \tag{2.54}$$

$$L S_{\Phi J} = 2k_B T \gamma_{\Phi J} L^2/R, \tag{2.55}$$

where L is the inductance of the SQUID and R is the shunt resistance of each junction. In terms of the dimensionless, the minimum noise temperature (Eq. 2.38 and Eq. 2.34) becomes,

$$T_{Nmin} = \frac{\gamma_\Phi}{\alpha^2}[(1+ Y/\omega L_i)^2 + 2\alpha^2 (\gamma_{\Phi J}/\gamma_\Phi)(1+ Y/\omega L_i) + \alpha^4(\gamma_J/\gamma_\Phi)]^{1/2} \frac{\omega}{\omega^0} T, \tag{2.56}$$

and those T_{Nmin} with special values of Y become

$$T_N^{un} = \frac{1}{\alpha^2}[\gamma_\Phi(\gamma_\Phi + 2\alpha^2 \gamma_{\Phi J} + \alpha^4 \gamma_J)]^{1/2} \frac{\omega}{\omega^0} T, \qquad (Y = 0) \tag{2.57}$$

$$T_N^{res} = (\gamma_\Phi \gamma_J)^{1/2} \frac{\omega}{\omega^0} T, \qquad (1+ Y/\omega L_i = 0) \tag{2.58}$$

$$T_N^0 = (\gamma_\Phi \gamma_J - \gamma_{\Phi J}^2)^{1/2} \frac{\omega}{\omega^0} T, \qquad (1+ Y/\omega L_i = -\alpha^2 \gamma_{\Phi J}/\gamma_\Phi) \tag{2.59}$$

where $\omega^0 = R/L$ is a characteristic frequency of the SQUID (see also Eq. 2.42, Eq. 2.46 and Eq. 2.51). For a SQUID with L = 0.4 nH and R = 6 Ω , $f^0 = \omega^0/2\pi = R/2\pi L = 2.4$ GHz.

Based on the numerical calculation by C. D. Tesche and J. Clarke, if a DC SQUID has parameters $\beta = 2I_0L/\Phi_0 = 1$ and is moderately noise rounded($2\pi k_BT/I_0\Phi_0 = 0.05$), γ_Φ, γ_J and $\gamma_{\Phi J}$ have following values [9],

$$\gamma_\Phi = 8, \tag{2.60}$$

$$\gamma_J = 5.5, \tag{2.61}$$

$$\gamma_{\Phi J} = 6. \tag{2.62}$$

Substituting these values into Eq. 2.56, we have

$$T_{Nmin} = \frac{8}{\alpha^2}[(1+ Y/\omega L_i)^2 + 1.5\,\alpha^2(1+ Y/\omega L_i) + 0.7\,\alpha^4]^{1/2}\frac{\omega}{\omega^0}T. \tag{2.63}$$

In Fig. 2.7, we plotted T_{Nmin}, in units of $(\omega/\omega^0)T$, as a function of Y with $\alpha^2=1$, $\alpha^2=0.5$ and $\alpha^2=0.2$. Those T_{Nmin} with special values of Y are given by

$$T_N^{un} = \frac{8}{\alpha^2}(1+ 1.5\,\alpha^2 + 0.7\,\alpha^4)^{1/2}\frac{\omega}{\omega^0}T, \quad (Y = 0) \tag{2.64}$$

$$T_N^{res} = 6.6\frac{\omega}{\omega^0}T, \qquad (1+ Y/\omega L_i = 0) \tag{2.65}$$

$$T_N^0 = 2.8\frac{\omega}{\omega^0}T. \qquad (1+ Y/\omega L_i = -0.75\alpha^2) \tag{2.66}$$

(see also Eq. 2.57, Eq. 2.58 and Eq. 2.59).

Here only T_N^{un} depends on α^2:

$$\text{for } \alpha^2 = 1.0,\ T_N^{un} = 14\frac{\omega}{\omega^0}T; \tag{2.67}$$

$$\text{for } \alpha^2 = 0.5,\ T_N^{un} = 22\frac{\omega}{\omega^0}T; \tag{2.68}$$

$$\text{for } \alpha^2 = 0.2,\ T_N^{un} = 46\frac{\omega}{\omega^0}T. \tag{2.69}$$

We note that for $\alpha^2 << 1$, $T_N^{un} \propto 1/\alpha^2$, so that it is important for an untuned amplifier to have a tight coupling coefficient, but it is not important for an tuned amplifier.

The minimum noise temperatures are linearly proportional to the signal frequency and the bath temperature. The varies minimum noise temperature (T_N^{un}, T_N^{res} and T_N^0) as a function of frequency f, at T =4.2K for the SQUID with L = 0.4 nH and R = 8 Ω and α^2 = 0.5, are given by following equations

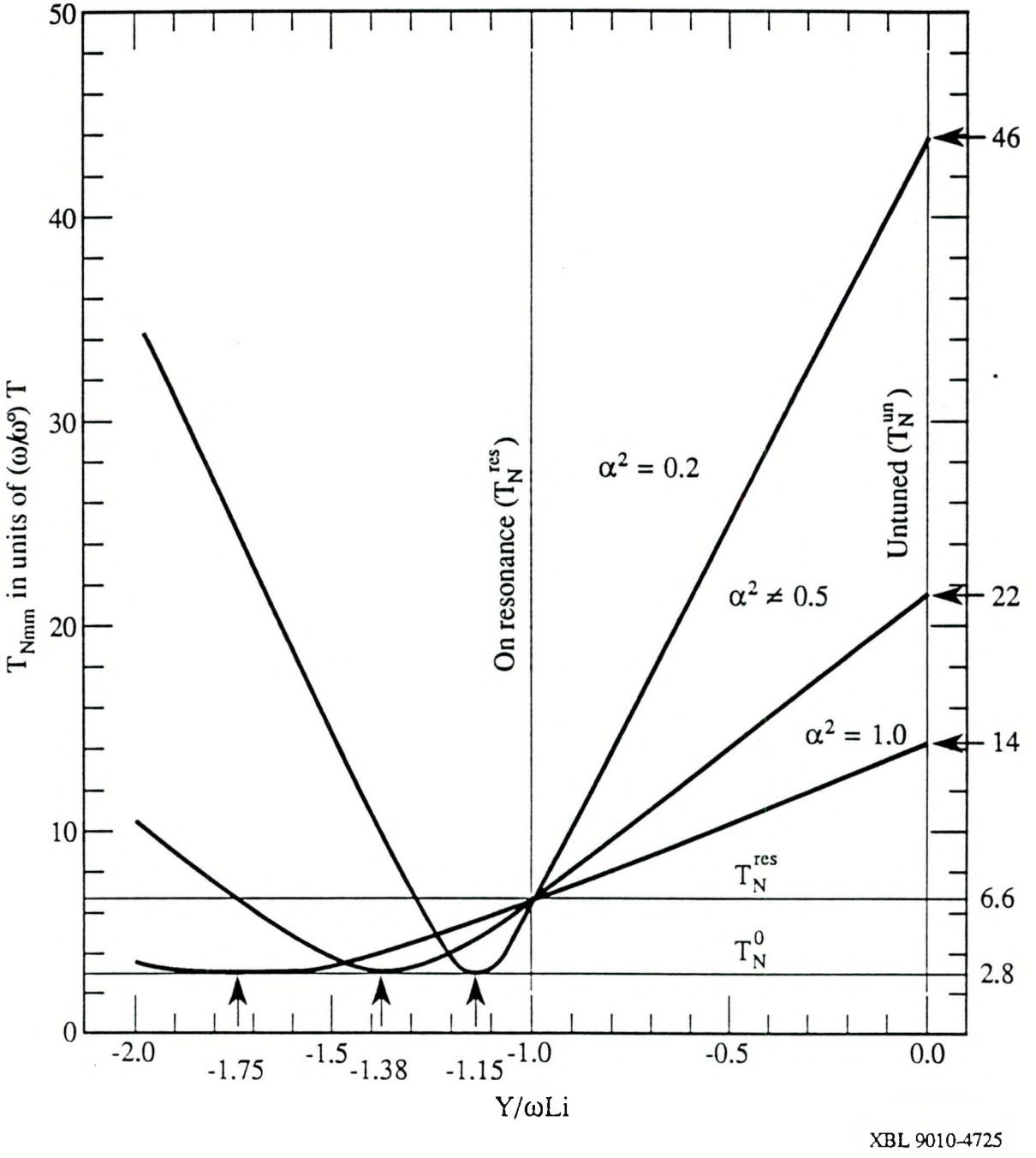

Fig. 2.7 Minimum noise temperature T_{Nmin} as function of Y.

$$T_N^{un} = 22\frac{\omega}{\omega^0}T = 39K(\frac{f}{GHz}) = 39mK(\frac{f}{MHz}) = 39\mu K(\frac{f}{kHz}), \quad (2.70)$$

$$T_N^{res} = 6.6\frac{\omega}{\omega^0}T = 12K(\frac{f}{GHz}) = 12mK(\frac{f}{MHz}) = 12\mu K(\frac{f}{kHz}), \quad (2.71)$$

$$T_N^{0} = 2.8\frac{\omega}{\omega^0}T = 4.9K(\frac{f}{GHz}) = 4.9mK(\frac{f}{MHz}) = 4.9\mu K(\frac{f}{kHz}), \quad (2.72)$$

and are plotted in Fig. 2.8. As a comparison, the noise temperature of the quantum limited amplifier is also plotted in the figure with a shadowed line.

C. Hillbert and J. Clarke [8] measured the noise temperatures of this kind of SQUID at 100 MHz and 4.2 K, and found $T_N^{un} = 3.8 \pm 0.9K$ and $T_N^{res} = 1.7 \pm 0.5K$; both of these data points are plotted in the Fig. 2.8.

To compare the noise temperatures of these SQUID amplifiers with that of conventional amplifiers, we plotted the noise temperature of PAR 113 as a function of frequency. P. Styles et. al.[9]achieved a noise temperature of 7 K with a GaAs FET operated at 45 MHz and at 4.2 K, which is also plotted in Fig. 2.8.

From Fig. 2.8, it is easy to conclude that SQUID amplifiers have a much lower noise temperature than conventional amplifiers, especially at low frequencies.

Since the minimum noise temperature of a SQUID is proportional to T/ω^0, lower noise temperatures can be achieved by decreasing the bath temperature T or increasing the characteristic frequency ω^0; $\omega^0=R/L$ is increased by decreasing L or increasing R. L is decreased by making a SQUID with smaller dimensions; R can be increased if at the same time the junction capacitance is decreased. Indeed, both of the approaches -- decreasing T and increasing ω^0 -- have been used to make SQUIDs with noise temperatures near quantum limit [10, 11].

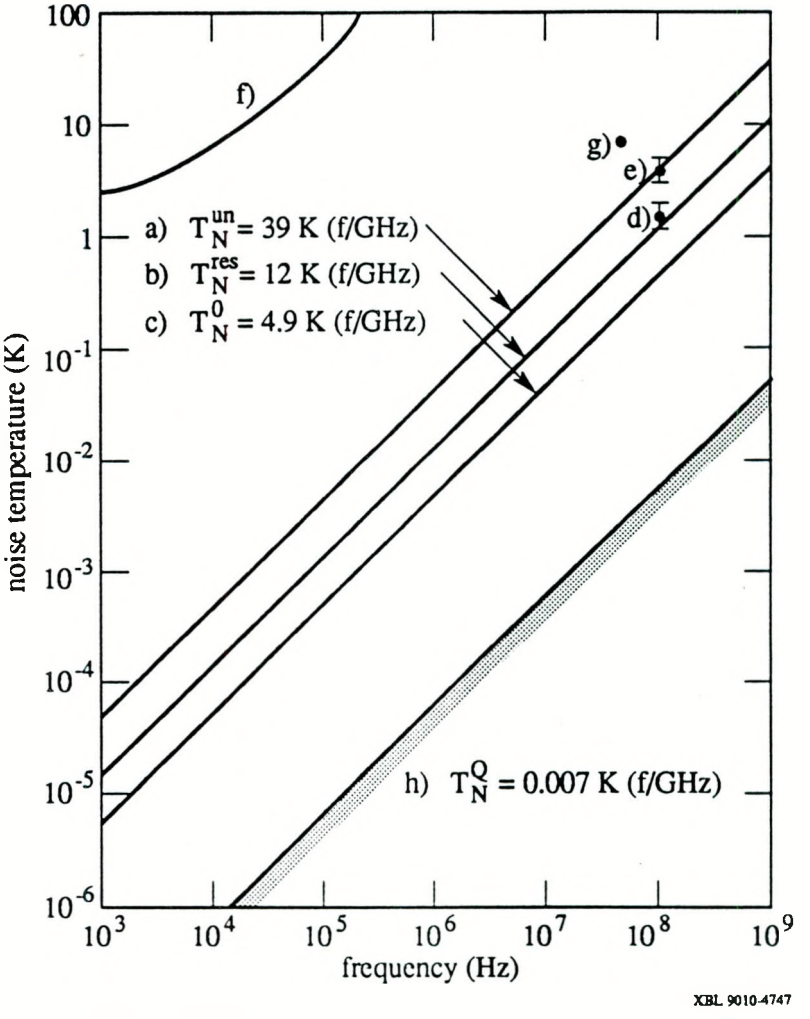

Fig. 2.8 Comparison of noise temperatures of SQUID and conventional amplifier.

SQUID amplifier at 4.2 K:

(a) Minimum noise temperature of untuned amplifier (theoretical value),

(b) Minimum noise temperature on resonance (theoretical value),

(c) Absolute minimum noise temperature (theoretical value),

(d) Tuned amplifier at 100 MHz(C. Hillbert & J. Clarke),

(e) Ununed amplifier at 100 MHz(C. Hillbert & J. Clarke);

Conventional amplifier:

(f) PAR 113 at room temperature (data sheet),

(g) GaAs FET at 4.2 K and at 45 MHz (P. Styles *et al.*);

Quantum limited amplifier:

(b) Noise temperature of quantum limited amplifier ($T_N = \hbar\omega / k_B \ln 2$).

II. Optimum Signal to Noise Ratio

In this section, I calculate the signal to noise ratio of a NMR signal in four detection schemes: (i) a tuned circuit with a conventional amplifier, (ii) an untuned circuit with a conventional amplifier, (iii) a tuned circuit with a SQUID amplifier and (iv) an untuned circuit with a SQUID amplifier.

In the following calculation, we assume the same sample is used, with a FID signal characterized by $M(t)= M_0 \exp(j\omega t - t/T_2)$, where M_0 is the initial magnetization, ω is the NMR resonance frequency and T_2 is the spin-spin relaxation time of the sample. We also assume the pickup coil has a cross sectional area A. We optimize the signal to noise ratio by varying the number of turns of the pickup coil N, and by varying other parameters of the input circuit that couples signals from the pickup coil ino the preamplifier.

The emf induced by the FID signal is

$$V_0= j\omega\, NAB_s, \tag{2.73}$$

where $B_s = 4\pi M$ is the magnetic field signal induced by the magnetization M. For the reason of simplicity in the calculation, we define

$$P_0= < V_0^2 >/\omega L_p, \tag{2.74}$$

where < > indicates a time average over one cycle of the sine wave, and L_p is the self inductance of the pick up coil. Since V_0 is proportional to the variable N and L_p is proportional to N^2, P_0 does not depend on N (assuming the filling factor does not change); therefore, in the following calculations of the signal to noise ratio, we may consider L_p as a variable and P_0 as a constant.

The meaning of P_0 is illustrated by an example in which the pickup coil is a solenoid with a length ℓ which has a self inductance $L_p = 4\pi N^2 A/\ell$. With the help of Eq.2.73, we have $P_0 = \omega(A\ell)(M_0^2/8\pi)$. Since Al is the volume of the coil and $M_0^2/8\pi$ is the energy density, $(A\ell)(M_0^2/8\pi)$ is the total energy of the signal

$$U_0 = (A\ell)(M_0^2/8\pi). \tag{2.75}$$

Thus, P_0 is related to the total energy of the signal U_0 by the equation

$$P_0 = \omega U_0 . \tag{2.76}$$

Because the magnetization M_0 is proportional to the population difference Δn of the two energy levels involved in the NMR or NQR transition, and Δn is proportional to the energy level splitting, $\Delta n \propto \Delta E/k_BT = \hbar\omega/k_BT$, we see that M_0 is proportional to ω and

$P_0 \propto \omega^3$.

A. Tuned circuit with conventional preamplifier

The tuned circuit, shown in Fig. 2.9, has a resonant frequency $\omega=1/\sqrt{LC}$ with a quality factor $Q= \omega L_p/R_s$. The resonant frequency is equal to the NMR frequency. The voltage signal across the circuit is

$$V_s=QV_0, \tag{2.77}$$

and the impedance is

$$Z= Q^2R_s . \tag{2.78}$$

At the resonant frequency, the total voltage noise across the circuit is

$$V_N=(S_V+S_I|Z|^2+4k_B|Z|T)^{1/2}\Delta B^{1/2}, \tag{2.79}$$

where S_V is the voltage noise density of the preamplifier, S_I is the current noise density of the preamplifier, T is the bath temperature of the pick up circuit and ΔB is the observation bandwidth.

Although the voltage signal to noise ratio can be used,

$$(SNR)_V=|V_s/V_N|, \tag{2.80}$$

it is more convenient to use the power signal to noise ratio,

$$SNR= \frac{P_s}{P_N} = \frac{<V_s^2>/|Z|}{<V_N^2>/|Z|} . \tag{2.81}$$

Since the signal power

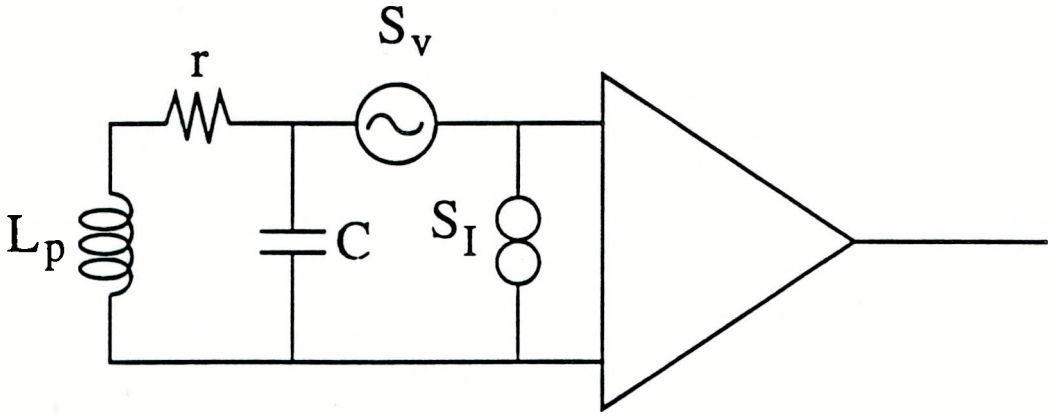

Fig. 2.9 Tuned input circuit with conventional amplifier.

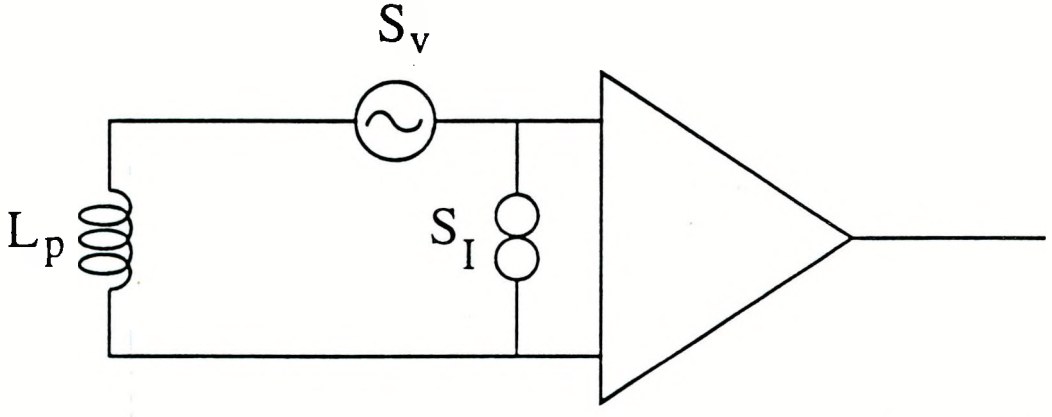

Fig. 2.10 Untuned input circuit with conventional amplifier.

$$P_s=<V_s^2>/|Z| \tag{2.82}$$

we have

$$P_s = QP_0, \tag{2.83}$$

which is obtained by substituting Eq. 2.77 and Eq. 2.78 into Eq. 82. The larger the Q, the larger the signal , and the better the signal to noise ratio. If the Q factor is fixed, the best signal to noise ratio is determined by minimizing the noise power

$$P_N=<V_N^2>/|Z| \tag{2.84}$$

or

$$P_N = (S_V/|Z|+S_I Z|+4k_B T)\Delta B, \tag{2.85}$$

which is obtained by substituting Eq. 2. 78 and Eq. 2.79 into Eq. 2.84. If the optimization condition,

$$Z= Q^2 r=\sqrt{S_V/S_I}, \tag{2.86}$$

is satisfied, the noise power is minimized, and found to be

$$P_N^0 = (2\sqrt{S_V S_I}+4k_B T)\Delta B. \tag{2.87}$$

It can be expressed in terms of the optimized noise temperature of the amplifier, $T_N^0 =\sqrt{S_V S_I}/2k_B$ (Eq. 2.14), that is,

$$P_N^0 = 4k_B(T_N^0 +T)\Delta B. \tag{2.88}$$

Thus, the best signal to noise ratio is given by

$$(SNR)^0 = \frac{QP_0}{4k_B(T_N^0 +T)\Delta B}. \tag{2.89}$$

B. Untuned circuit with conventional preamplifier

Fig. 2.10 shows the untuned circuit with a conventional preamplifier. The voltage signal across the coil is

$$V_s=V_0, \tag{2.90}$$

and the impedance of the coil is

$$Z= j\omega L_p. \tag{2.91}$$

The voltage noise across the coil is $V_N=(S_V+S_I|Z|^2)^{1/2}B^{1/2}$. The power signal to noise ratio is is given by

$$SNR= \frac{P_s}{P_N} = \frac{<V_s^2>/|Z|}{<V_N^2>/|Z|} . \tag{2.92}$$

where the signal power

$$P_s= <V_s^2>/|Z|,, \tag{2.93}$$

or

$$P_s = QP_0, \tag{2.94}$$

obtained by substituting Eq. 2.90 and Eq. 2.91 into Eq. 2.93. The noise power

$$P_N =<V_N^2>/|Z| =(S_V/|Z|+S_I|Z|)\Delta B. \tag{2.95}$$

The total noise power is minimized if the optimization condition,

$$|Z|=\sqrt{S_V/S_I}, \tag{2.96}$$

is satisfied and the minimal noise power is

$$P_N^0 = 2\sqrt{S_V S_I}\,\Delta B. \tag{2.97}$$

Expressing P_N^0 in terms of the optimized noise temperature of the amplifier, $T_N^0 =\sqrt{S_V S_I}/2k_B$ (Eq*), we have the minimal noise power

$$P_N^0 = 4k_B\, T_N^0\, \Delta B, \tag{2.98}$$

and the best signal to noise ratio

$$(SNR)^0 = \frac{P_0}{4k_B\, T_N^0\, \Delta B} . \tag{2.99}$$

C. Tuned circuit with SQUID preamplifier

Fig. 2.11 shows a tuned circuit with a SQUID amplifier. The tuned circuit has a resonant frequency $\omega=1/\sqrt{(L_p+L_i)C}$ with a quality factor $Q=\omega(L_p+L_i)/R_s$. The resonant frequency is equal to the NMR frequency. The total imaginary part of the impedance in the circuit is $Y+\omega L_i$, where Y is given by

$$Y = \omega L_p - \frac{1}{\omega C}. \tag{2.100}$$

The time average of the square of the flux signal Φ_s coupled into the SQUID is

$$< \Phi_s^2 >= \frac{< V_s^2 > M^2}{R_s^2 + (Y+\omega L_i)^2}. \tag{2.101}$$

The time average of the square of the total flux noise in the SQUID is given by Eq. 2.53,

$$< \Phi_{N\Sigma}^2 >= \frac{4k_B(T_N+T)R_s M^2}{R_s^2 + (Y+\omega L_i)^2}\Delta B, \tag{2.102}$$

where T_N is the noise temperature of the SQUID amplifier. With the help of Eq. 101 and Eq. 2.102, we have the signal to noise ratio

$$SNR = \frac{< \Phi_s^2 >}{< \Phi_{N\Sigma}^2 >} = \frac{< V_s^2 > / R_s}{4k_B(T_N+T)\Delta B}. \tag{2.103}$$

At the resonant frequency, $< V_s^2 > / R_s$ is the signal power P_s coupled into the input circuit,

$$P_s = < V_s^2 > / R_s; \tag{2.104}$$

correspondingly, $4k_B(T_N+T)\Delta B$ is the noise power P_N in the input circuit,

$$P_N = 4k_B(T_N+T)\Delta B. \tag{2.105}$$

We can write the signal power P_s in terms of P_0 and Q,

$$P_s = \frac{QP_0}{1+L_i/L_p}. \tag{2.106}$$

The signal power P_s decreases as the ratio L_i/L_p increases; therefore, we choose L_i/L_p much smaller than 1, and have

$$P_s = QP_0. \tag{2.107}$$

To maximize the signal, we chose Q as large as possible (assume that there is no requirement on the bandwidth within which signals need to be coupled into the SQUID).

At the resonant frequency, if the optimization condition (Eq. 2.47),

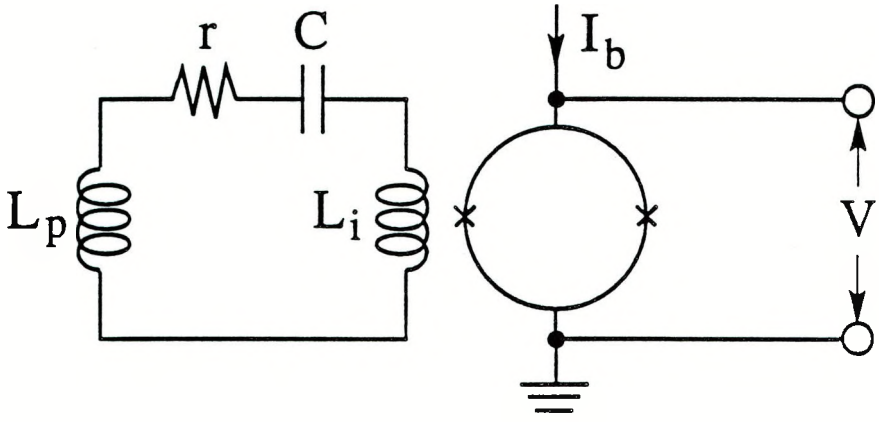

Fig. 2.11 Tuned input circuit with SQUID amplifier.

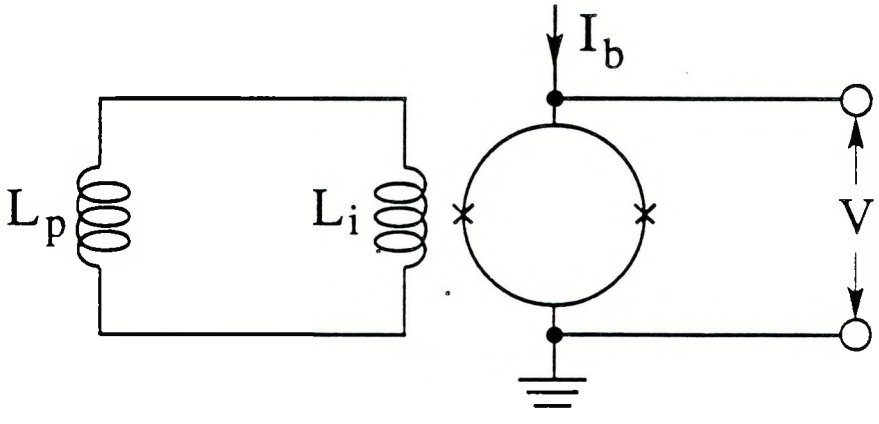

XBL 9010-4723

Fig. 2.12 Untuned input circuit with SQUID amplifier.

$$R_s = \omega L_i (\alpha^4 L^2 S_J/S_\Phi)^{1/2}, \tag{2.108}$$

is satisfied, the noise temperature in Eq. 2.105 is equal to the minimum noise temperature at the resonant frequency T_N^{Res} given by Eq. 2.46,

$$T_N^{res} = (S_J S_\Phi)^{1/2}/ 2k_B. \tag{2.109}$$

Under the optimization condition, the minimum noise power is

$$P_N = 4k_B(T_N^{res}+T)\Delta B, \tag{2.110}$$

and the best signal to noise ratio is

$$(SNR)^0 = \frac{QP_0}{4k_B(T_N^{res}+T)\Delta B}. \tag{2.111}$$

D. Untuned circuit with SQUID preamplifier

Fig 2.12 shows an untuned circuit with a SQUID amplifier. The time average of the square of the flux signal Φ_s coupled into the SQUID is obtained from Eq. 2.101 by setting $R_s = 0$ and $Y = \omega L_p$,

$$< \Phi_s^2 > = \frac{< V_s^2 > M^2}{\omega^2(L_p+L_i)^2}. \tag{2.112}$$

The time average of the square of the total flux noise in the SQUID is obtained from Eq. 2.33 and Eq. 2.34 by setting $R_s = 0$ and $Y = \omega L_p$,

$$< \Phi_{N\Sigma}^2 > = \frac{L_i^2 \tilde{S_\Phi}}{(L_p+L_i)^2} \Delta B, \tag{2.113}$$

where

$$\tilde{S_\Phi} = S_\Phi (1+ L_p/L_i)^2 + 2\alpha^2 L S_{\Phi J} (1+ L_p/L_i) + \alpha^4 L^2 S_J. \tag{2.114}$$

With the help of Eq. 2.11, Eq. 2.113 and Eq. 2.114, we have the signal to noise ratio,

$$SNR = \frac{< \Phi_s^2 >}{< \Phi_{N\Sigma}^2 >} = \frac{P_0}{2\omega\varepsilon/\alpha^2} \left[\frac{u}{(1+u)^2 + 2\alpha^2(1+u)LS_{\Phi J}/S_\Phi + \alpha^4 L^2 S_J/S_\Phi} \right], \tag{2.115}$$

where $\varepsilon = \frac{S_\Phi}{2L}$, and $u = L_p/L_i$.

In the limit $\alpha^2 << 1$, the SNR becomes

$$SNR = \frac{P_0}{2\omega\varepsilon/\alpha^2}\,\frac{u}{(1+u)^2}\,. \tag{2.116}$$

When the optimization condition u =1, or

$$L_p = L_i, \tag{2.117}$$

is satisfied, the SNR has the maximal value

$$(SNR)^0 = \frac{P_0}{8\omega\varepsilon/\alpha^2}\,. \tag{2.118}$$

This $(SNR)^0$ along with the optimization condition (Eq. 2.117) can also be obtained by maximizing the flux signal coupled into the SQUID $<\Phi_s^2>$. In the limit $\alpha^2 << 1$, maximizing SNR is the same as maximizing $<\Phi_s^2>$, since in that limit $\tilde{S}_\Phi = S_\Phi (1+ L_p/L_i)^2$, and the total flux noise in the SQUID given by Eq. 2.113 is a constant (independent of the parameters of the input circuit),

$$<\Phi_{N\Sigma}^2> = S_\Phi \Delta B, \tag{2.119}$$

and the SNR is proportional to $<\Phi_s^2>$,

$$SNR = \frac{<\Phi_s^2>}{<\Phi_{N\Sigma}^2>} = \frac{<\Phi_s^2>}{S_\Phi \Delta B} \propto <\Phi_s^2>. \tag{2.120}$$

Maximizing $<\Phi_s^2>$ given by Eq. 2.112, we have the same optimization condition as Eq. 2.117, $L_p = L_i$. The maximal flux signal is

$$<\Phi_s^2>_{max} = \frac{\alpha^2 L}{4L_p}\,\frac{<V_s^2>}{\omega^2}\,, \tag{2.121}$$

and the best signal to noise ratio is

$$(SNR)^0 = \frac{<\Phi_s^2>_{max}}{S_\Phi \Delta B} = \frac{P_0}{8\omega\varepsilon/\alpha^2}\,,$$

which is the same as Eq. 2.118. (2.122)

When α^2 is not small, the best signal to noise ratio is obtained by maximizing the SNR given by Eq. 2.115. The optimization condition is

$$u = 1+ 2\alpha^2 L S_{\Phi J}/S_\Phi + \alpha^4 L^2 S_J/S_\Phi\,. \tag{2.123}$$

and the best signal to noise ratio is

$$(SNR)^0 = \frac{P_0}{8\omega\varepsilon/\alpha^2} \frac{2}{1+\alpha^2 LS_{\Phi J}/S_\Phi + (1+2\alpha^2 LS_{\Phi J}/S_\Phi + \alpha^4 L^2 S_J/S_\Phi)^{1/2}}. \quad (2.124)$$

In terms of the minimal noise temperature of an untuned SQUID amplifier T_N^{un} (Eq. 2.24), we have

$$(SNR)^0 = \frac{P_0}{4k_B T_N^{un}} \kappa(\alpha^2), \quad (2.125)$$

where $\kappa(\alpha^2)$ is a correction factor,

$$\kappa(\alpha^2) = \frac{(1+2\alpha^2 LS_{\Phi J}/S_\Phi + \alpha^4 L^2 S_J/S_\Phi)^{1/2}}{1+\alpha^2 LS_{\Phi J}/S_\Phi + (1+2\alpha^2 LS_{\Phi J}/S_\Phi + \alpha^4 L^2 S_J/S_\Phi)^{1/2}} \quad (2.126)$$

$$\approx \frac{1}{2} + \frac{\alpha^2}{8} \frac{(L^2 S_J/S_\Phi)-(LS_{\Phi J}/S_\Phi)^2}{1+\alpha^2(LS_{\Phi J}/S_\Phi)}.$$

In terms of γ_Φ, $\gamma_{\Phi J}$ and γ_J, we have

$$\kappa(\alpha^2) \approx \frac{1}{2} + \frac{\alpha^2}{8} \frac{(\gamma_J/\gamma_\Phi)-(\gamma_{\Phi J}/\gamma_\Phi)^2}{1+\alpha^2(\gamma_{\Phi J}/\gamma_\Phi)}. \quad (2.127)$$

The correction factor $\kappa(\alpha^2)$ is almost a constant ; for the SQUID discussed in Sec. I.D ($\gamma_\Phi = 8$ $\gamma_J = 5.5$ and $\gamma_{\Phi J} = 6$),

$$\kappa(\alpha^2) - 1/2 \approx \frac{\alpha^4}{64}(1+0.75\alpha^2) << 1. \quad (2.128)$$

Therefore , $(SNR)^0$ becomes

$$(SNR)^0 \approx \frac{P_0/2}{4k_B T_N^{un}}. \quad (2.129)$$

In reality, if α^2 not so small, Eq. 2.125 --with $\kappa(\alpha^2)$ given by Eq. 2.126-- is only an approximation of the best signal to noise ratio, because of the screening effect: the inductance L of the SQUID is reduced by the presence of the input circuit [12], and the reduced inductance $L' = L(1-\alpha^2 L_p/L_i)$. The SQUID L in Eq. 2.114 and Eq. 2.115 should be replaced by L', and the change of the SQUID noise parameters (S_Φ, S_J and $S_{\Phi J}$) due to the change of L should also be taken into account. As our purpose is not to calculate accurately but to estimate reasonably the best signal to noise ratio $(SNR)^0$, we will continue the discussion about the $(SNR)^0$ of an untuned SQUID amplifier based on Eq. 2.129.

We summarize the signal to noise ratios of the above four circuits (Eq. 2.89, Eq. 2.99, Eq. 2.111 and Eq. 2.129 by one equation:

$$(SNR)^0 = \frac{QP_0}{4k_B T_\Sigma B}, \tag{2.130}$$

where we take Q=1 for an untuned circuit with a conventional amplifier and Q =1/2 for an untuned circuit with a SQUID amplifier. we have also introduced the concept of the system noise temperature T_Σ, which is defined as follows: for an untuned circuit, the system noise temperature is equal to the preamplifier noise temperature, and for an tuned circuit, the system noise temperature is equal to the sum of the bath temperature and the preamplifier noise temperature. The complete definitions of T_Σ are listed in Table 2.2.

The minimum detectable power P_{0min} is defined by $(SNR)^0 = 1$, or

$$P_{0min} = 4k_B T_\Sigma \Delta B / Q. \tag{2.131}$$

The minimal detectable voltage defined by $P_{0min} = < V^2_{smin} > /\omega L_p$ (c.f. Eq. 2.74), or

$$(< V^2_{smin} >)^{1/2} = \sqrt{4k_B T_\Sigma \Delta B \omega L_p / Q}. \tag{2.132}$$

The minimal detectable energy U_{0min} is defined by $P_{0min} = \omega U_{0min}$ (c.f. Eq. 2.76), or

$$U_{0min} = 4k_B T_\Sigma \Delta B / \omega Q, \tag{2.133}$$

and the minimal detectable magnetization by $U_{0min} = (M^2_{0min}/8\pi)\, V^*$ (c.f. Eq. 2.75), or

$$M_{0min} = \left(\frac{8\pi}{V^*} \frac{4k_B T_\Sigma \Delta B}{\omega Q} \right)^{1/2}. \tag{2.134}$$

Here V^* is the effective volume of the sample (V^* depends on coil geometry and the filling factor; for a solonoid with filling factor 1, V^* is equal to the value of the sample). The larger the product $\omega Q V^*$, the smaller the minimal detectable magnetization M_{0min}. The minimal detectable NMR signal M_{0min} is proportional to the square root of the system noise temperature, so that the sensitivity of a NMR spectrometer can be improved by decreasing the system noise temperature.

	Tuned Circuit (on resonance)	Untuned Circuit
Conventional Amplifier	$T_\Sigma = T + T_N^0$	$T_\Sigma = T_N^0$
SQUID Amplifier	$T_\Sigma = T + T_N^{res}$	$T_\Sigma = T_N^{un}$

Table 2.2 Definition of system noise temperature

III. Conclusion

Whether or not one should use a SQUID preamplifier obviously depends on its effect on system sensitivity. For an untuned circuit, the system sensitivity always improves as the noise temperature of the preamplifier is decreased, until the noise temperature reaches its quantum limit $k_B T_N^Q \sim h\omega$. For a tuned circuit, if the preamplifier noise temperature is larger than or comparable to the bath temperature, the system sensitivity can be improved by using a preamplifier with a lower noise temperature, for example, a SQUID preamplifier. But, on the other hand, if the bath temperature is much larger than the noise temperature of the preamplifier, the system sensitivity cannot be improved by using a preamplifier with a lower noise temperature; In this case, the sensitivity only can be improved by decrease the bath temperature.

As an example we consider the case tof a tuned circuit at 4.2K. If a conventional preamplifier with a noise temperature 50 K is used, the system noise temperature is 54 K, dominated by the preamplifier noise. By replacing the preamplifier with a SQUID preamplifier with a noise temperature of 1K, one achieves a system noise temperature of 5 K, which is a factor of 10 improvement in signal to noise ratio. The use of a SQUID with a noise temperature lower than 1K will not improve the system sensitivity any further. However, if the bath temperature of the input coil is lowered to 1.5 K, the system noise temperature changes to 2.5 K , which is another improvement of factor of 2.

Whether one should use a tuned circuit depends on how big the Q factor of the tuned circuit is . The signal power coupled into a tuned circuit is a factor of Q larger than the power coupled into the untuned circuit, but the system noise temperature of a tuned circuit is larger than that of an untuned circuit: by a factor of $(T_N^0 + T)/ T_N^0$ times larger for a conventional amplifier, and a factor of $(T_N^{rcs}+T)/T_N^{un}$ times larger for a SQUID amplifier. Therefor, for a conventional amplifier, a tuned circuit has a better sensitivity, if one can make the Q large enough so that $Q > 1+T/T_N$; otherwise, an untuned circuit is better. For

a SQUID amplifier, if one can make Q large enough so that $Q > T/T_N^{un}$ (we neglected T_N^{res} because $T_N^{res} << T$ in most applications), then a tuned circuit has a better sensitivity; otherwise, an untuned circuit is better. For the SQUID discussed in Sec. I.D, using Eq. 2.70 we can write the condition as $Q > 100$ MHz/f at T= 4.2 K. Applying this condition to a specific example, at 50 kHz to make a tuned SQUID amplifier more sensitive than an untuned SQUID amplifier, we need the Q factor larger than 2×10^3, which is formidably difficult at liquid helium temperature. The condition implies that in sensitivity the lower the frequency the more favorable it is to an untuned amplifier to obtain the best sensitivity. .

Finally, why can only a SQUID be used to detect directly ZFNMR and low frequency NQR spectra ? The reason is that ZFNMR and the NQR spectra from some of the nuclei (e.g. ^{2}D) have a very low resonant frequency [13], typically below 200 kHz; at these low frequencies the ZFNMR and NQR signals are very weak, and a SQUID amplifier has a much better noise temperature than that of a conventional amplifier (c.f. Fig. 2.8). Because $P_0 \propto \omega^3$, the signal coupled to an untuned circuit is proportional to ω^3 and the signal coupled to a tuned circuit is proportional to $Q\omega^3$. The lower the resonant frequency the weaker the signal. because of the requirement that the input circuit has to cover signals over a large bandwidth (from a few kHz to 200 kHz), one must use an untuned amplifier. And because an untuned SQUID amplifier is much more sensitive than an untuned conventional amplifier at low frequency (at 50kHz, the noise temperature of best semiconductor amplifier is more than 10^3 times higher than that of the best SQUID amplifier), to detect ZFNMR and low frequency NQR spectra, an untuned SQUID amplifier is essential.

1. J. Clarke, NATO ASI Series Vol. 59, *Superconductive Electronics*, edited by M.Nisenoff and H. Weinstock (Springer, Berlin, 1989), p.87.

2. C. Hilbert, J. Clarke, T. Sleator and E. L. Hahn, Appl. Phys. Lett. **47**, 637 (1985).

3. N. Q. Fan, M. B. Heaney, J. Clarke, D. Newitt, L. Wald, E. L. Hahn, A. Bielecke, and A. Pines, IEEE Trans. **MAG-25**, 1193 (1989).

4. C. G. Caves (1982) (unpublished).

5. J. Clarke, *Advances in superconductivity*, edited by B. Deaver and J. Ruvalds (Plenum Publishing Corporation, 1983), p13.

6. C. D. Tesche and J. Clarke, J. Low Temp. Phys. **37**, 397 (1979).

7. J. Clarke, C. D. Tesche and R. P. Giffard, J. Low Temp. Phys. **37**, 405 (1979).

8. C. Hilbert and J. Clarke, J. Low Temp. Phys. **61**, 263 (1985).

9. P. Styles, N. F. Soffe, C. A. Scott, D. A. Cragg, F. row, D. J. White and P. C. J. White, J. of Mag. Res. **60**, 397-404 (1984)

10. Van Harlingen, R. H. Koch and J. Clarke, Appl. Phys. Lett. **41**, 197 (1982).

11. F. C. Wellstood, C. Urbina and J. Clarke, Appl. Phys. Lett. **54**, 2599 (1989).

12. J. E. Zimmerman, J. Appl. Phys. **41**, 4483 (1971).

13. D. B. Zax, A. Bielecki, K. W. Zilm, A. Pines and D. P. Weitekamp, J. Chem. Phys. 83, 4877 (1985).

CHAPTER 3

COMPARISON BETWEEN HIGH FIELD NMR SPECTRA AND ZERO FIELD NMR OR PURE NQR SPECTRA

In this chapter I will discuss the difference in spectral resolution between the high field NMR spectra and two other kind of spectra: zero field NMR and pure NQR spectra[1]. The high field NMR spectra of a powder sample are broadened mainly by two types of interactions: the dipole-dipole interaction and the quadrupole interaction. The dipole-dipole interaction can be measured directly from the zero field NMR spectra; the quadruple interaction can be measured directly from the pure NQR spectra. I will discuss the dipole-dipole interaction and the ZFNMR spectra in Sec. I , and the quadrupole interaction and the NQR spectra in Sec. II. In Sec. III, I will calculate the transient response of a quadrupole system after a rf pulse is applied to the system.

In the following, I will use two frames: the laboratory frame and the molecular frame. The laboratory frame is fixed in space; the molecular frame is fixed on the molecule of interest, which rotates along with the molecule. I will use $\mathbf{x}^0$, $\mathbf{y}^0$ and $\mathbf{z}^0$ to represent respectively the unit vectors along the x, y and z axes of the laboratory frame, and $\mathbf{X}^0$, $\mathbf{Y}^0$ and $\mathbf{Z}^0$ to represent respectively the unit vectors along axes X, Y and Z of the molecular frame; I will use O_x, O_y and O_z to represent the components of a vector O in the laboratory frame, and O_X, O_Y and O_Z in the molecular frame.

I. Dipole-Dipole Interaction

We consider a system that consists of two nuclei, coupled together by their dipole-dipole interaction -- each spin interacts with the magnetic field generated by the other. The Hamiltonian of the system is the dipole Hamiltonian,

$$H_d = \hbar\, \omega_d[\, \mathbf{I}_1\cdot\mathbf{I}_2 - 3\, (\mathbf{I}_1\cdot\mathbf{n})(\mathbf{I}_2\cdot\mathbf{n})], \tag{3.1}$$

where $\mathbf{n}$ is the unit vector pointing from one spin to other and ω_d is a frequency characterizing the strength of the dipole-dipole interaction. The frequency $\omega_d = \gamma_1\gamma_2\,\hbar^2/r^3$, where γ_1 and γ_2 are the gyromagnetic ratios of the two nuclei, and r is the distance between the two spins. The frequency $\omega_d/2\pi$ is typically between 1 kHz and 30 kHz; for example, the distance between the two protons in a water molecular in a hydrated crystal is about 1.8 Å and $\omega_d/2\pi$ is about 28 kHz.

In a molecular frame where the Z axis is along the $\mathbf{n}$ direction, the Hamiltonian is written as

$$H_d = \hbar\, \omega_d[\, \mathbf{I}_1\cdot\mathbf{I}_2 - 3\, I_{1Z}I_{2Z}]. \tag{3.2}$$

In the laboratory frame, by substituting the unit vector

$$\mathbf{n} = \sin\theta\cos\phi\ \mathbf{x}^0 + \sin\theta\sin\phi\ \mathbf{y}^0 + \cos\theta\ \mathbf{z}^0 \tag{3.3}$$

into Eq. 3.1, we can write the Hamiltonian as

$$H_d = \hbar\, \omega_d \sum_q (-1)^q T_2^q\, Y_2^{-q}, \tag{3.4}$$

where Y_2^{-q} is the second order spherical harmonic function, and T_2^q is defined as

$$T_2^0 = \sqrt{4\pi/5}\ (\mathbf{I}_1\cdot\mathbf{I}_2 - 3\, I_{1z}I_{2z}), \tag{3.5}$$

$$T_2^{\pm1} = \mp\sqrt{6\pi/5}\ (I_{1z}I_{2\pm} + I_{1\pm}I_{2z}), \tag{3.6}$$

$$T_2^{\pm2} = -\sqrt{6\pi/5}\ (I_{1\pm}I_{2\pm}). \tag{3.7}$$

One property of T_2^q that will be used in the following calculation is the selection rule on the matrix element $\langle m | T_2^q | m' \rangle$, where $| m \rangle$ and $| m' \rangle$ are the eigenstates of $I_z = I_{1z} + I_{2z}$ with eigenvalues m and m' respectively. The selection rule is

$$\langle m | T_2^q | m' \rangle \neq 0, \quad \text{only if } m = m' + q. \tag{3.8}$$

For simplicity, in the following discussion we assume the two spins are identical spin 1/2 nuclei with gyromagnetic ration γ.

A. High magnetic field

In a magnetic field H_0, the total Hamiltonian is the sum of the Zeeman Hamiltonian $H_z = -\hbar\omega_0 (I_{1z} + I_{2z})$ and the dipole Hamiltonian H_d, where ω_0 is the Larmor frequency, $\omega_0 = \gamma H_0$. In the limit that $\omega_0 >> \omega_d$, the dipole Hamiltonian can be truncated by H_z. We define the total angular momentum operator $I^2 = (I_1+I_2)^2$ and the z component of the total angular momentum $I_z = I_{1z} + I_{2z}$.

Without the dipole Hamiltonian, the eigeinstate of the Zeeman Hamiltonian is $| m \rangle$, which is the eigeinstate of I_z with eigenvalue m. The truncated Hamiltonian is calculated with the help of Eq. 3.8:

$$\begin{aligned} H &= \langle m | H_z + H_d | m \rangle \\ &= - m \hbar \omega_0 + \hbar \omega_d T_2^0 Y_2^0 \\ &= - m \hbar \omega_0 - \frac{\hbar \omega_d}{2} (1 - 3\cos^2\theta)(I_1 \cdot I_2 - 3 I_{1z} I_{2z}). \end{aligned} \tag{3.9}$$

Since the Hamiltonian commutes with both I^2 and I_z, the four energy levels can be labeled by the eigeinvalues of these two operators. Three energy levels labeled with I=1 are triplet state; one energy level labeled with I = 0 is singlet state.

The transitions between different states can be induced by applying a rf magnetic field H_1 to the system. Since the total angular momentum I commutes with the

perturbation Hamiltonian $H' = -\gamma\hbar H_1 \cdot (I_1+I_2)$, there is no transition between the triplet states and the singlet state. We can consider the two classes of states separately. The singlet state has no contribution to NMR spectra. The three triplet states are $|1\ 1\rangle$, $|1\ 0\rangle$ and $|1\ -1\rangle$; they are the eigenstates of I with I=1 and the eigenstates of I_Z with eigenvalues 1, 0 and -1 respectively. The energies of the three states are:

$$E_{1\,1} = \langle 1\ 1 | H | 1\ 1 \rangle = \hbar\omega_0 + \frac{\hbar\,\omega_d}{4}(1-3\cos^2\theta), \tag{3.10}$$

$$E_{1\,0} = \langle 1\ 0 | H | 1\ 0 \rangle = 0 - \frac{\hbar\,\omega_d}{2}(1-3\cos^2\theta), \tag{3.11}$$

$$E_{1\,-1} = \langle 1\ -1 | H | 1\ -1 \rangle = -\hbar\omega_0 + \frac{\hbar\,\omega_d}{4}(1-3\cos^2\theta). \tag{3.12}$$

The energy levels, shown in Fig. 3.1, are shifted by the dipole-dipole interaction. The amount of the energy level shift depends on the orientation of the molecule relative to the external magnetic field. As illustrated in Fig. 3.2, the two resonant frequencies also depend on the molecular orientation,

$$\omega_+ = \omega_0 + \frac{3\omega_d}{4}(1-3\cos^2\theta), \tag{3.13}$$

$$\omega_- = \omega_0 - \frac{3\omega_d}{4}(1-3\cos^2\theta). \tag{3.14}$$

With a powder sample, the spectrum is an average over all the possible molecular orientations[2]. The probability of finding a molecular within solid angle $d\Omega$ is $dn = d\Omega / 4\pi$. The probability that the resonant frequency is between ω to $\omega+d\omega$ is

$$dn = \left[\frac{1}{4\pi} \left| d\Omega/d\omega_+ \right| + \frac{1}{4\pi} \left| d\Omega/d\omega_- \right| \right] d\omega, \tag{3.15}$$

with $\omega_+=\omega$ and $\omega_-=\omega$. Thus, the spectrum of a powder sample is given by

$$\frac{dn}{d\omega} = \frac{1}{2}\left[\left| d\omega_+/d\cos\theta \right|^{-1} + \left| d\omega_-/d\cos\theta \right|^{-1} \right]. \tag{3.16}$$

With the aid of Eq. 3.13 and Eq. 3.14, the equation describing the spectrum becomes

$$f(\omega) = \begin{cases} \left[1 - \dfrac{\Delta\omega}{3\omega_d/4} \right]^{-1/2} & \left(-3\omega_d/2 < \Delta\omega < -3\omega_d/4 \right) \\ \left[1 - \dfrac{\Delta\omega}{3\omega_d/4} \right]^{-1/2} + \left[1 + \dfrac{\Delta\omega}{3\omega_d/4} \right]^{-1/2} & \left(-3\omega_d/4 \le \Delta\omega \le 3\omega_d/4 \right) \\ \left[1 + \dfrac{\Delta\omega}{3\omega_d/4} \right]^{-1/2} & \left(3\omega_d/4 < \Delta\omega < 3\omega_d/2 \right). \end{cases} \tag{3.17}$$

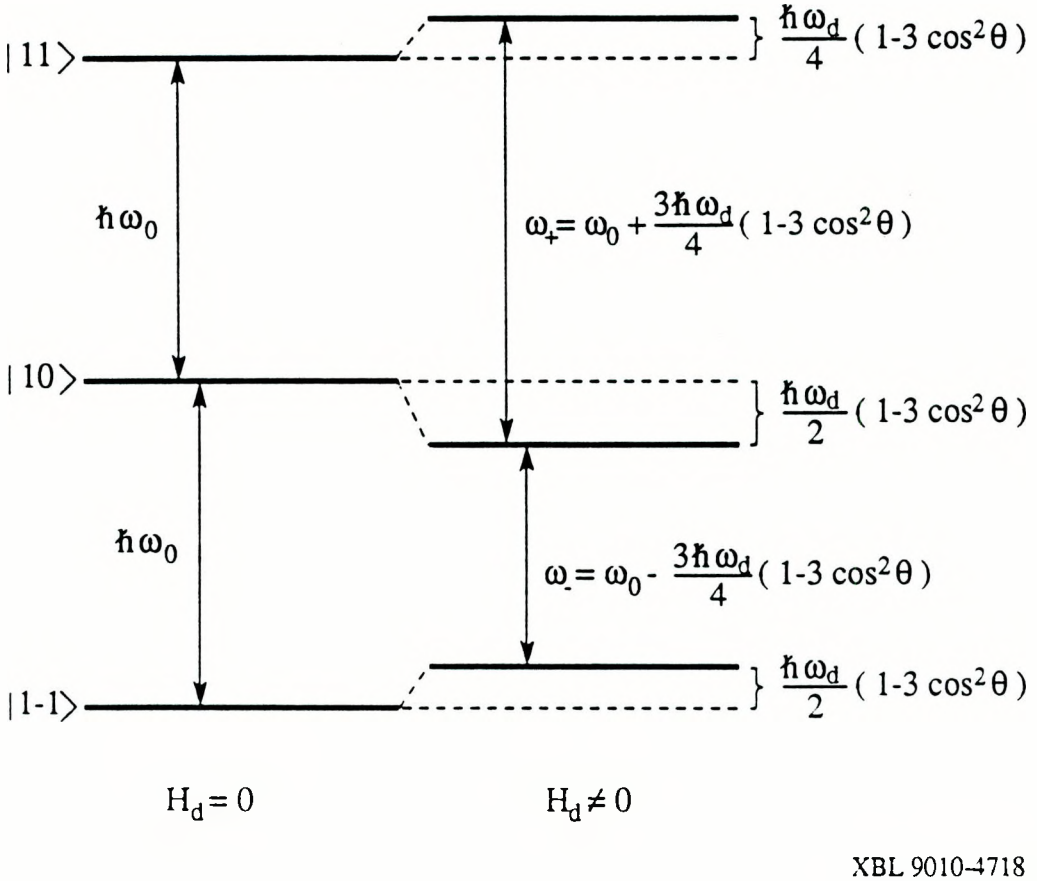

Fig. 3.1 Energy levels of a pair of identical spin 1/2 nuclei.

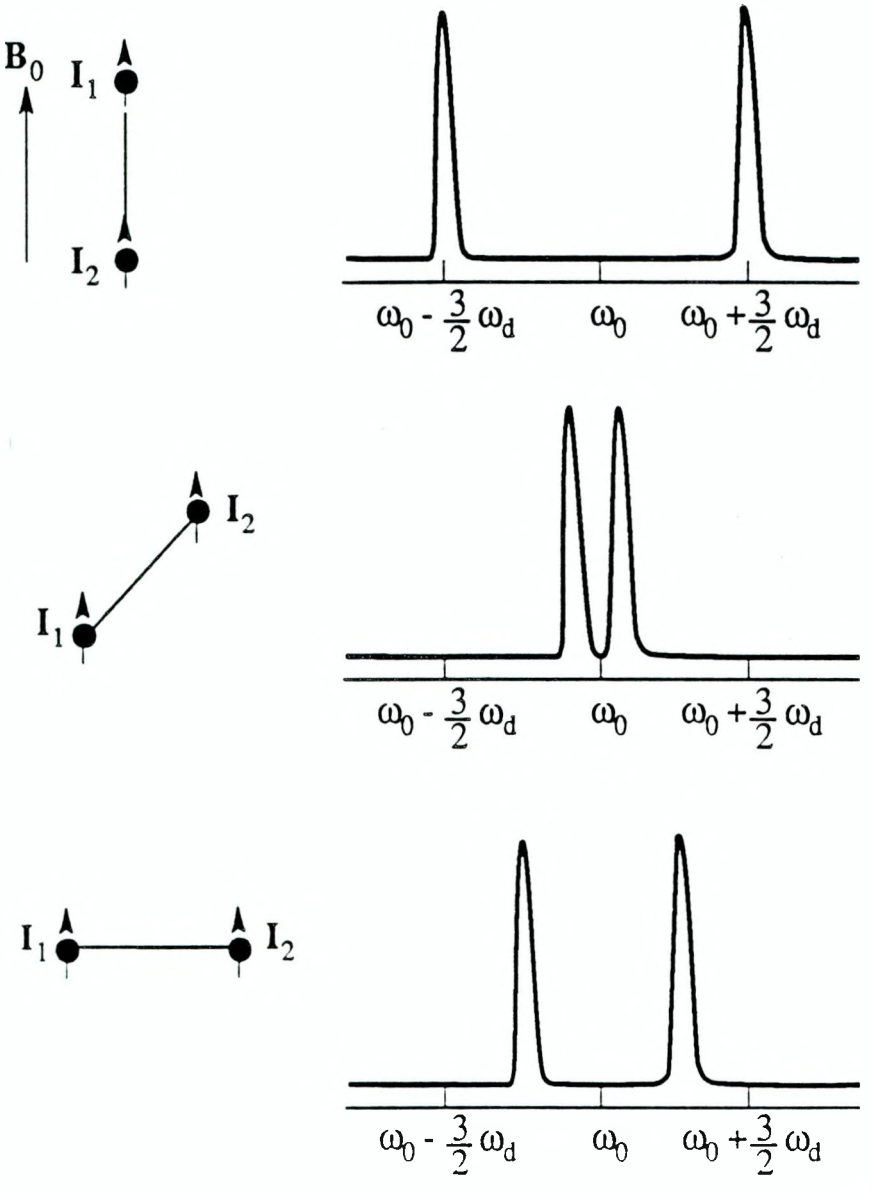

XBL 9010-4719

Fig. 3.2 Spectra of two spins system with molecules in different orientations relative to external magnetic field.

It is plotted in Fig. 3.3. Without other broadening mechanisms, the spectrum diverges at frequencies $\omega = \omega_0 \pm 3\omega_d/4$. In reality, the two spins in the molecule are not completely isolated; they interact with the local magnetic field generated by the spins from other nearby molecules. This interaction broadens the spectrum and removes the divergence.

B. Zero magnetic field

In zero magnetic field, the total Hamiltonian consists of the dipole Hamiltonian only. In the molecular frame the Hamiltonian is $H = H_d = \hbar\, \omega_d[\, I_1 \cdot I_2 - 3\, I_{1Z} I_{2Z}]$. Since the Hamiltonian commutes with I^2, the eigenstates can be classified as triplet and singlet. Only the transitions between the triplet states contribute to the zero field NMR spectrum. The Hamiltonian also commutes with I_Z, and the eigenstates of the Hamiltonian are $| I, I_Z \rangle$. The singlet state is $| 0\ 0 \rangle$. The triplet states are $|1\ 1\rangle$, $|1\ 0\rangle$ and $|1\ -1\rangle$. The energy levels of the triplet states are given by

$$E_{1\,1} = \langle 1\ \ 1 | H_d | 1\ \ 1 \rangle = -\omega_d/2, \tag{3.18}$$

$$E_{1\,0} = \langle 1\ \ 0 | H_d | 1\ \ 0 \rangle = \omega_d, \tag{3.19}$$

$$E_{1\,-1} = \langle 1\ -1 | H_d | 1\ -1 \rangle = -\omega_d/2, \tag{3.20}$$

and are shown in Fig. 3.4. The resonant transition frequency is $3\omega_d/2$, independent of the orientation of the molecules. It is important to realize that the spectrum of a powder sample is the same as that of a single crystal.

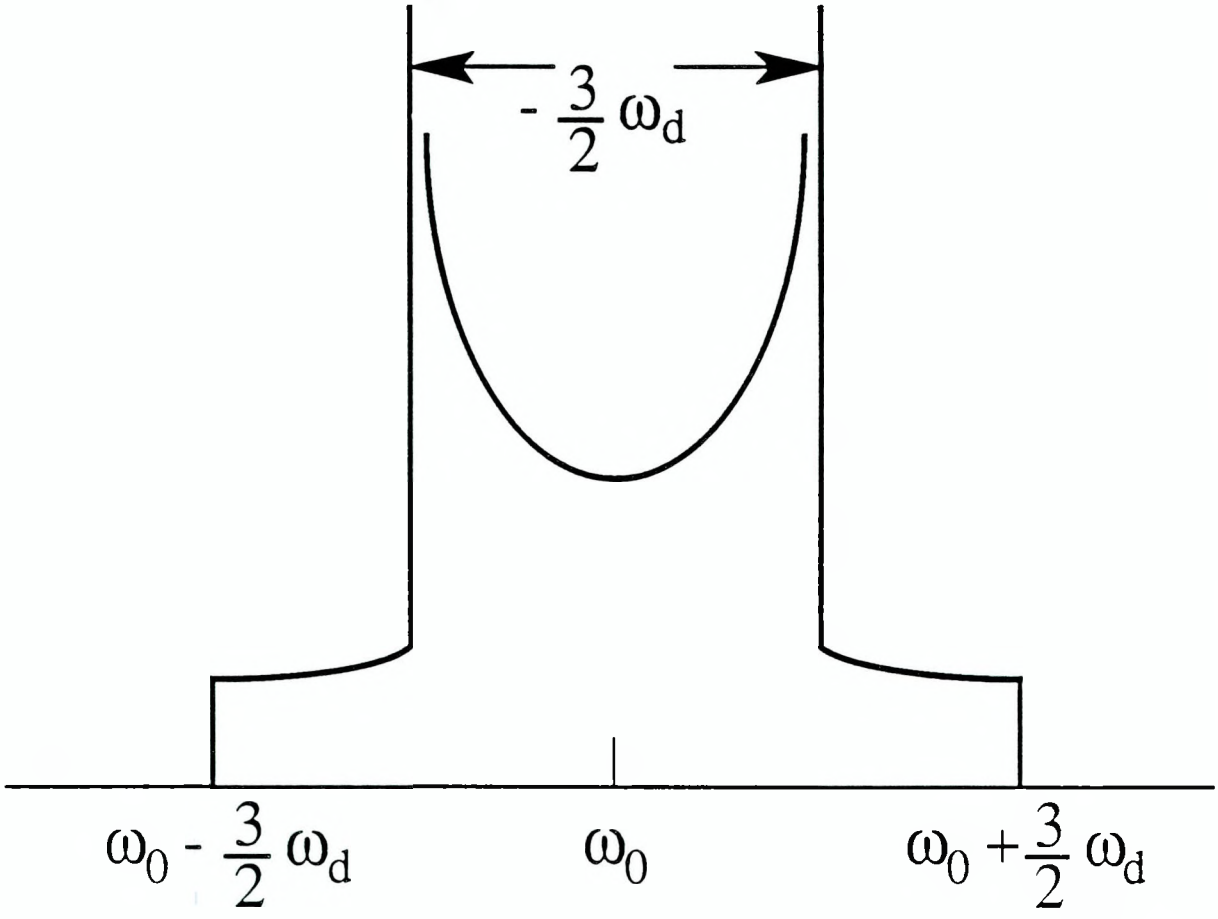

Fig. 3.3 High field NMR spectra of powder sample.

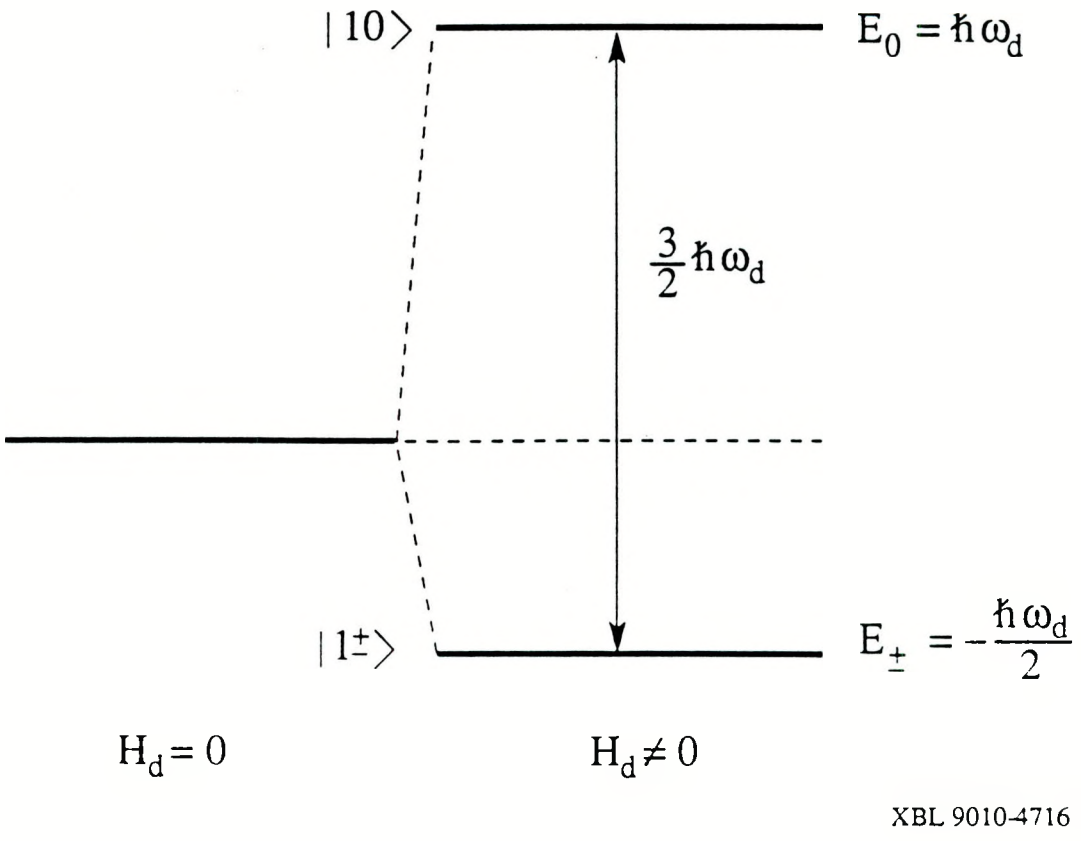

Fig. 3.4 Energy levels of a pair of identical spin 1/2 nuclei in zero magnetic field.

II. Quadruple Interaction

Nuclei with spin $I \geq 1$ have an electric quadruple moment Q, which, in materials interacts with the local electric field gradient. The interaction Hamiltonian is

$$H_Q = \hbar \omega_Q [3 I_Z^2 - I (I+1) + \frac{1}{2} \eta (L_+^2 + I_-^2)], \tag{3.21}$$

where $\omega_Q H = e^2 qQ/4I(2I-1)\hbar$, q is defined by $eq = V_{ZZ}$ and η ($0 \leq \eta \leq 1$) is $(V_{XX} - V_{YY}) / V_{ZZ}$. V_{XX}, V_{YY} and V_{ZZ} are the electric field gradients along the principal axes.

In the laboratory frame, if $\eta = 0$, the Hamiltonian can be written as

$$H_Q = \hbar \omega_Q \sum_q (-1)^q Q_2^q Y_2^{-q}, \tag{3.22}$$

where Y_2^{-q} is the second order spherical harmonic function and Q_2^q is defined as

$$Q_2^0 = \sqrt{4\pi/5} (I^2 - 3 I_z^2), \tag{3.23}$$

$$Q_2^{\pm 1} = \pm \sqrt{6\pi/5} (I_z I_\pm + I_\pm I_z), \tag{3.24}$$

$$Q_2^{\pm 2} = - \sqrt{6\pi/5} (I_\pm^2). \tag{3.25}$$

Q_{2q} obeys the selection rule:

$$\langle m | Q_2^q | m' \rangle \neq 0, \quad \text{only if} \quad m = m' + q, \tag{3.26}$$

where $| m \rangle$ and $| m' \rangle$ are the eigenstates of I_z with eigenvalues m and m' respectively.

A. High Magnetic Field.

In a magnetic field H_0, the total Hamiltonian is the sum of the Zeeman Hamiltonian $H_Z = - \gamma \hbar I_z H_0$ and the quadruple Hamiltonian H_Q given by Eq. 3.21. We now calculate the effect of the quadruple interaction on a high field NMR spectrum. We consider only the case $\eta = 0$. In the limit $\omega_0 >> \omega_Q$, the energy level shift due to the quadruple interaction is calculated with first order perturbation theory. With only the Zeeman

interaction, the eigenstate of the Hamiltonian is also an eigenstate of I and I_z (I_z =m), which is $|\, I\ m \rangle$. The energy level shift due to the quadruple interaction is

$$\Delta E_m = \langle I\ m | H_Q | I\ m \rangle$$
$$= \hbar \omega_Q Q_2^0 Y_2^0$$
$$= \frac{\hbar \omega_Q}{2}(1-3\cos^2\theta)\,[\,3m^2 - I(I+1)\,]. \qquad (3.27)$$

The resonant frequency due to the transition between $|\, I\ m \rangle$ and $|\, I\ m-1 \rangle$ is changed by

$$\Delta \omega_m = \frac{\omega_Q}{2}(1-3\cos^2\theta)\,(m - \frac{1}{2}). \qquad (3.28)$$

This frequency change depends on the orientation of the molecule relative to the external magnetic field. Therefore, the linewidth of a powder sample is broadened by the quadrupole interaction. In a high magnetic field, the line shape of a spin I=1 due to the quadrupole interaction is the same as that of two identical spin 1/2 nuclei due to the dipole-dipole interaction, which is shown in Fig. 3.3.

B. Zero magnetic field

1. $\eta = 0$

In zero magnetic field, the total Hamiltonian is equal to the quadrupole Hamiltonian. If $\eta = 0$, the Hamiltonian is given by

$$H = H_Q = \hbar \omega_Q [\ 3 I_Z^2 - I(I+1)\ ], \qquad (3.29)$$

Since H commutes with I_Z, the energy level can be labeled with $I_Z = M$. The energy of the state $|\, I\ M \rangle$ is given by

$$E_M = \langle I\ M | H_Q | I\ M \rangle = \hbar \omega_Q [\ 3M^2 - I(I+1)\ ]. \qquad (3.30)$$

The transition frequency from the state $|\, I\ M \rangle$ to the state $|\, I\ M-1 \rangle$ is

$$\omega_M = \frac{3\omega}{2}(M - \frac{1}{2}). \qquad (3.31)$$

2. $\eta \neq 0$

For $\eta \neq 0$, we consider only the system of nuclei with spin I=1, the simplest system with a quadruple interaction. In the representation with basis $|1\ 1\rangle$, $|1\ 0\rangle$ and $|1\ -1\rangle$, the Hamiltonian is

$$H = \begin{bmatrix} \omega_Q & 0 & \eta\omega_Q \\ 0 & -2\omega_Q & 0 \\ \eta\omega_Q & 0 & \omega_Q \end{bmatrix} \quad (3.32)$$

Solving the Hamiltonian, we find the three eigenstates

$$|+\rangle = (|1\ 1\rangle + |1\ -1\rangle)/\sqrt{2}, \quad (3.33)$$

$$|-\rangle = (|1\ 1\rangle - |1\ -1\rangle)/\sqrt{2}, \quad (3.34)$$

$$|0\rangle = |1\ 0\rangle; \quad (3.35)$$

the energy level is given by

$$E_+ = \omega_Q (1 + \eta), \quad (3.36)$$

$$E_- = \omega_Q (1 - \eta), \quad (3.37)$$

$$E_0 = -2\omega_Q. \quad (3.38)$$

The three transition frequencies are

$2\omega_Q\eta$, $3\omega_Q(1-\eta/3)$ and $3\omega_Q(1+\eta/3)$.

III. Transient Response

In this section, we calculate the NQR signal from spin I=1 nuclei after a magnetic pulse is applied to the nuclei. The energy level of the system is calculated in Sec. II B. The eigenstates $(|1\ 1\rangle - |1\ -1\rangle)/\sqrt{2}$, $(|1\ 1\rangle + |1\ -1\rangle)/\sqrt{2}$ and $|1\ 0\rangle$ are the eigenstates of I_X, I_Y, and I_Z, respectively, with eigenvalues equal to zero:

$$I_X(|1\ 1\rangle - |1\ -1\rangle)/\sqrt{2} = 0, \quad (3.39)$$

$$I_Y(|1\ 1\rangle + |1\ -1\rangle)/\sqrt{2} = 0, \quad (3.40)$$

$$I_Z|1\ 0\rangle = 0. \quad (3.41)$$

For convenience, we introduce the symbols:

$$|X\rangle = (|1\ 1\rangle - |1\ {-1}\rangle)/\sqrt{2}, \tag{3.42}$$

$$|Y\rangle = (|1\ 1\rangle + |1\ {-1}\rangle)/\sqrt{2}, \tag{3.43}$$

$$|Z\rangle = |1\ 0\rangle ; \tag{3.44}$$

$$E_X = (1-\eta)\,\omega_Q, \tag{3.45}$$

$$E_Y = (1+\eta)\,\omega_Q, \tag{3.46}$$

$$E_Z = -2\,\omega_Q ; \tag{3.47}$$

$$\omega_{YX} = (E_Y - E_X)/\hbar, \tag{3.48}$$

$$\omega_{XZ} = (E_X - E_Z)/\hbar, \tag{3.49}$$

$$\omega_{YZ} = (E_Y - E_Z)/\hbar . \tag{3.50}$$

The energy diagram labeled with the new symbols is shown in Fig. 3.5.

If we assume the perturbation magnetic field is

$$H_1 = H_{1X}\mathbf{X}^0 + H_{1Y}\mathbf{Y}^0 + H_{1Z}\mathbf{Z}^0, \tag{3.51}$$

the perturbation Hamiltonian is

$$H' = 2\gamma\hbar\, H_1 \cdot I \cos\omega t$$

$$= 2\cos\omega t\,(\gamma\hbar H_{1X} I_X + \gamma\hbar H_{1Y} I_Y + \gamma\hbar H_{1Z} I_Z). \tag{3.52}$$

In the representation with basis $|X\rangle$, $|Y\rangle$ and $|Z\rangle$,

$$I_X = \begin{bmatrix} 0 & 0 & 0 \\ 0 & 0 & 1 \\ 0 & 1 & 0 \end{bmatrix}, \qquad I_Y = \begin{bmatrix} 0 & 0 & -i \\ 0 & 0 & 0 \\ i & 0 & 0 \end{bmatrix}, \quad I_Z = \begin{bmatrix} 0 & 1 & 0 \\ 1 & 0 & 0 \\ 0 & 0 & 0 \end{bmatrix}. \tag{3.53}$$

In the limit that the pulse length τ is long, $1/\tau \ll \omega_{YX}$, ω_{YZ} and ω_{XZ}, we can calculate the three transitions between the three states separately. The transition between the states $|X\rangle$ and $|Y\rangle$ is calculated by writing the spin operators and the Hamiltonian operator in the subspace spaned by the bases $|X\rangle$ and $|Y\rangle$. The spin operators are given by

$$I_X = \begin{bmatrix} 0 & 0 \\ 0 & 0 \end{bmatrix}, \quad I_Y = \begin{bmatrix} 0 & 0 \\ 0 & 0 \end{bmatrix}, \quad I_Z = \begin{bmatrix} 0 & 1 \\ 1 & 0 \end{bmatrix}, \text{ or} \tag{3.54}$$

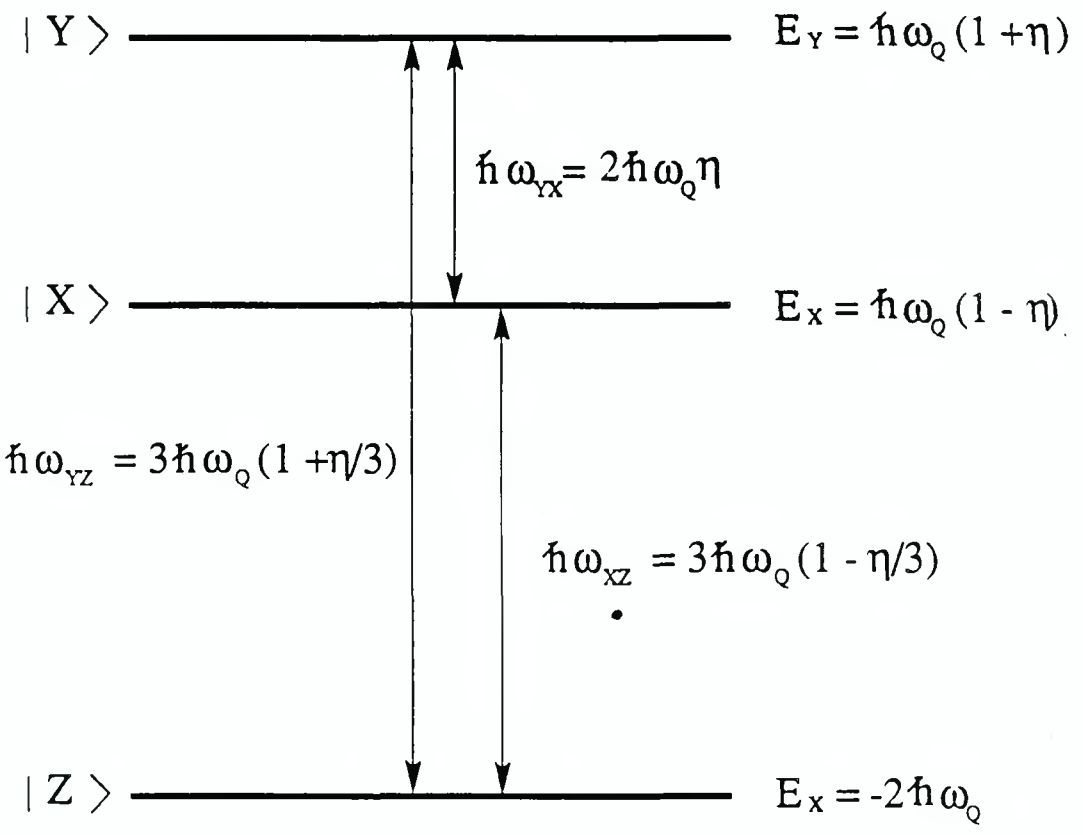

$$\begin{cases} |X\rangle = \frac{1}{\sqrt{2}} \left(|11\rangle - |1\,{-1}\rangle\right) \\ |Y\rangle = \frac{1}{\sqrt{2}} \left(|11\rangle + |1\,{-1}\rangle\right) \\ |Z\rangle = |1\,0\rangle \end{cases}$$

XBL 9010-4715

Fig. 3.5 Energy levels of spin 1 nuclei due to quadrupole interaction.

$$\mathbf{I} = \begin{bmatrix} 0 & 1 \\ 1 & 0 \end{bmatrix} \mathbf{Z}^0 . \tag{3.55}$$

The total Hamiltonian is given by

$$H = \begin{bmatrix} E_X & 2\gamma\hbar H_{1Z}\cos\omega t \\ 2\gamma\hbar H_{1Z}\cos\omega t & E_Y \end{bmatrix}. \tag{3.56}$$

Only the component of $\mathbf{H}_1$ along the $\mathbf{Z}^0$ direction can induce transitions between states $|X\rangle$ and $|Y\rangle$. Similarly, only the component of $\mathbf{H}_1$ along the $\mathbf{X}^0$ direction can induce transitions between states $|Y\rangle$ and $|Z\rangle$, and only the component of $\mathbf{H}_1$ along the $\mathbf{Y}^0$ direction can induce transitions between states $|X\rangle$ and $|Z\rangle$.

Expressing the wave function at time t in the subspace spanned by $|X\rangle$ and $|Y\rangle$,

$$|t\rangle = C_1(t)\,|X\rangle + C_2(t)\,|Y\rangle, \tag{3.57}$$

we can write the equation of motion as

$$i\hbar \frac{d}{dt}\begin{bmatrix} C_1(t) \\ C_2(t) \end{bmatrix} = \begin{bmatrix} E_X & 2\gamma\hbar H_{1Z}\cos\omega t \\ 2\gamma\hbar H_{1Z}\cos\omega t & E_Y \end{bmatrix}\begin{bmatrix} C_1(t) \\ C_2(t) \end{bmatrix}. \tag{3.58}$$

In the interaction representation

$$\tilde{C}_1(t) = \exp\left(i\frac{E_X t}{\hbar}\right) C_1(t), \tag{3.59}$$

$$\tilde{C}_2(t) = \exp\left(i\frac{E_Y t}{\hbar}\right) C_2(t), \tag{3.60}$$

the equation of motion becomes

$$i\frac{d}{dt}\begin{bmatrix} \tilde{C}_1(t) \\ \tilde{C}_2(t) \end{bmatrix} = \begin{bmatrix} 0 & 2\gamma H_{1Z}\cos\omega t \exp(i\omega_{YX}t) \\ 2\gamma H_{1Z}\cos\omega t \exp(i\omega_{YX}t) & 0 \end{bmatrix}\begin{bmatrix} \tilde{C}_1(t) \\ \tilde{C}_2(t) \end{bmatrix}. \tag{3.61}$$

Assuming the frequency of the pulse ω equal to the resonant frequency ω_{YX}, at time $t >> 1/\omega$, we can write Eq. 3.61 approximately as

$$i\frac{d}{dt}\begin{bmatrix} \tilde{C}_1(t) \\ \tilde{C}_2(t) \end{bmatrix} = \begin{bmatrix} 0 & \gamma H_{1Z} \\ \gamma H_{1Z} & 0 \end{bmatrix} \begin{bmatrix} \tilde{C}_1(t) \\ \tilde{C}_2(t) \end{bmatrix}. \tag{3.62}$$

Solving the equation, we find the wave function at the end of the pulse is

$$\tilde{C}_1(\tau) = \cos(\gamma H_{1Z}\tau)\,\tilde{C}_1(0) - i\sin(\gamma H_{1Z}\tau)\,\tilde{C}_2(0), \tag{3.63}$$

$$\tilde{C}_2(\tau) = -i\sin(\gamma H_{1Z}\tau)\,\tilde{C}_1(0) + \cos(\gamma H_{1Z}\tau)\,\tilde{C}_2(0). \tag{3.64}$$

Thus, in the Schrödinger representation, the wave function at time t , $t > \tau$, is given by

$$C_1(t) = [\cos(\gamma H_{1Z}\tau)C_1(0) - i\sin(\gamma H_{1Z}\tau)C_2(0)]\,\exp(-i\frac{E_X t}{\hbar}) \tag{3.65}$$

$$C_2(t) = [-i\sin(\gamma H_{1Z}\tau)\,C_1(0) + \cos(\gamma H_{1Z}\tau)\,C_2(0)]\,\exp(-i\frac{E_Y t}{\hbar}) \tag{3.66}$$

The total magnetization is

$$\mathbf{M}(t) = N\gamma\hbar\,\langle\overline{I}\rangle, \tag{3.67}$$

where N is the total number of spins and $\langle I \rangle$ is the expectation value of the spin operator. $\langle\overline{I}\rangle$ indicates the assemble average of the expectation value $\langle I \rangle$, obtained by taking $\overline{C_1(0)\,C_2^*(0)} = 0$ and $\overline{|C_1(0)|^2} - \overline{|C_2(0)|^2} = -\hbar\omega_{XY}/3k_BT$. Using Eq. 3.65 and 3.66, we find

$$\langle\overline{I}\rangle = \frac{\hbar\omega_{XY}}{k_BT}\sin(\frac{\gamma H_{1Z}\tau}{\hbar})\sin(\omega_{YX}t)\,\mathbf{Z}^0. \tag{3.68}$$

Thus, the NQR signal is given by

$$\mathbf{M}(t) = \frac{2}{3}N\gamma\hbar\,\frac{\hbar\omega_{XY}}{k_BT}\sin(2\gamma H_{1Z}\tau)\sin(\omega_{YX}t)\,\mathbf{Z}^0.$$

In the laboratory frame, the NQR signal is expressed as

$$\mathbf{M}(t) = \frac{2}{3}N\gamma\hbar\,\frac{\hbar\omega_{XY}}{k_BT}\sin(2\gamma H_1\cos\theta\,\tau)\sin(\omega_{YX}t)\,\mathbf{Z}^0,$$

where $\mathbf{Z}^0 = \sin\theta\sin\phi\,\mathbf{x}^0 + \sin\theta\sin\phi\,\mathbf{y}^0 + \cos\theta\,\mathbf{z}^0$. (3.69)

Similarly, if the pulse has a frequency $\omega = \omega_{YZ}$ and the pulse length $\tau >> 1/\omega_{YZ}$, the NQR signal is given by

$$\mathbf{M}(t) = \frac{2}{3} N\gamma\hbar \frac{\hbar\omega_{YZ}}{k_B T} \sin(2\gamma H_{1Z}\tau)\sin(\omega_{YZ} t)\,\mathbf{X}^0. \tag{3.70}$$

If the pulse has a frequency $\omega = \omega_{XZ}$ and the pulse length $\tau >> 1/\omega_{XZ}$, the NQR signal is given by

$$\mathbf{M}(t) = \frac{2}{3} N\gamma\hbar \frac{\hbar\omega_{XZ}}{k_B T} \sin(2\gamma H_{1Z}\tau)\sin(\omega_{XZ} t)\,\mathbf{Y}^0. \tag{3.71}$$

In the above calculation, we assume all the molecules are oriented in the same direction. In the following, we calculate the signal from a powder sample[3], assumeing $\omega = \omega_{XY}$, $\tau >> 1/\omega_{XZ}$, and $\mathbf{H}_1$ is in the $\mathbf{z}^0$ direction. In the laboratory frame, the NQR signal is expressed as

$$\mathbf{M}(t) = \frac{2}{3} N\gamma\hbar \frac{\hbar\omega_{XY}}{k_B T} \sin(2\gamma H_1 \cos\theta\,\tau)\sin(\omega_{YX} t)\,\mathbf{Z}^0, \tag{3.72}$$

where $\mathbf{Z}^0 = \sin\theta\sin\phi\,\mathbf{x}^0 + \sin\theta\sin\phi\,\mathbf{y}^0 + \cos\theta\,\mathbf{z}^0$. Averaging over all orientations, we have

$$\mathbf{M}(t) = \frac{2}{3} N\gamma\hbar \frac{\hbar\omega_{XY}}{k_B T} \sin(\omega_{XY} t)\mathbf{Z}^0 \left[\frac{1}{4\pi}\int \sin(2\gamma H_1\tau\cos\theta)\sin\theta\cos\phi\, d\Omega\,\mathbf{x}^0 \right.$$

$$\left. + \frac{1}{4\pi}\int \sin(2\gamma H_1\tau\cos\theta)\cos\theta\cos\phi\, d\Omega\;\mathbf{y}^0 + \frac{1}{4\pi}\int \sin(2\gamma H_1\tau\cos\theta)\cos\theta\; d\Omega\,\mathbf{z}^0 \right].$$

The first two terms in the bracket are zero, and the above expression becomes

$$\mathbf{M}(t) = \frac{2}{3} N\gamma\hbar \frac{\hbar\omega_{XY}}{k_B T} \sin(\omega_{XY} t)\frac{1}{\omega_1\tau}\left[\cos(\omega_1\tau) - \frac{\sin(\omega_1\tau)}{\omega_1\tau}\right]\mathbf{z}^0, \tag{3.73}$$

where ω_1 is defined by $\omega_1 = 2\gamma H_1$. The induced magnetization $\mathbf{M}(t)$ is in the same direction as the applied rf magnetic field.

1. D. P. Weitekamp, A. Bielecki, D. Zax, K. Zilm, and A. Pines, Phys. Rev. Lett. 43, 1791 (1979); D. B. Zax, A. Bielecki, K. W. Zilm, A. Pines and D. P. Weitekamp, J. Chem. Phys. 83, 4877 (1985).

2. G. F. Pake, J. Chem. Phys. 16, 327 (1948).

3. E. L. Hahn, Phys. Rev. 80, 580 (1950).

CHAPTER 4

SPECTROMETER AND SPECTRA

In this Chapter, I begin in Section I by describing the design and the performance of the SQUID amplifier. Section II is concerned with the construction of the spectrometer. Section III presents examples of some data, and Section IV contains concluding remarks.

I. SQUID Amplifier

We designed the SQUID-based amplifier, shown in Fig. 4.1(a), with three major criteria in mind. First, to detect signals at low frequency, the sensitivity should be as high as possible. Second, to cover most of the ^{2}D NQR spectra of practical interest, the bandwidth should extend to at least 200 kHz. Third, to detect signals from a solid sample with a short T_2, the preamplifier should be able to recover quickly (say in a few tens of μs) after the magnetic pulse has been turned off.

A. SQUID and input circuit

We use our standard design[1] of planar dc SQUID, which we fabricate in batches of 36 on 50 mm-diameter oxidized Si wafers. Each SQUID consists of a square washer of Nb with inner and outer dimensions of 0.2 and 0.9 mm. The Josephson junctions are formed in a plasma discharge in Ar (10% O_2), and the counter-electrode is Pb (5% In). Nominal values of the parameters are: critical current per junction, 5μA; shunt resistance per junction, 8W; inductance of SQUID loop, 0.4 nH; inductance of 20-turn spiral input coil: L_i =120 nH; mutual inductance between input coil and SQUID, 6nH.

The SQUID-based amplifier is shown in Fig. 4.1(a); the SQUID and its input circuit are immersed in liquid ^{4}He. The sample is placed in the pickup coil (inductance L_p) which

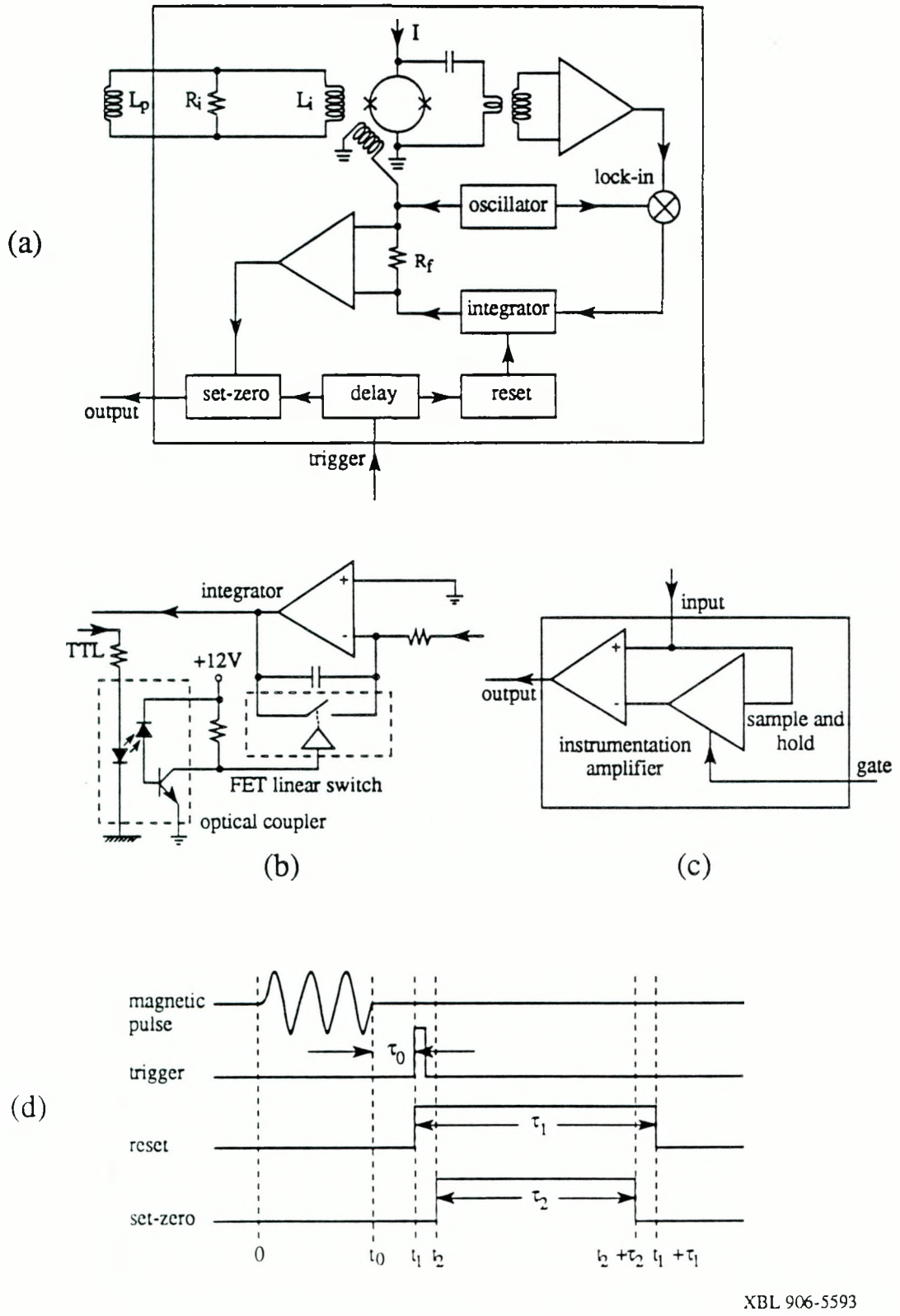

XBL 906-5593

Fig. 4.1 Schematic drawing of amplifier based on dc SQUID; (b) reset circuit of Fig. 1(a) ; (c) set-zero circuit of Fig. 1(a); (d) timing sequence of the TTL signals that control reset and set-zero circuits.

is coupled to the input coil (inductance L_i) of the SQUID. The pickup coils have an inductance L_p approximately equal to the inductance L_i = 120 nH of the input coil. The presence of the resistor R_i = 100 Ω provides a low-pass filter [2] to reduce the level of interference reaching the SQUID at frequencies above about 60 MHz. The Nyquist noise generated in the SQUID by the resistor is negligible, about $10^{-6}\ \Phi_o Hz^{-1/2}$. Because the entire input flux transformer is superconducting, the SQUID detects changes in the magnetization of the sample at frequencies down to zero. We choose an untuned circuit, as opposed to a tuned circuit, first, because we require a wide bandwidth, and, second, because of the impracticality of obtaining sufficiently large capacitors for use at liquid ^{4}He temperatures. A discussion of the comparative sensitivity of tuned and untuned circuits is given in the Appendix.

B. Flux-locked loop

The SQUID is operated in a flux-locked loop [Fig. 4.1(a)], which is a modified version of that described by Wellstood[3] et al. A 500 kHz modulation signal with a peak-to-peak amplitude of $\Phi_o/2$ is applied to the SQUID (Φ_o = h/2e is the flux quantum), and the resulting oscillating voltage across the SQUID is amplified by a room-temperature transformer with a turns ratio of 15. After further amplification, the signal is lock-in detected, integrated, and fed back via a resistor R_f = 5kΩ into a coil coupled to the SQUID with a mutual inductance M_f = 0.1 nH. For any change of flux DF in the SQUID loop, a change of feedback current , $\Delta I = \Delta\Phi/M_f$, cancels $\Delta\Phi$ and induces a voltage $\Delta V = R_f\Delta I = \Delta\Phi R_f/M_f$ across R_f. Thus, the SQUID amplifier has a transfer coefficient $\Delta V/\Delta\Phi = R_f/M_f \approx 0.1 V/\Phi_o$.

The feedback circuit enables the SQUID to operate at a fixed flux bias provided the changes in flux do not exceed the slew rate, which is about $2 \times 10^5\ \Phi_o$/sec at 40 kHz. In pulsed NMR and NQR applications, however, a large magnetic pulse is applied to the sample, and despite one's best efforts to minimize the fraction of this pulse coupled into the

SQUID, the integrator is inevitably driven into saturation. After the pulse is turned off, the integrator remains saturated for a long period. We overcome this problem by shorting the integrator capacitor with a FET linear switch (Siliconix DG 308) during the pulse, and opening the switch after the pulse has been turned off. The FET switch is controlled by a voltage pulse derived from a TTL pulse via an optical coupler (Hewlett Packard 6N135) that prevents digital noise being injected into the SQUID circuit [Fig. 4.1(b)]. When the flux-locked loop reaches stable operation, it produces a large voltage step at the output reflecting the feedback current necessary to flux-lock the SQUID. It is therefore necessary to provide a set-zero circuit to cancel this step while the free induction decay of the spins is recorded. This circuit [Fig. 4.1(c)] consists of a sample-and-hold $(S/H)^4$ device (LF198) with unity gain and an instrumentation amplifier (AD 625). The S/H mode is determined by a TTL pulse. Before the flux-locked loop reaches stable operation, the S/H device is in the sample mode, and the output of the instrumentation amplifier is zero since its two inputs are at the sample voltage. After the flux-locked loop settles into stable operation, the S/H is switched into the hold mode in which its output is held constant. The output of the amplifier is then proportional to the changes of the voltage produced by the flux-locked loop, with the large voltage step subtracted. The integrator reset circuit and the set-zero circuit are operated by TTL pulses from a delay circuit, which is constructed from three 555 timers.

The SQUID preamplifier is controlled by the timing sequence shown in Fig.4.1(d). At time $t = 0$, the magnetic pulse to the sample is turned on; it is turned off at t_0. During this time, the flux-locked loop is disabled and the output of the set zero stage is zero. At time t_0, even though the pulse is off, the residual signal induced by the pulse still changes too rapidly for the flux-locked loop to follow. After a further time t_0, the time-derivative of the residual signal is smaller than the slew rate of the flux-locked loop, and at time $t_1 = t_0 + \tau_0$, a trigger pulse is sent to the delay circuit, which produces two pulses to enable the integrator and the set-zero circuit. The time t_0 is about $20\mu s$ for a magnetic pulse with

peak-to-peak value of 0.1 mtesla, and about 80μs for a peak-to-peak value of 10 mtesla. At time t_1, the switch across the integrator capacitor is opened. The flux-locked loop settles into stable operation within 20μs, and at $t_2 = t_1 + 20\mu s$ the S/H circuit is switched to the hold mode so that data collection can begin. The output of the set-zero produces a signal for a time $t_2 \approx$ 50 ms, which is sufficiently long for the complete data aquisition of the FID signal from a solid sample. At time $t_2 + \tau_2$, the S/H circuit is switched to the sample mode, and the output returns to zero. Slightly later , at time $t_1 + \tau_1$ the flux-locked loop is disabled in preparation for another magnetic pulse.

C. Performance

The frequency response of the flux-locked SQUID is flat (± 3dB) from 0 to 200 kHz, and the equivalent flux noise of the SQUID is typically $6\mu\Phi_0 Hz^{-1/2}$ from 10 kHz to 110 kHz. The noise is higher than the intrinsic SQUID noise ($2\mu\Phi_0 Hz^{-1/2}$), probably because of spurious noise coupled into the SQUID by the transmitter circuit.

We tested the integrator reset and set zero circuits by applying a continuous sinusoidal signal to the SQUID and monitoring the voltage from the flux-locked loop at both the input and the output of the set-zero circuit. In Fig.4.2, the upper trace shows the signal at the input of the set-zero circuit; when the switch across the integrator is opened, the flux-locked loop reaches stable operation within 20μs, but with a large voltage offset; the lower trace of Fig.4.2 is the signal at the output of the set-zero circuit, showing the action of the set-zero circuit, which effectively subtracts the large offset.

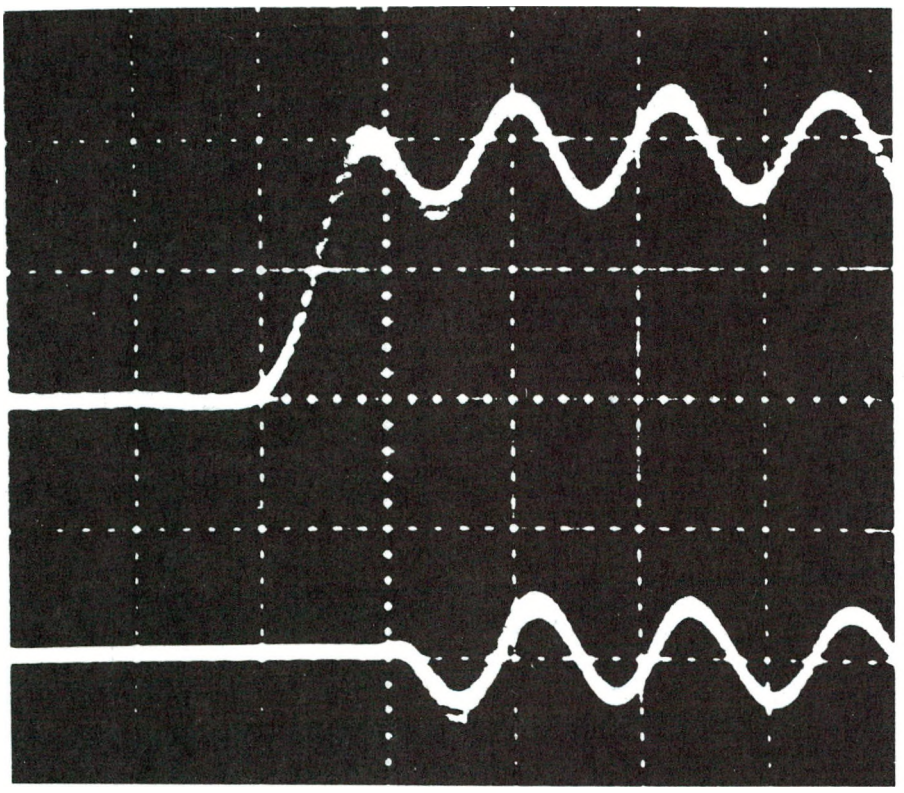

Fig. 4.2 Observed signals at input of set-zero circuit (upper trace) and output of set-zero (lower trace). Horizontal scale is 20 μs per division.

II. Spectrometer

The spectrometer is shown in Fig. 4.3; the SQUID amplifier described in Sec. I is represented by a box, with its input, output and trigger labeled. A function generator (Hewlett Packard 3314A), on receiving a trigger signal from the time base (Stanford Research Systems DG 535), produces a sinusoidal signal that typically contains 1 to 30 cycles, starting at zero phase. For spin echo experiments, a second function generator is also used. This pulse is amplified by a power amplifier (ENI 1040L) and coupled to the transmitter coil via a low pass filter (cutting off at about 300kHz) and 4 stages of cross-diodes (only one is shown in Fig. 4.3). These diodes present a high impedance to the transmitter coil when the pulse is turned off, thereby minimizing the noise coupled into the SQUID during the measurement. The pulse tips the nuclear spins, which precess to produce a free induction decay signal in the pick-up coil. This signal is amplified by the SQUID amplifier, which produces an output after receiving a trigger pulse from the time base , as explained in Sec. I.B. The amplified signal is coupled to a spectrum analyzer (Hewlett Packard 3561A) and a digital oscilloscope (Tektronix 2430A), both of which are triggered by the time base and store their data in a Hewlett Packard 9000-216 computer (not shown in the figure). The computer is also used to control the parameters of the digital osilloscope, spectrum analyzer, time base and function generators (e.g. frequency, amplitude and pulse length).

We made two cells for the spectrometer: one to detect low field NMR, and the other to detect low frequency NQR and zero field NMR. One or other of the cells is attached to a probe on which the SQUID is mounted, and which is immersed in liquid helium in a cryostat surrounded by a double mu-metal shield. The whole assembly rests on an vibration-isolation table to minimize microphonic noise. The cryostat and SQUID electronics are in a shielded room, while the remaining electronics are outside this room to

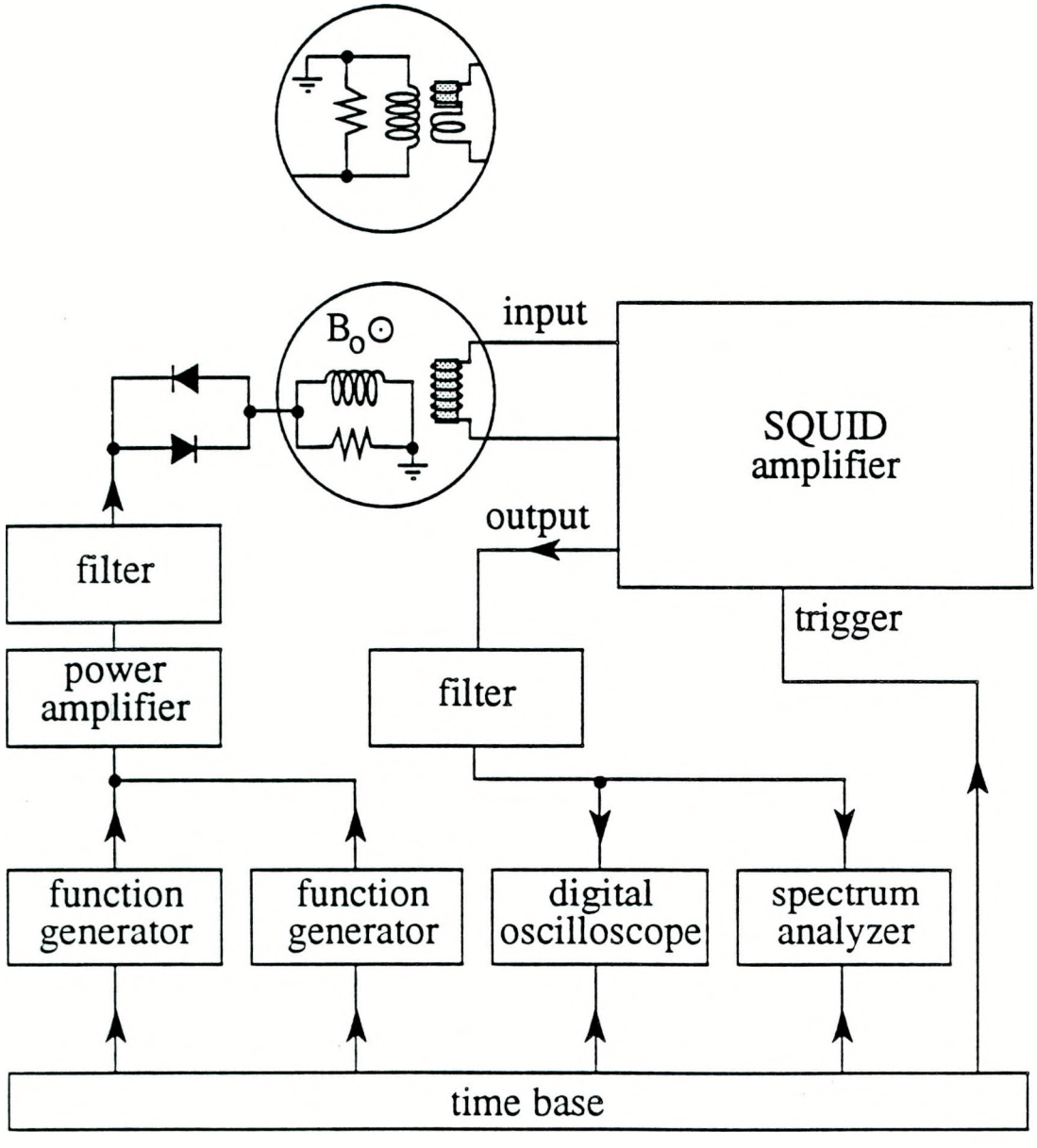

Fig. 4.3 Schematic of spectrometer. Circuit shown in circle is for NMR; circle above shows circuit for NQR.

eliminate spurious digital noise. The design and the construction of the low frequency NMR cell (circled in Fig. 4.3) and the low frequency NQR cell (inset of Fig. 4.3) are described below.

A. Low-frequency NMR cell

The sample and the various coils are enclosed in a cylindrical superconducting shield with internal length and diameter of 130mm and 30mm, respectively [Fig. 4.4]. The shield has a wall thickness of 3 mm, and was machined from a solid cylinder of lead. The materials inside the shield were chosen to minimize spurious resonance signals. The pickup and transmitter saddle coils are wound from 125μm diameter insulated Nb wire and attached orthogonally to quartz tubes 6.4 mm and 10 mm in diameter respectively. The tubes are rigidly held apart by spacers. The pickup coils have 2 turns each, and are about 6 x 8 mm in size with a total inductance of about 150 nH. The leads are twisted together, glued to the quartz tube and brought out of the cell into a second Pb cell containing the SQUID. The transmitter coils have 20 turns each, and are about 9 x 16 mm in size. The static field is provided by a superconducting solenoid wound from 225 μm diameter Cu-clad NbTi wire coated with Formvar. A thermal switch enabled us to operate the coil in the persistent current mode. The magnetic field was attenuated by the Pb tube to a value of approximately 9.5 mtesla /A. Each sample (0.2 ml) was packed in a 5 mm diameter pyrex NMR tube, and could be inserted into the middle of the pickup coil through an o-ring seal at the top of the cryostat.

B. Low-frequency NQR cell

The sample and coils are surrounded by the same Pb cell as in the NMR cell (Fig. 4.5). The pickup coil consists of a pair of two coils, each consisting of two turns of 125 μm diameter Nb wire, wound in opposition 15 mm apart on a 8.5 mm diameter quartz tube. We estimate the total inductance of this coil to be 150 nH. The transmitter coil is a

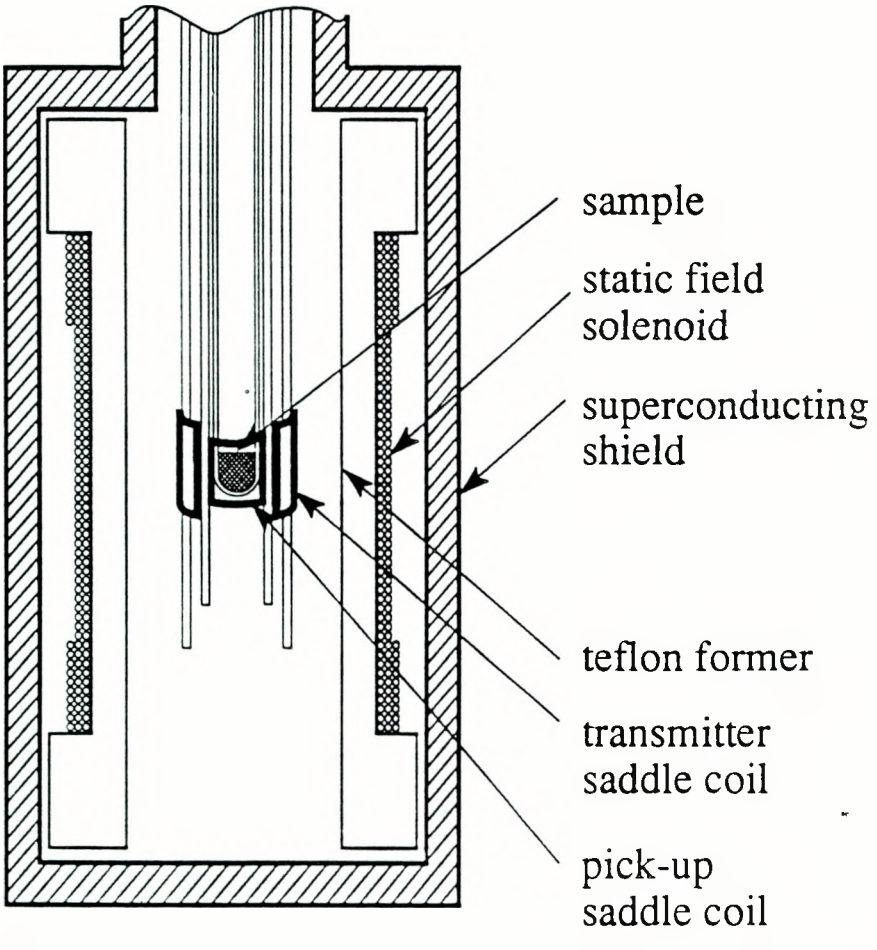

XBL 9010-4755

Fig. 4.4 Cell used to detect low-frequncy NMR.

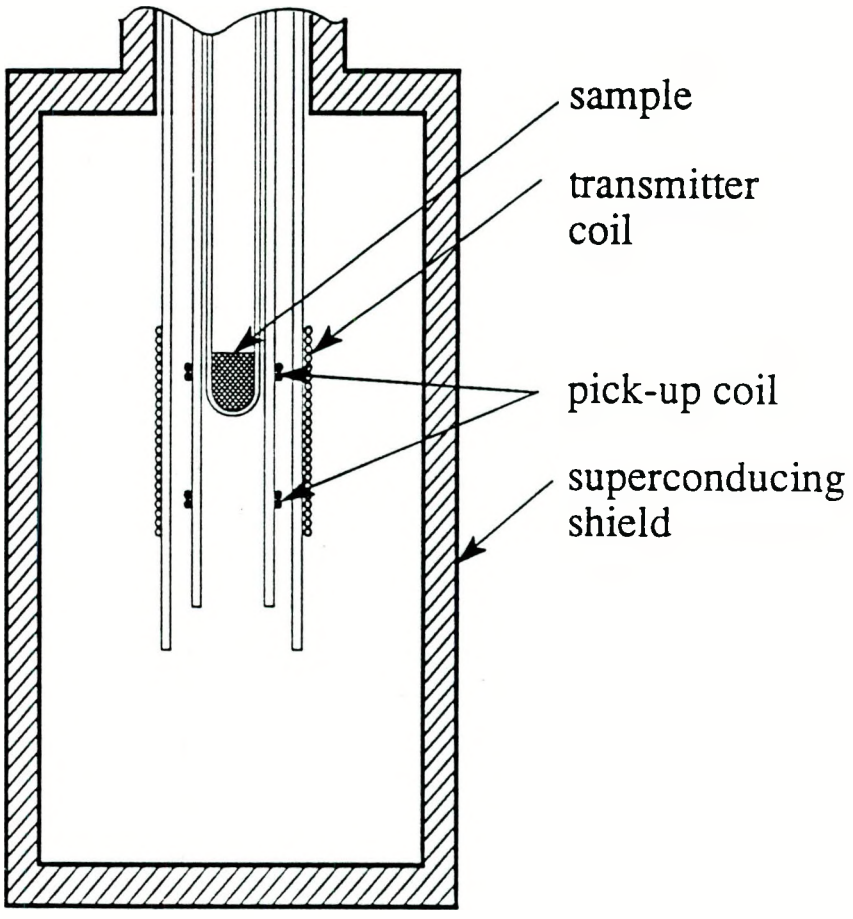

XBL 906-5597

Fig. 4.5 Cell used to detect low-frequency NQR.

30 mm long, single layer solenoid wound from 225 μm diameter Nb wire on a quartz tube with an outer diameter of 14 mm. The relative positions of the pickup and transmitter coils are adjusted empirically to achieve a balance of about 50 ppm in the pickup gradiometer. The sample, typically 0.5 ml, is packed into a 8 mm diameter pyrex NMR tube.

III. Results

A. Low-field NMR spectra

We have used two metal powders to illustrate the detection of low field NMR. The first was ^{195}Pt, which has spin 1/2 and a gyromagnetic ratio of 9.2 kHz/mtesla. At 4.2K, it has a short T_1 (10 ms), because of free electron assisted relaxation,[5] and a long T_2 (1.1 ms), because of spin exchange interaction [6]. Figure 4.6(a) shows the FID, averaged 250 times, in a 6 mtesla magnetic field. In this experiment, a 56 kHz sinewave with a peak-to-peak amplitude of about 50 μtesla and a duration of 0.4 ms was applied to the sample every 0.5s. The Fourier transform of a FID averaged 40 times is shown in Fig. 4.6(b); the resonant peak is somewhat broadened by the inhomogeneity in the magnetic field. We repeated the experiment in static fields ranging from 3 to 12 mtesla, and found the expected linear dependence of the NMR frequency.

Figure 4.7 shows the FID of ^{63}Cu and ^{65}Cu in a magnetic field of 6 mtesla averaged 256 times. The NMR frequencies of the two isotopes are too close to be resolved with such a short value of T_2. This result demonstrates that the spectrometer is able to detect signals from nuclei with T_2 as short as 50 μs.

B. Low-frequency NQR spectra

To illustrate the direct detection of low frequency NQR, we have performed experiments on three samples. Figure 4.8(a) shows the ^{2}D NQR spectrum of the quantum

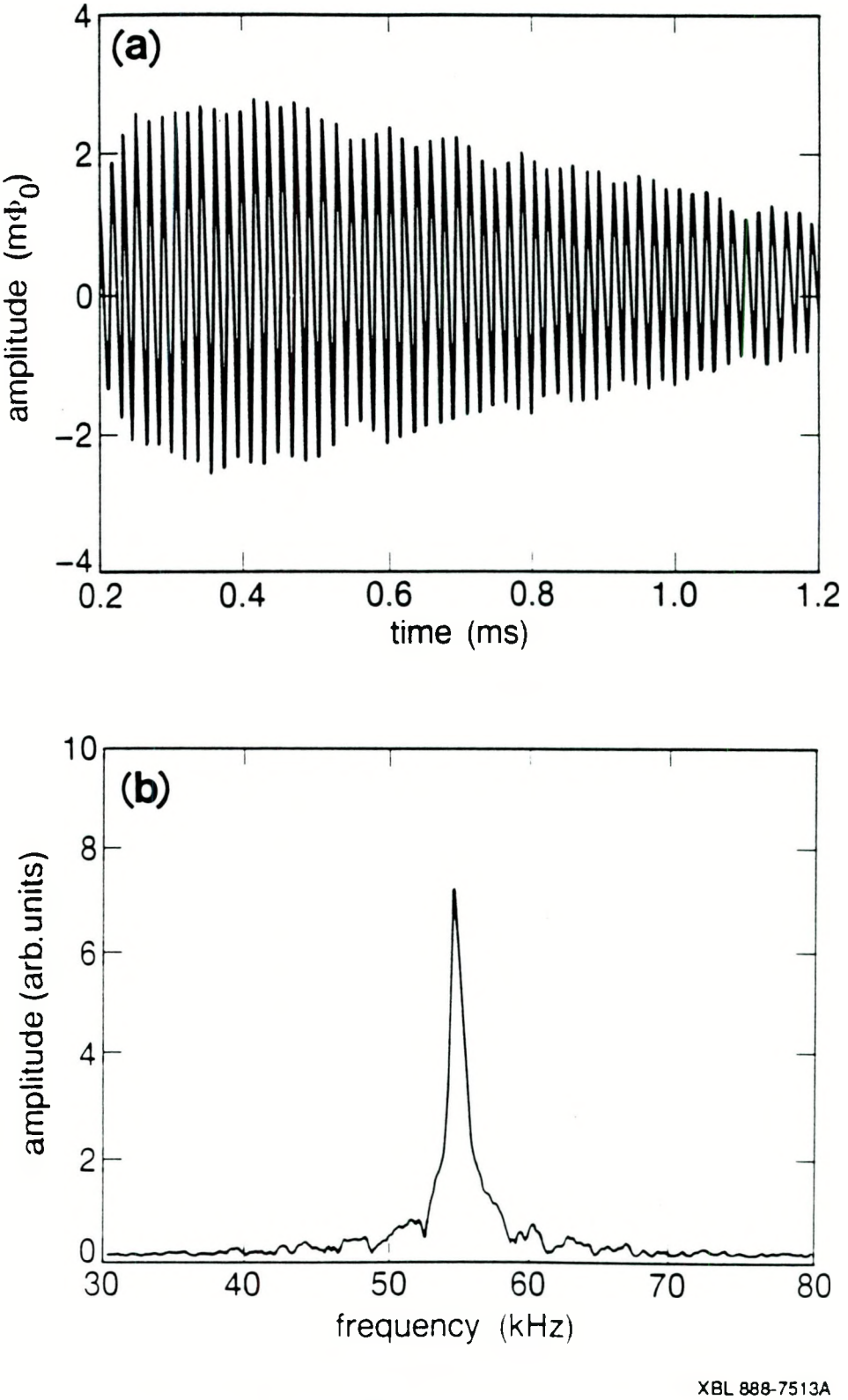

Fig. 4.6 (a) FID of ^{195}Pt in 6mT magnetic field;

(b) Fourier transform of FID in Fig. 6(a).

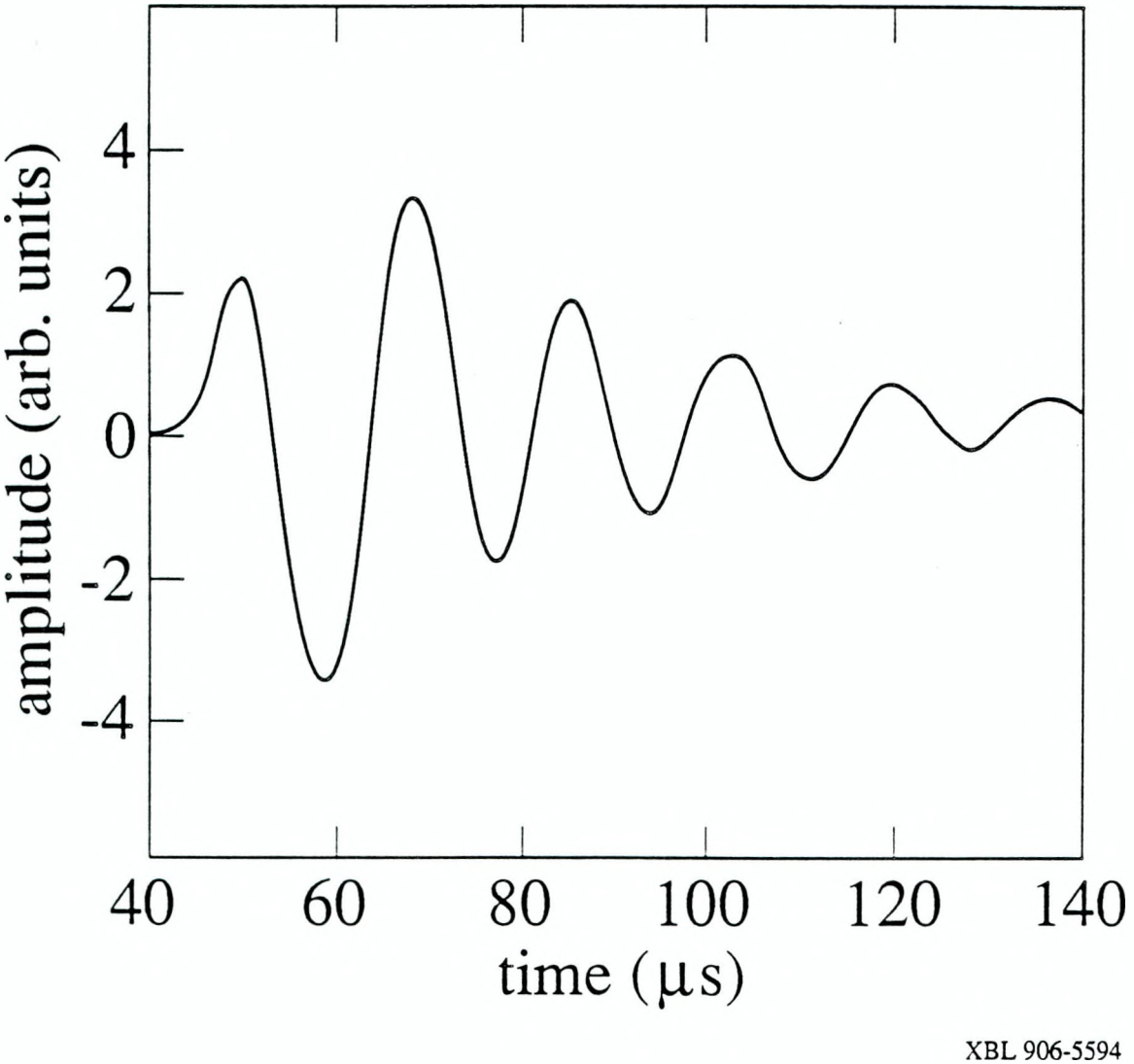

Fig. 4.7 FID from Cu metal powder in 6mT magnetic field.

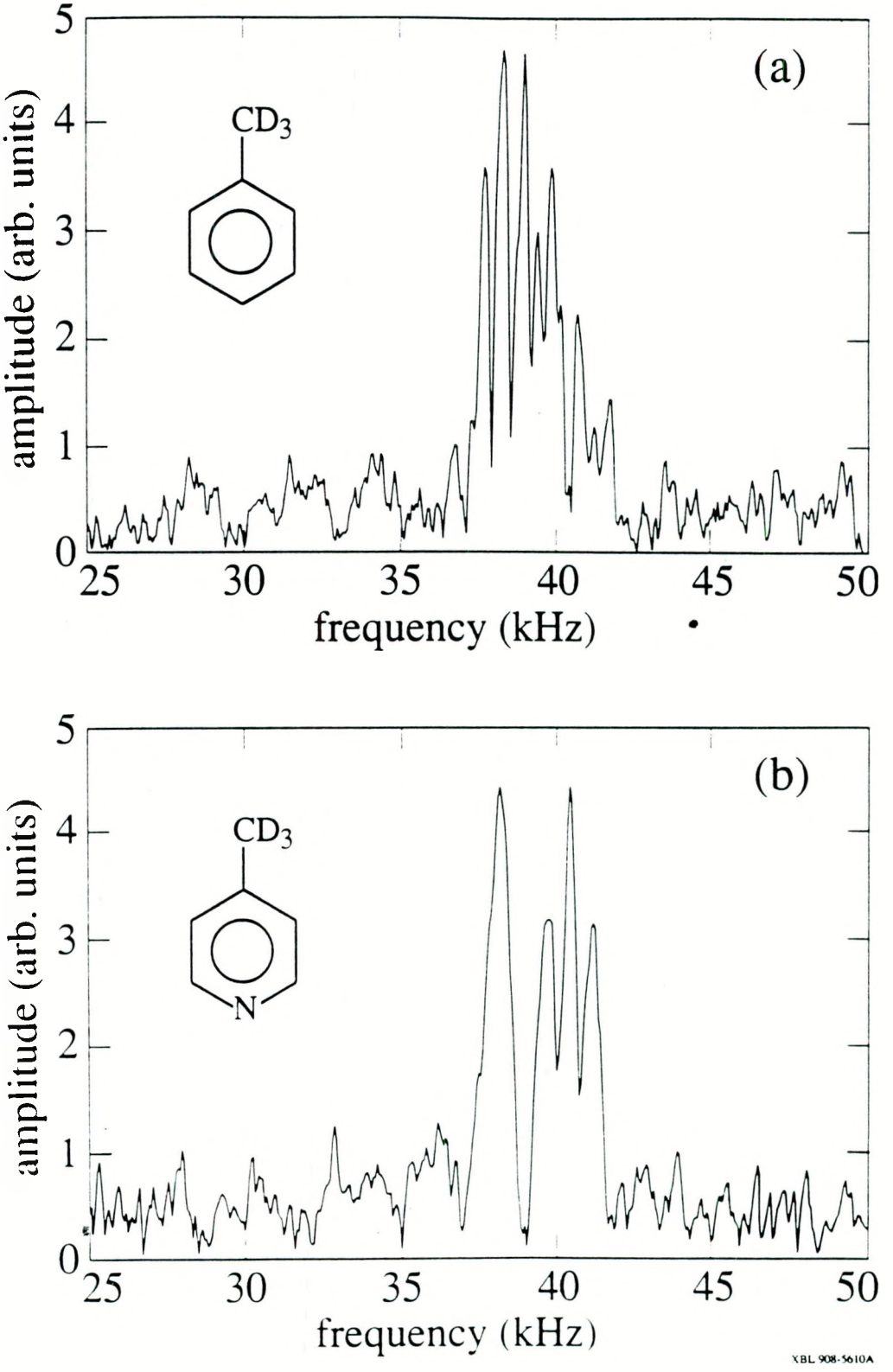

Fig. 4.8 ^{2}D NQR spectrum of tunneling methyl group in (a) perdeuterated toluene, and (b) perdeuterated picoline.

tunneling methyl group [7] in perdeuterated toluene at 1.2K, averaged 1,000 times. The pulses applied to the sample were at 44kHz with a duration of 0.2 ms, a peak-to-peak amplitude of 0.5 mtesla and a repetition rate of 0.2 Hz. Using the same pulse parameters, we also obtained the ^{2}D NQR spectrum, shown in Fig. 4.8(b) , of the tunneling methyl group in perdeuterated picoline. We believe the multiple splittings in the spectra arise partly from the magnetic dipole interactions among the ^{2}D nuclei in the methyl group, and partly from the distorted methyl groups occupying inequivalent sites in solids [8].

In the second experiment, we performed a NQR experiment with a powered NH_4ClO_4 sample. To confirm that the signals are due to the ^{14}N NQR, we measured the signal amplitude as a function of tipping angle, as shown in Fig. 4.9. We fitted the exprimental data with the expectated function $[\cos(\omega\tau)- \sin(\omega\tau)/\omega\tau]/\omega\tau$, given by Eq. 3.73, and found the gyromagnetic ratio of the nuclei responsible for the signal are within 5% of that of ^{14}N; the difference is attributed to experimental error.

In the third experiment, we performed a spin echo experiment [9] on ^{14}N nuclei in powdered NH_4ClO_4 at 1.2K. Two pulses are applied to the sample: the first is a single cycle at 45kHz with a peak-to-peak amplitude of 4 mtesla, and the second, a time Δt later, is a single cycle at the same frequency with twice the amplitude. The first pulse initiates a FID, which has a decay constant T_2^* of about 1 ms (the decay rate, $[\ T_2^*\ ]^{-1}$, includes both inhomogeneous and homogeneous contributions). The second pulse initiates a second FID, and results in an NQR echo which peaks Δt later. The sequence is repeated three times per second, and the FIDs and the spin echo are recorded with the digital oscilloscope and the spectrum analyzer. The spin echo for Δt = 4 ms, averaged 16,000 times, is shown in Fig. 4.10(a), and its Fourier transform in Fig. 4.10 (b). The spectrum consists of three peaks, at 17.4 kHz, 38.8 kHz and 56.2 kHz, arising from the ^{14}N nuclear energy levels shown inset in Fig. 4.10(b). By measuring the magnitude of the echo as a function of Δt, as shown in Fig. 4.11, we were able to deduce the decay rate $1/T_2$ due to homogeneous broadening; we found T_2 = 17.6 ms for the 17.4kHz resonant line, T_2 = 23.8 ms for the

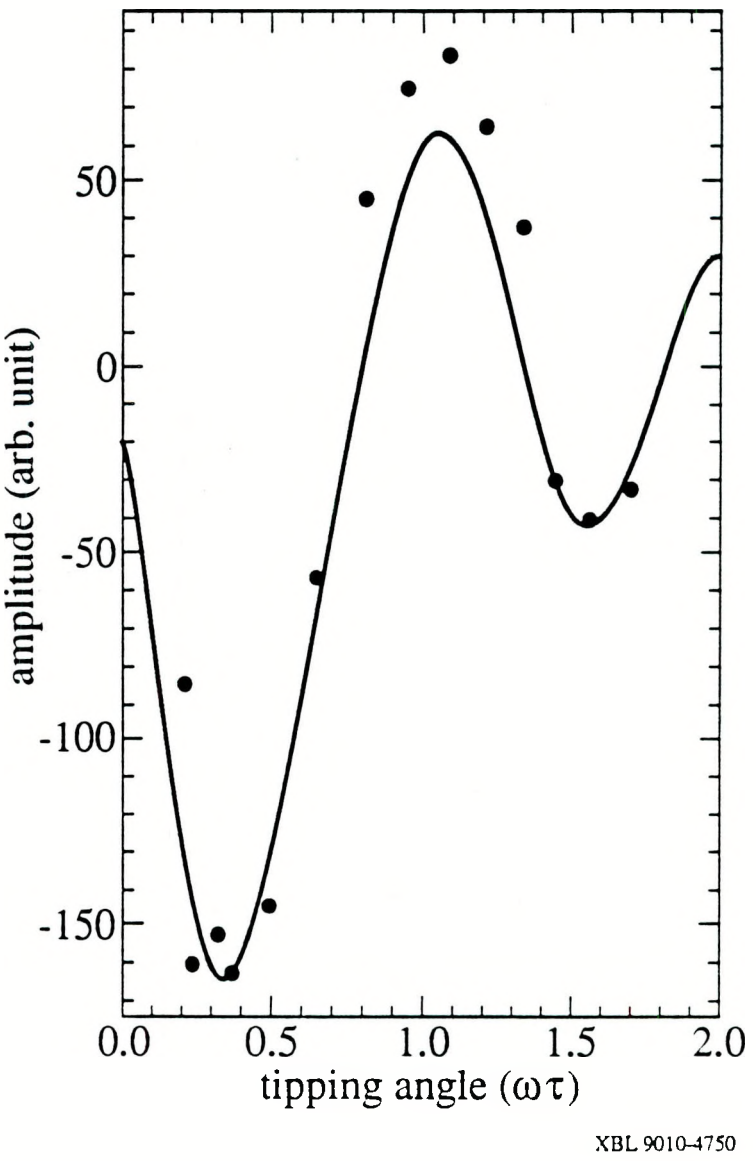

Fig. 4.9 Signal amplitude as a function of tipping angle ($\omega\tau$).
Solid lines are fitted to the theoretical function $M \propto [\cos(\omega\tau)-\sin(\omega\tau)/\omega\tau]/\omega\tau$.

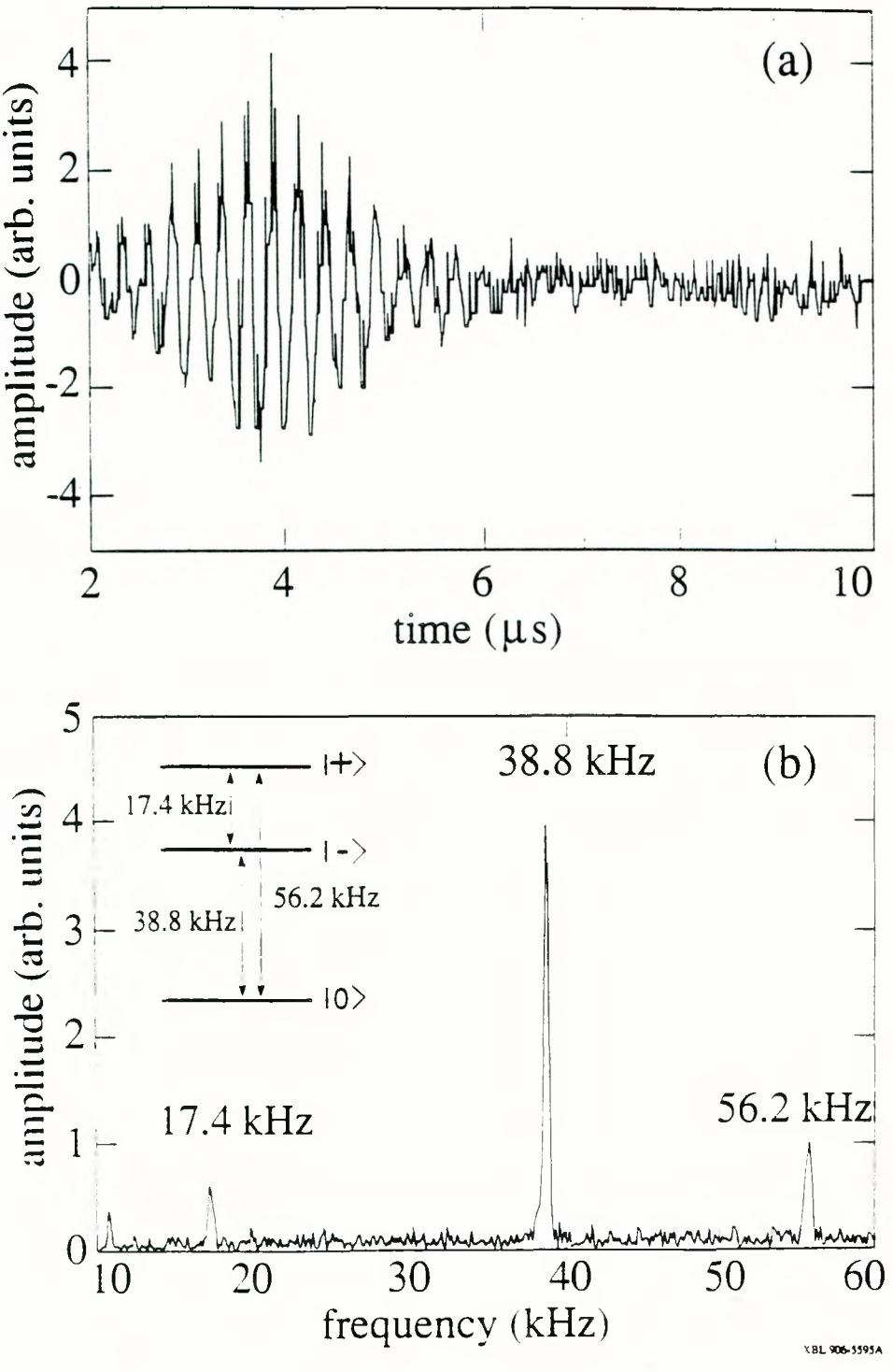

Fig. 4.10(a) Spin echo of ^{14}N nuclei in NH_4ClO_4 obtained from real-time signal demodulated with 35 kHz; (b) Fourier transform of spin echo. Three resonant peaks are due to transitions between energy levels (shown inset) of ^{14}N nuclei in presence of electric field gradient in NH_4ClO_4.

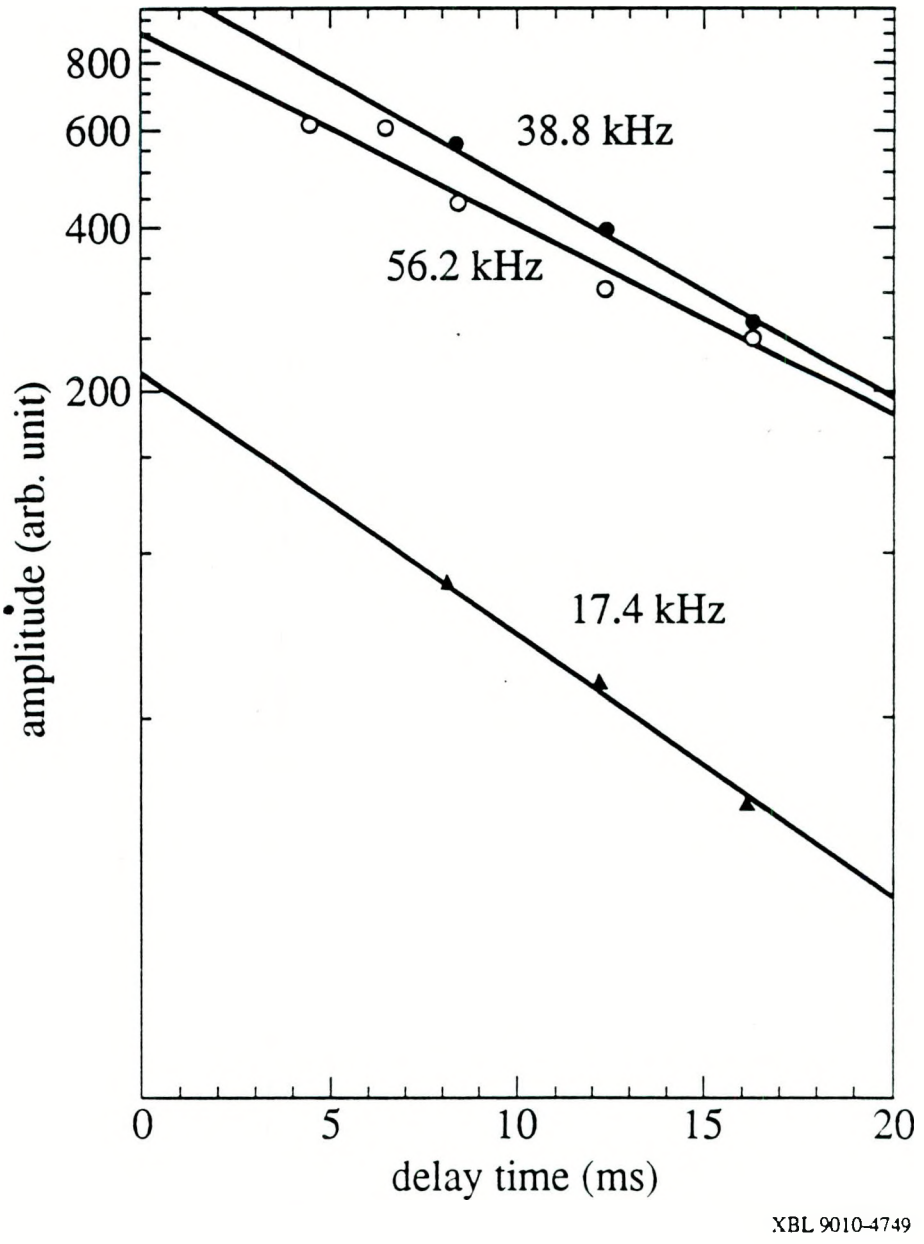

Fig. 4.11 Spin echo experiment: signal amplitude as a function of delay time.

38.8 kHz resonant line, and T_2 = 26.2 ms for the 56.2kHz resonant line. We also measured the T_1 of the sample with a stimulated echo experiment [9], in which three pulses are applied to the sample. As shown in Fig.4.12, by measuring the amplitude as a function of the delay time between the second and third pulse, we found T_1= 40 ms.

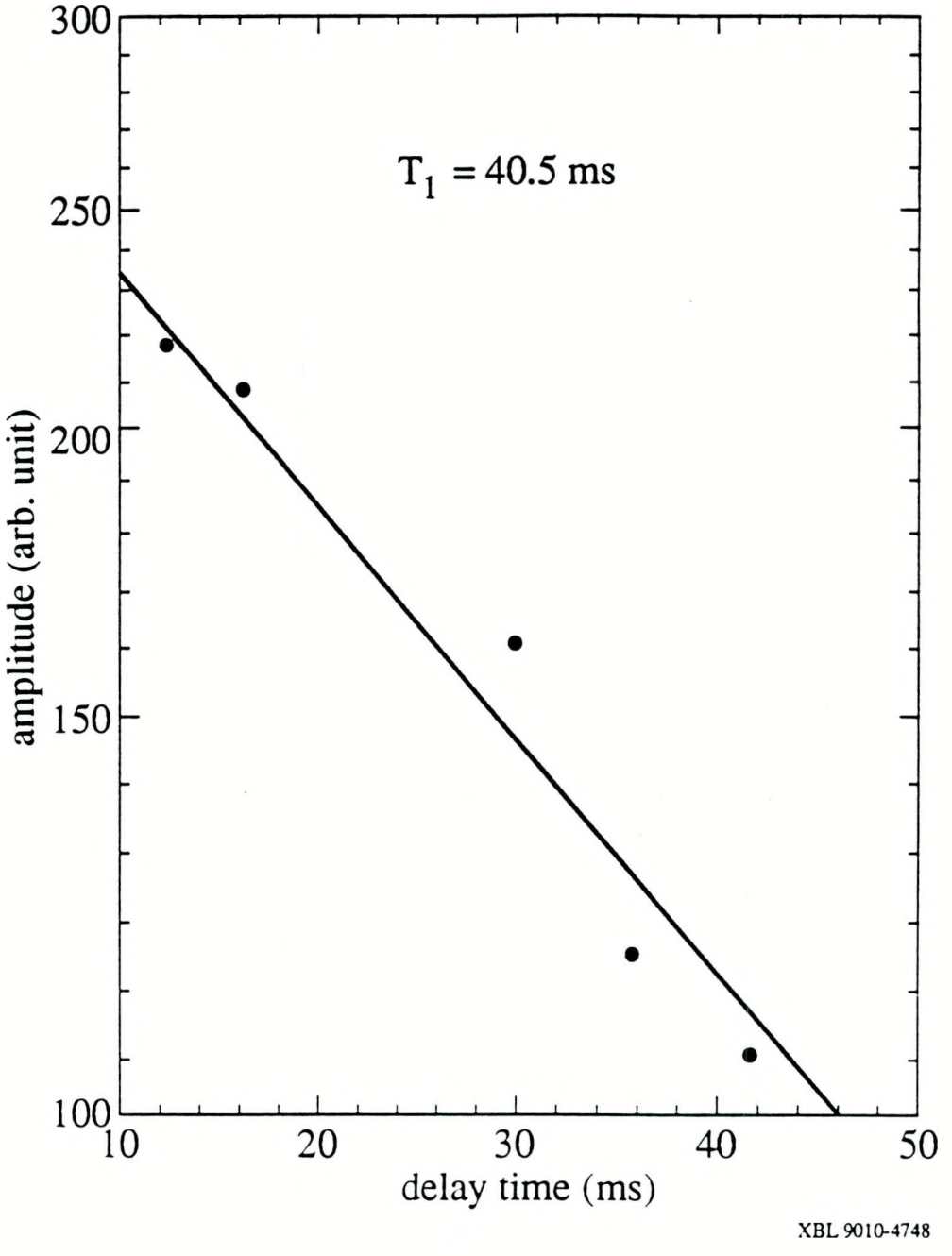

Fig. 4.12 Stimulated echo experiment: signal amplitude as a function of delay time between second and third pulse.

IV. Concluding Remarks

We have demonstrated the feasibility of measuring low-frequency NMR and NQR directly with a SQUID-based spectrometer, and are able to measure FID signals from samples with T_2 as short as 50μs. We observed all three NQR lines from ^{14}N in NH_4^+ simultaneously by using a short, large amplitude magnetic pulse. We have also obtained high resolution NQR spectra of ^2D nuclei in tunneling methyl groups, revealing detailed structure which has not previously been observed in high-field NMR spectrum of ^2D nuclei where the linewidth is broad.

The fact that we can detect low-frequency NQR suggests that we should be able to obtain ZFNMR spectra, which is detected in a similar manner and should produce signals comparable in amplitude and frequency. Our major difficulty in detecting ZFNMR has been that many suitable samples have very long T_1 (>> 100 sec) at liquid ^4He temperatures. Our choice of NQR samples has been similarly restricted.

Because of the restriction that the sample must be cooled to 4.2K or lower, we are currently constructing a second spectrometer that will allow us to vary the temperature of the sample from the bath temperature to 100K or higher while maintaining the SQUID and input circuit at the bath temperature. This system will not only greatly broaden the choice of samples, but also enable us to study the temperature dependence of a given resonance. To reduce the averaging time in obtaining a spectrum, we also hope to improve the sensitivity of the SQUID amplifier by decreasing the inductance of the SQUID and adding a second, cooled transformer.

1. J. Clarke, NATO ASI Series Vol. 59, *Superconductive Electronics*, edited by M.Nisenoff and H. Weinstock (Springer, Berlin, 1989), p.87.

2. R. A. Webb, Rev. Sci. Instrum. **48**, 1585 (1977).

3. F. Wellstood, C. Heiden, and J. Clarke, Rev. Sci. Instrum. **55**, 952 (1984).

4. L. J. Friedman, A. K. M. Wennberg, S. N. Ytterboe, and H. M. Bozler, Rev. Sci. Instrum. **57**,410 (1986).

5. A. Abragram, ref.(2), Chap.IX; C. P. Slichter, ref.(2), Chap. 5.

6. R. E. Walstedt, Phys. Rev. **138**, A1097 (1965).

7. R. A. Wind, S. Emid, D. J. Lighthelm, J. F. J. M. Pourquie, and J. Smidt, Bulletin of Magnetic Resonance **6**, 71 (1980).

8. M. Anderson, L. Bosio, J. Bruneaux-Poulle and R. Fourme, J. Chimie Physique **74**, 68 (1977).

9. E. L. Hahn, Phys. Rev. **80**, 580 (1950).

CHAPTER 5

ZERO FIELD NMR SPECTRA OF METHYL GROUP

In the last chapter of this thesis, I will discuss the possibility of detecting zero field NMR directly with our spectrometer. In principle, ZFNMR can be detected the same way that NQR is detected -- if their resonant frequencies are comparable, their signal strengths are also comparable. In practice, however, it is extremely difficult to find a sample that has a ZFNMR signal which has a long T_2 and short T_1 at liquid helium temperature. I believe the most promising samples are those molecular solids in which the molecule contains methyl groups (or ammonia ions) which undergo fast quantum tunneling at liquid helium temperature. In sec. I, I discuss the motion of a methyl group without taking into account the nuclear spin wave functions. In sec. II, I discuss the energy levels of a methyl group with nuclear dipole- dipole interactions taken into account, and calculate the ZFNMR frequency from a methyl group.

I. Energy Levels of Methyl Groups

A. Free rotation and hindered rotation

To illustrate the symmetry properties of a methyl group, I start this chapter with a discussion of the simplest case involving a methyl group -- the methyl group rotating freely about its symmetrical axis (the axis passing through the C atom and the center of the triangle formed by the three H atoms). The Hamitonian of this one dimensional free rotor is

$$H = \frac{J_Z^2}{2I} , \tag{5.1}$$

where J_Z is the angular momentum of the rotor and I is its momentum of inertia. The

angular momentum is always along the symmetry axis which I choose to be the Z axis. The energy levels of the rotor are

$$E = M^2 \frac{\hbar^2}{2I}, \quad M = 0, \pm 1, \pm 2, \ldots \tag{5.2}$$

and the eigenstate is $| M \rangle$, the eigenstate of J_Z,

$$J_Z | M \rangle = M\hbar | M \rangle. \tag{5.3}$$

In spacial representation, the eigenstate is

$$\Psi_M (\phi) = \frac{1}{\sqrt{2\pi}} \exp (i M\phi). \tag{5.4}$$

The symmetry of the wave function is classified according its transformation under the operator C_3 which rotates the CH_3 group by 120^0. Since

$$C_3 \Psi_M (\phi) = \exp (i 2\pi M/3) \Psi_M (\phi) \tag{5.5}$$

and $\exp (i 2\pi M/3)$ can take three values (1, ε, and ε^*, where $\varepsilon = \exp [i2\pi/3]$), the wave functions have three kinds of symmetries:

(i) if $M = 3n$, $n = 0, \pm 1, \pm 2, \ldots$

$$C_3 \Psi_M (\phi) = \Psi_M (\phi), \tag{5.6}$$

and $\Psi_M (\phi)$ has A symmetry;

(ii) if $M = 3n+1$, $n = 0, \pm 1, \pm 2, \ldots$

$$C_3 \Psi_M (\phi) = \varepsilon \Psi_M (\phi), \tag{5.7}$$

and $\Psi_M (\phi)$ has E_a symmetry;

(iii) if $M = 3n+2$, $m = 0, \pm 1, \pm 2, \ldots$

$$C_3 \Psi_M (\phi) = \varepsilon^* \Psi_M (\phi), \tag{5.8}$$

and $\Psi_M (\phi)$ has E_b symmetry.

The energy levels along with their symmetries are plotted in Fig. 5.1. Except for $M = 0$, all the energy levels are doubly degenerate.

A methyl group can be considered as a free rotor only in the most ideal situation, for example, when the methyl group is isolated from all other atoms or molecules in a material.

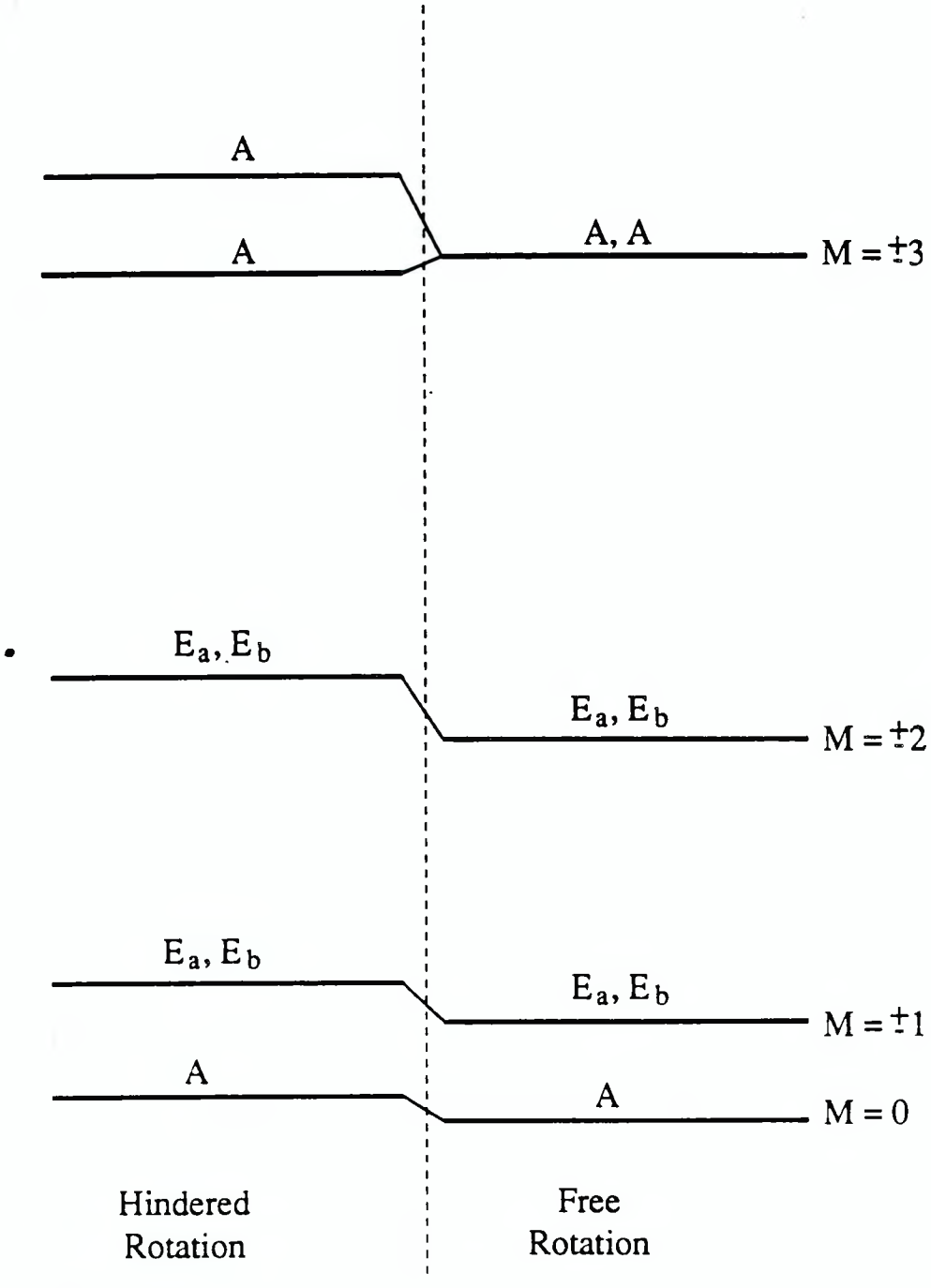

Fig. 5.1 Energy levels of CH_3 for free and hindered rotation.

In reality, however, a methyl group is electrically coupled to other atoms or molecules and the motion of a methyl group is described by the Hamiltonian

$$H = \frac{J_Z^2}{2I} + V(\phi), \tag{5.9}$$

where the potential term $V(\phi)$ has a three fold symmetry,

$$C_3\, V(\phi)\, C_3^{-1} = V(\phi). \tag{5.10}$$

The simplest example of $V(\phi)$ is of the form

$$V(\phi) = V_3 \cos 3\phi. \tag{5.11}$$

If the barrier $|V(\phi)|$ is much smaller than $\hbar^2/2I$, the energy levels and the eigenstates can be calculated by perturbation theory; the motion of the methyl group in this limit are usually referred to as hindered rotation. Figure 5.1 also shows the energy levels of a methyl group that undergoes hindered rotation. Compares with the case of free rotation, energy levels with A symmetry are now no longer degenerate, but those with E_a and E_b symmetries are still degenerate and they are shifted together by the potential term. This degeneracy is due to time reversal symmetry and can be lifted only by magnetic fields.

In zero magnetic field, the system is invariant under the time reversal operation K. Under the operation K,

$$K\,|\,E_a\rangle = |\,E_b\rangle, \tag{5.12}$$

$$K\,|\,E_b\rangle = |\,E_a\rangle, \tag{5.13}$$

where $|\,E_a\rangle$ and $|\,E_b\rangle$ represent a state with E_a and E_b symmetry, respectively. The subspace spanned by all the eigenstates within an energy level must be invariant under both the time reversal operation K and the symmetry operation C_3. Such kind of subspace must contain both $|\,E_a\rangle$ and $|\,E_b\rangle$ states; therefore, $|\,E_a\rangle$ and $|\,E_b\rangle$ are always degenerate in zero magnetic field.

B. Torsional vibration and quantum tunneling

The hindered rotation discussed above usually describes the motion of a methyl group in molecules which are in gas form, where the potential term is small. If the potential term is not small as in the case for a solid, the motion of a methyl group is best described by torsional vibration and quantum tunneling.

Torsional vibration describe the case when a methyl group interacts so strongly with the surrounding atoms and molecules in a solid that the orientations of its three hydrogen atoms are almost fixed in space. If we imaging the methyl group as a rigid rotor, the rotor is so strongly confined that it can not rotate any more; instead, it undergoes torsional vibration about its equilibrium position. Because the three hydrogen atoms are identical particles, the rigid rotor has three equilibrium positions. We represent these three states by $|\upsilon, \alpha\rangle$, $|\upsilon, \beta\rangle$ and $|\upsilon, \gamma\rangle$, and they can be transformed into each other by the symmetry operation C_3, that is

$$C_3 |\upsilon, \alpha\rangle = |\upsilon, \beta\rangle, \tag{5.14}$$

$$C_3 |\upsilon, \beta\rangle = |\upsilon, \gamma\rangle, \tag{5.15}$$

$$C_3 |\upsilon, \gamma\rangle = |\upsilon, \alpha\rangle, \tag{5.16}$$

where υ is the quantum number of the torsional vibration. The torsional vibration of a methyl group is equivalent to a particle confined in a three-well potential $V(\phi)$, as shown in Fig. 5.2. Figure 5.2 also shows the vibration energy levels. Since the rigid rotor can be in one of the three equilibrium positions, the particle in Fig. 5.2 can be in one of the three wells. If the barriers between the wells are infinite, the particle will be confined in one of the wells. Because there are three wells, each vibrational energy level is three fold degenerate. However, if the barrier is finite, the particle can tunneling from one well into another and the three fold degeneracy is lifted. This is the situation when the methyl group undergoes quantum tunneling in solids.

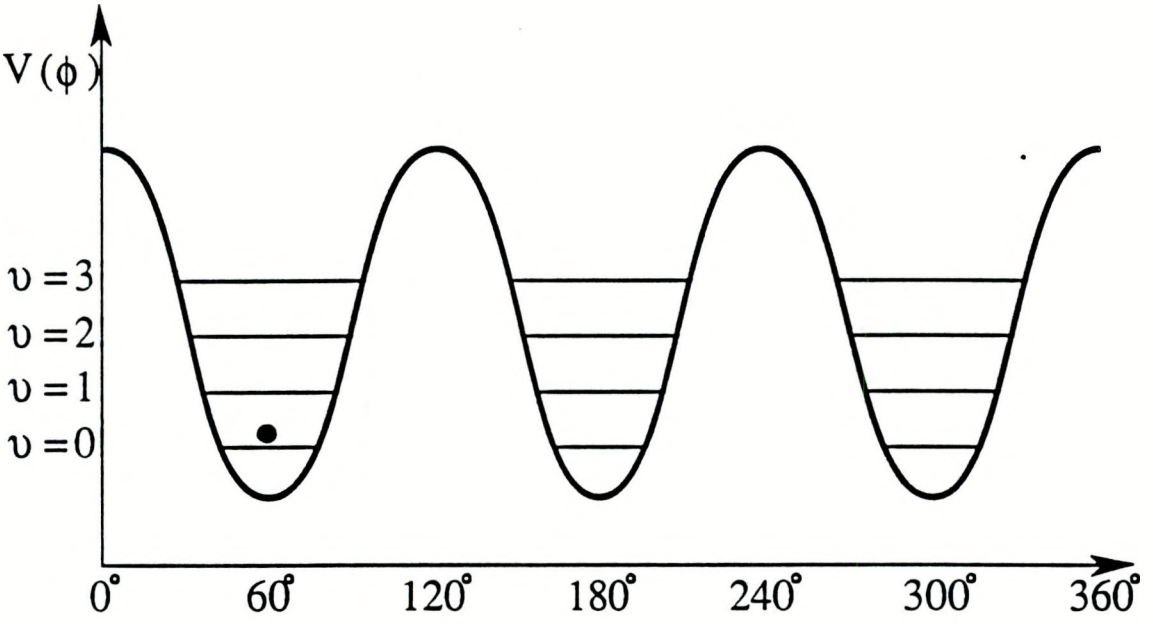

XBL 9011-4770

Fig. 5.2 Particle in three-well potential.

The quantum tunneling of a methyl group at torsional vibration state υ can be described by a tunneling Hamitonian H_T^{υ}. In the subspace spanned by $|\upsilon, \alpha\rangle$, $|\upsilon, \beta\rangle$ and $|\upsilon, \gamma\rangle$, H_T^{υ} is given by

$$H_T^{\upsilon} = -\begin{bmatrix} 0 & \Delta_\upsilon & \Delta_\upsilon \\ \Delta_\upsilon & 0 & \Delta_\upsilon \\ \Delta_\upsilon & \Delta_\upsilon & 0 \end{bmatrix}. \tag{5.17}$$

Here, the parameter Δ_υ is positive if υ is even and negative if υ is odd, and Δ_υ decreases as υ increases. The eigenstates of the Hamitonian are

$$|\upsilon, A\rangle = (|\upsilon, \alpha\rangle + |\upsilon, \beta\rangle + |\upsilon, \gamma\rangle)/\sqrt{3}, \tag{5.18}$$

$$|\upsilon, E_a\rangle = (|\upsilon, \alpha\rangle + \varepsilon|\upsilon, \beta\rangle + \varepsilon^*|\upsilon, \gamma\rangle)/\sqrt{3}, \tag{5.19}$$

$$|\upsilon, E_b\rangle = (|\upsilon, \alpha\rangle + \varepsilon^*|\upsilon, \beta\rangle + \varepsilon|\upsilon, \gamma\rangle)/\sqrt{3}, \tag{5.20}$$

where states $|\upsilon, A\rangle$, $|\upsilon, E_a\rangle$ and $|\upsilon, E_b\rangle$ have A, E_a and E_b symmetries respectively, that is

$$C_3|\upsilon, A\rangle = |\upsilon, A\rangle, \tag{5.21}$$

$$C_3|\upsilon, E_a\rangle = \varepsilon|\upsilon, E_a\rangle, \tag{5.22}$$

$$C_3|\upsilon, E_b\rangle = \varepsilon^*|\upsilon, E_b\rangle. \tag{5.23}$$

States $|\upsilon, A\rangle$, $|\upsilon, E_a\rangle$ and $|\upsilon, E_b\rangle$ have energies $-2\Delta_\upsilon$, Δ_υ and Δ_υ respectively, as shown in Fig. 5.3. Because of the time reversal symmetry in zero magnetic field, $|\upsilon, E_a\rangle$ and $|\upsilon, E_b\rangle$ are degenerate. The quantum tunneling frequency ω_t is determined by

$$\hbar\omega_t = 3\Delta_\upsilon. \tag{5.24}$$

The quantum tunneling frequency of a methyl CH_3 group can be as small as a few kHz and as large as 200 GHz. The smaller the barrier the larger the tunneling frequency. Figure 5.4 shows that as the barrier decrease from infinity to zero, the motion of the methyl group changes from pure torsional vibration to quantum tunneling, then to hindered rotation, and finally to free rotation.

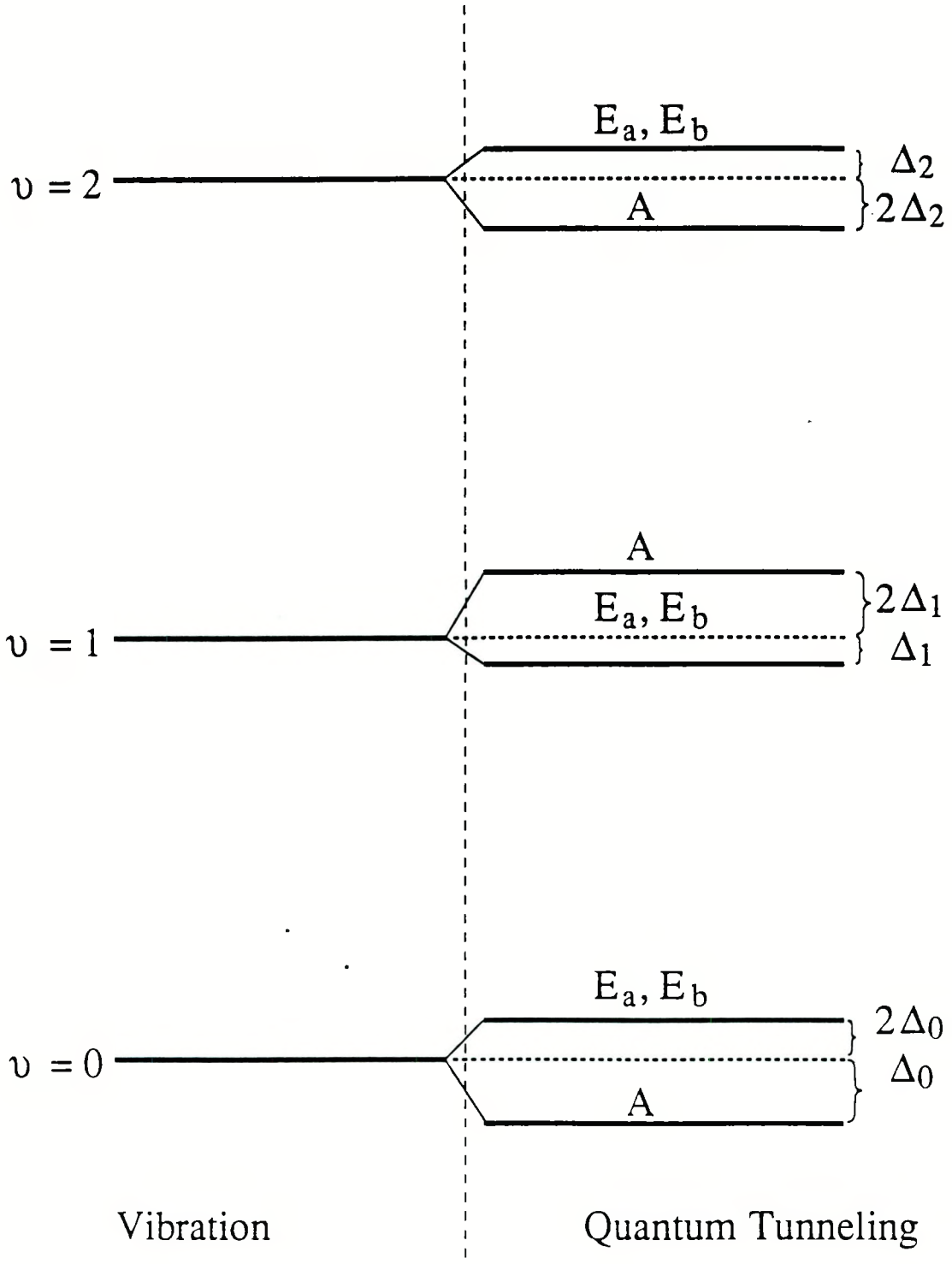

XBL 9011-4767

Fig. 5.3 Energy levels of CH_3 for tosional vibration and quantum tunneling.

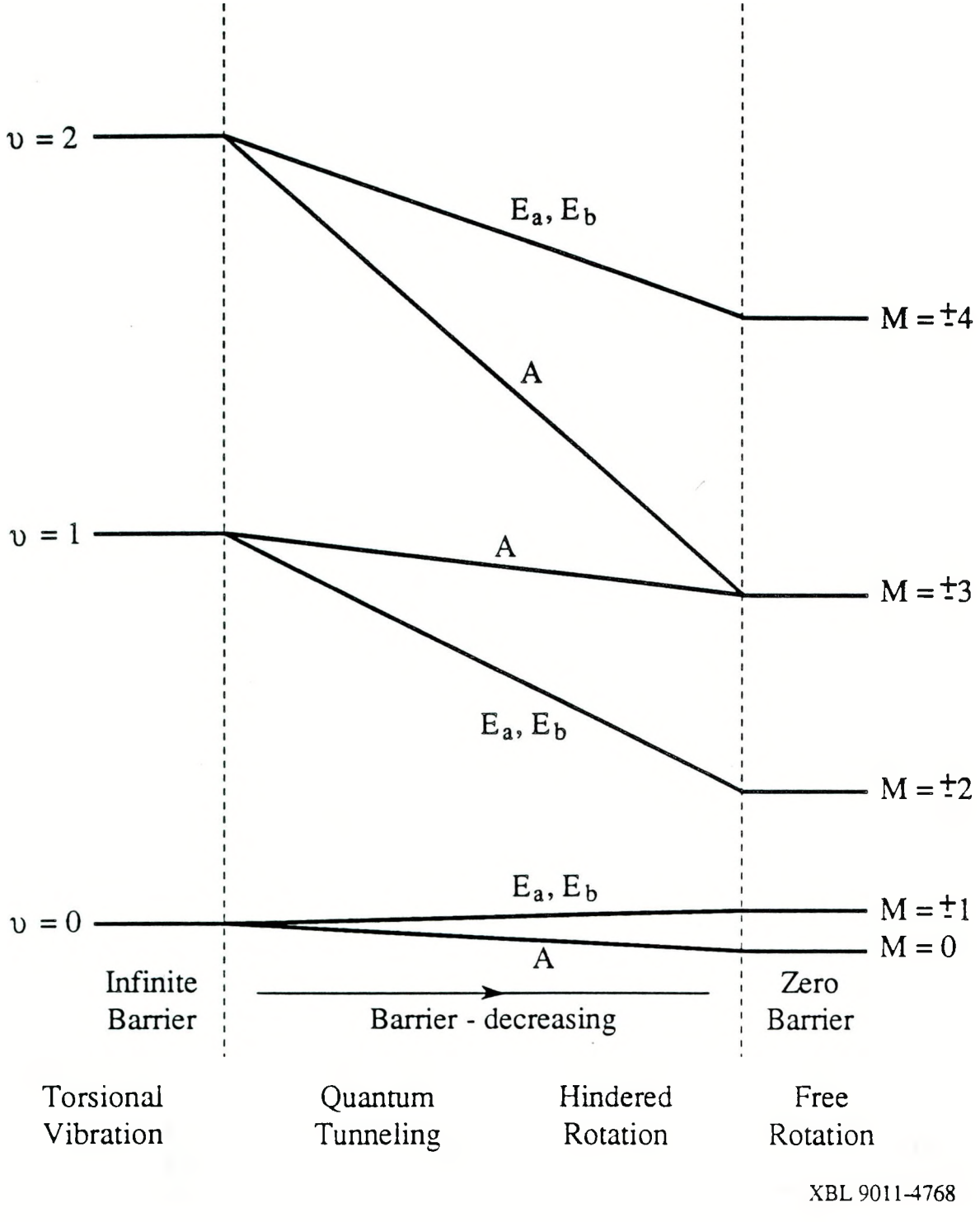

Fig. 5.4 Energy levels of CH_3 as the barrier decreases from infinity to zero.

II. ZFNMR Spectra of Methyl Group

A. Symmetry of spin wave functions

The total wave function of a methyl group is the product of the spacial wave function $|\Psi\rangle$ and the spin wave function $|\chi\rangle$ Since the methyl group CH_3 contains three identical fermions, the total wave function is antisymmetric with respect to the exchange of two protons. And since the symmetry operation C_3 can be achieved by two exchange operations, the total wave function must be symmetric with respect to C_3 operation,

$$C_3 |\Psi\rangle|\chi\rangle = |\Psi\rangle|\chi\rangle. \tag{5.25}$$

This equation requires th efollowing combinations of special wave functions and spin wave functions:

i) if $|\Psi\rangle$ has A symmetry, $|\chi\rangle$ must have A symmetry;

ii) if $|\Psi\rangle$ has E_a symmetry, $|\chi\rangle$ must have E_b symmetry;

iii) if $|\Psi\rangle$ has E_b symmetry, $|\chi\rangle$ must have E_a symmetry.

The spacial wave functions are discussed in Sec. I, and the total spin wave functions are constructed from the wave functions of the three spin 1/2 nuclei. If we use $|+\rangle$ and $|-\rangle$ to indicate spin up spin down states, respectively, the wave functions with A symmetry are given by

$$|A\ 3/2\ \ 3/2\rangle = |+\rangle|+\rangle|+\rangle, \tag{5.26}$$

$$|A\ 3/2\ \ 1/2\rangle = (|-\rangle|+\rangle|+\rangle + |+\rangle|-\rangle|+\rangle + |+\rangle|+\rangle|-\rangle)/\sqrt{3}, \tag{5.27}$$

$$|A\ 3/2\ -1/2\rangle = (|+\rangle|-\rangle|-\rangle\ + |-\rangle|+\rangle|-\rangle + |-\rangle|-\rangle|+\rangle)/\sqrt{3}, \tag{5.28}$$

$$|A\ 3/2\ -3/2\rangle = |-\rangle|-\rangle|-\rangle. \tag{5.29}$$

These states have I = 3/2 and I_Z = + 3/2, 1/2, -1/2, -3/2, respectively (I is the total spin and I_Z is the projection of the total spin in Z axis). Wave functions with E_a symmetry are given by

$$| E_a\ 1/2\ \ 1/2 \rangle = (|-\rangle|+\rangle|+\rangle + \varepsilon |+\rangle|-\rangle|+\rangle + \varepsilon^* |+\rangle|+\rangle|-\rangle)/\sqrt{3}, \quad (5.30)$$

$$| E_a\ 1/2\ -1/2 \rangle = (|+\rangle|-\rangle|-\rangle + \varepsilon |-\rangle|+\rangle|-\rangle + \varepsilon^* |-\rangle|-\rangle|+\rangle)/\sqrt{3}, \quad (5.31)$$

and are states with I =1/2 and I = 1/2, -1/2, respectively. Wave functions with E_b symmetry are given by

$$| E_b\ 1/2\ \ 1/2 \rangle = (|-\rangle|+\rangle|+\rangle + \varepsilon^* |+\rangle|-\rangle|+\rangle + \varepsilon |+\rangle|+\rangle|-\rangle)/\sqrt{3}, \quad (5.32)$$

$$| E_b\ 1/2\ -1/2 \rangle = (|+\rangle|-\rangle|-\rangle + \varepsilon^* |-\rangle|+\rangle|-\rangle + \varepsilon |-\rangle|-\rangle|+\rangle)/\sqrt{3}, \quad (5.33)$$

and are states with I =1/2 and I = 1/2, -1/2, respectively.

B. Energy levels of methyl groups due to dipole-dipole interaction

Figure 5.5 shows the energy levels of a methyl group. The energy difference between vibration states are so large that at liquid helium temperature only the ground state is occupied; therefore, we concentrate our attention on that energy level. Because of the quantum tunneling, this energy level is split. The new ground state has A symmetry, and has a total spin 3/2 (four fold degeneracy in spin states). The first excitation states are doubly degenerate in the spacial wave function with E_a and E_b symmetry, and each of them has a total spin 1/2 (additional two-fold degeneracy in spin states for each spacial state).

While the dipole- dipole interaction will not influence the states in the first excitation energy level, the interaction will make the energy level of the ground state split into two levels, both of which are doubly degenerate. In the following, I will discuss this effect of the dipole-dipole interaction in detail.

The Hamitonian describing the dipole- dipole interaction is (c.f. Chp. 3, Sec. II)

$$H_d = \hbar\,\omega_d \sum_{i<j} \sum_{q} (-1)^q T^{\,q}_{\,2}(i,j) Y^{-q}_{\,2}(\theta_{ij}), \quad i, j = 1, 2, 3, \quad (5.34)$$

where

$$\hbar\,\omega_d = \gamma^2\hbar^2/r^3, \quad (5.35)$$

$Y^{-q}_{\,2}(\theta_{ij})$ is the second order spherical harmonic function (θ_{ij} is the angle between the Z

axis and the vector pointing from spin i to spin j, in this case, $\theta_{ij} = \pi/2$), and T_2^q (i, j) is defined by

$$T_2^0 (i, j) = \sqrt{4\pi/5} \, (I_i \cdot I_j - 3 I_{iz} I_{jz}), \tag{5.36}$$

$$T_2^{\pm 1} (i, j) = \mp \sqrt{6\pi/5} \, (I_{iz} I_{j\pm} + I_{i\pm} I_{jz}), \tag{5.37}$$

$$T_2^{\pm 2} (i, j) = - \sqrt{6\pi/5} \, (I_{i\pm} I_{j\pm}) . \tag{5.38}$$

Because $\Theta_{ij} = \pi/2$, $Y_2^0(\pi/2) = - \sqrt{5/16\pi}$, $Y_2^{\pm 1} (\pi/2) = 0$ and

$Y_2^{\pm 2} (\pi/2) = \sqrt{15/32\pi} \exp(\pm 2i\phi)$.

(1) First excitation energy level

Since $T_2^{\pm 2} (i, j)$ flips two spins at the same time and results in a change $|\Delta I_Z| = 2$, this term makes no contribution to the first excitation state where I =1/2 and the maximum change of I_Z is 1. To calculate the influence of the dipole-dipole interaction on the first excitation states, we need to calculate $\langle 0\, E_a | H_d | 0\, E_b \rangle$, $\langle 0\, E_a | H_d | 0\, E_a \rangle$ and $\langle 0\, E_b | H_d | 0\, E_b \rangle$ (cf. Eqs. 5.19 and 5.20):

$$\langle 0\, E_a | H_d | 0\, E_b \rangle = \hbar \omega_d \sum_{i<j} T_2^0 (i, j) \langle 0\, E_a | Y_2^{-0} (\pi/2) | 0\, E_b \rangle = 0, \tag{5.39}$$

$$\langle 0\, E_a | H_d | 0\, E_a \rangle = \hbar \omega_d \sum_{i<j} T_2^0 (i, j) \langle 0\, E_a | Y_2^{-0} (\pi/2) | 0\, E_a \rangle$$

$$= - \frac{\hbar \omega_d}{2} \sum_{i<j} T_2^0 (i, j), \tag{5.40}$$

$$\langle 0\, E_b | H_d | 0\, E_b \rangle = \hbar \omega_d \sum_{i<j} T_2^0 (i, j) \langle 0\, E_b | Y_2^{-0} (\pi/2) | 0\, E_b \rangle$$

$$= - \frac{\hbar \omega_d}{2} \sum_{i<j} T_2^0 (i, j). \tag{5.41}$$

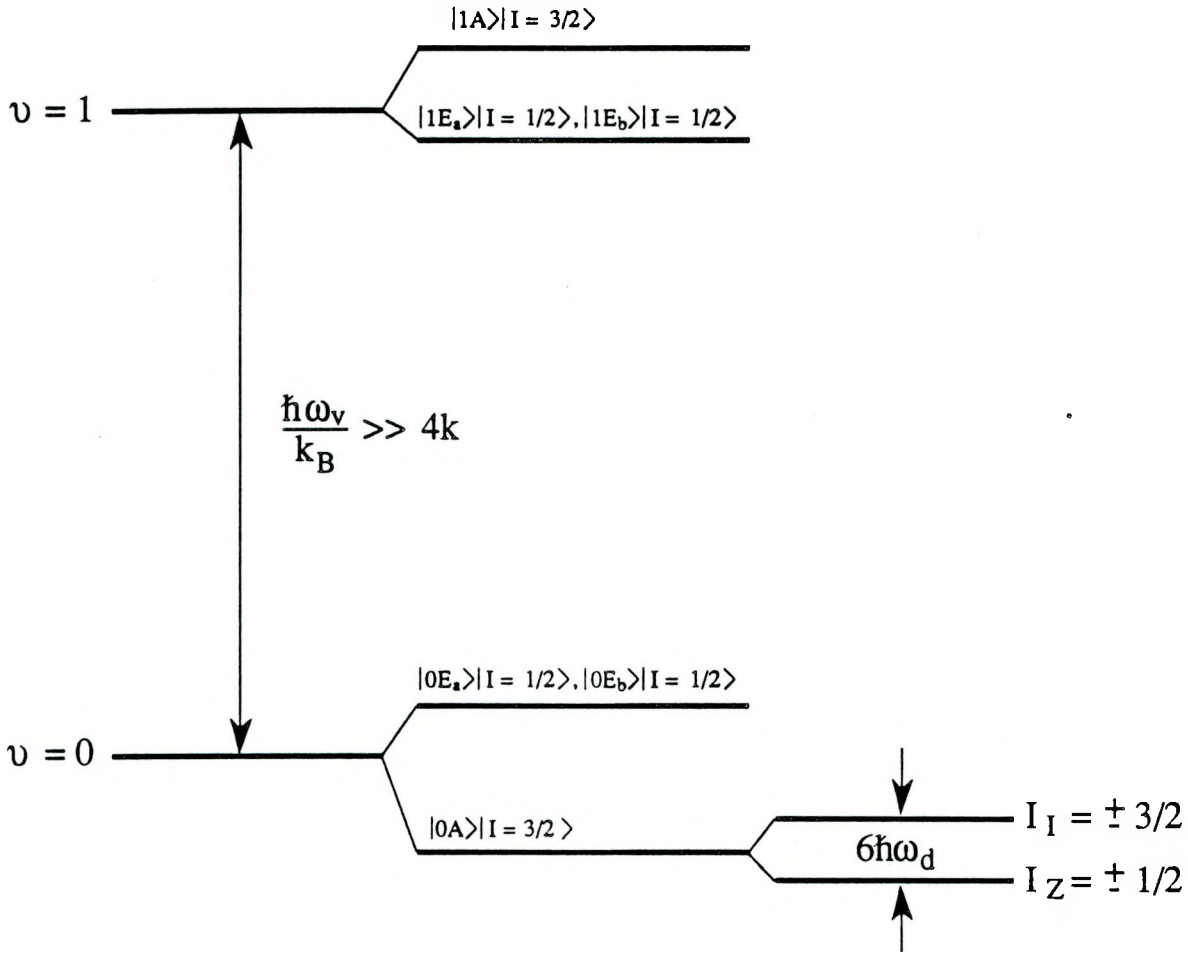

Fig. 5.5 Energy level splittings due to dipole-dipole interaction.

Because

$$\langle \delta\ 1/2\ \ 1/2 \mid \sum_{i<j} T^0_2\ (i,j) \mid \delta\ 1/2\ -1/2 \rangle = 0, \tag{5.42}$$

$$\langle \delta\ 1/2\ \ 1/2 \mid \sum_{i<j} T^0_2\ (i,j) \mid \delta\ 1/2\ \ 1/2 \rangle = 0, \tag{5.43}$$

$$\langle \delta\ 1/2\ -1/2 \mid \sum_{i<j} T^0_2\ (i,j) \mid \delta\ 1/2\ -1/2 \rangle = 0, \tag{5.44}$$

where $\delta = E_a , E_b$, we have

$$H_d = 0 \tag{5.45}$$

within the subspace spaned by the four states in the first excitation energy level. Thus, the dipole-dipole interaction has no effect on this level.

(2) Ground energy level

To calculate the influence of the dipole-dipole interaction on the ground state, we need to calculate $\langle 0\ A \mid H_d \mid 0\ A \rangle$ (cf. Eq. 5.18). Because

$$\langle 0\ A \mid Y^{\pm 2}_2 (\pi/2) \mid 0\ A \rangle = 0, \tag{5.46}$$

we have

$$\langle 0\ A \mid H_d \mid 0\ A \rangle = \hbar\, \omega_d \sum_{i<j} T^0_2\ (i,j) \langle 0\ A \mid Y^{-0}_2 (\pi/2) \mid 0\ A \rangle$$

$$= - \frac{\hbar\, \omega_d}{2} \sum_{i<j} T^0_2\ (i,j). \tag{5.47}$$

The reduced Hamiltonian is

$$H^A_d = - \frac{\hbar\, \omega_d}{2} [\ (I_1 \cdot I_2 + I_2 \cdot I_3 + I_3 \cdot I_1) - 3(I_{1Z}\, I_{2Z} + 3I_{2Z}\, I_{3Z} + 3I_{3Z}\, I_{1Z})]. \tag{5.48}$$

Since $[\ H^A_d , I_Z\ ] = 0$, the energy levels can be labeled by I_Z , and are given by

$$E_{3/2} = \langle A\ 3/2\ \ 3/2 \mid H^A_d \mid A\ 3/2\ \ 3/2 \rangle = \frac{3\hbar\, \omega_d}{4}, \tag{5.49}$$

$$E_{1/2} = \langle A\ 3/2\ \ 1/2 \mid H^A_d \mid A\ 3/2\ \ 1/2 \rangle = - \frac{3\hbar\, \omega_d}{4}, \tag{5.50}$$

$$E_{-1/2} = \langle A\ 3/2\ -1/2 \mid H^A_d \mid A\ 3/2\ -1/2 \rangle = - \frac{3\hbar\, \omega_d}{4}, \tag{5.51}$$

$$E_{-3/2} = \langle A\ 3/2\ -3/2 \mid H^A_d \mid A\ 3/2\ -3/2 \rangle = \frac{3\hbar\, \omega_d}{4}, \tag{5.52}$$

and they are plotted in Fig. 5.5. The resonant frequency is determined by

$$\hbar\omega_0 = E_{3/2} - E_{-1/2} = 3\hbar\,\omega_d/2. \tag{5.53}$$

For a CH_3 group, r = 1.758 Å,

$$\omega_d/2\pi = 21.1\text{kHz}, \tag{5.54}$$

and

$$\omega_0/2\pi = 31.6\ \text{kHz}.$$

For a NH_3D^+ ion, r = 1.652

$$\omega_d/2\pi = 25.4\ \text{kHz}, \tag{5.55}$$

and

$$\omega_0/2\pi = 38.1\ \text{kHz}. \tag{5.56}$$

Because H are coupled to N and D, this resonant frequency will be split.

LAWRENCE BERKELEY LABORATORY
UNIVERSITY OF CALIFORNIA
INFORMATION RESOURCES DEPARTMENT
BERKELEY, CALIFORNIA 94720